ELECTROSTATIC INTERACTIONS BETWEEN BIOMOLECULES AND SILICA PARTICLES USING TIME-RESOLVED FLUORESCENCE ANISOTROPY

STUDIES ON ELECTROSTATIC INTERACTIONS BETWEEN BIOMOLECULES AND SILICA PARTICLES USING TIME-RESOLVED FLUORESCENCE ANISOTROPY

By

JIE SUI, M.Sc.

A Thesis

Submitted to the School of Graduate Studies

in Partial Fulfillment of the Requirements

for the Degree

Master of Science

McMaster University

MASTER OF SCIENCE (2005)
McMaster University
(Chemistry)
Hamilton, Ontario

Title: Studies on Electrostatic Interactions between Biomolecules and Silica Particles using Time-Resolved Fluorescence Anisotropy

Author: Jie Sui, M.Sc. (Beijing University of Science and Technology)

Supervisor: Dr. John Brennan

Number of Pages: xvi, 128

ABSTRACT

This thesis focuses on the use of time-resolved fluorescence anisotropy (TRFA) for the analysis of peptide-silica and protein-silica interactions. Previous studies from our group have shown that strong ionic binding of the cationic probe rhodamine 6G (R6G) to the anionic surface of silica particles in water provides a convenient labeling procedure to study both particle growth kinetics and surface modification by time-resolved fluorescence anisotropy (TRFA). The decays for R6G dispersed in diluted Ludox silica sols usually fit to a sum of picosecond and nanosecond decay components, along with a significant residual anisotropy component. The first objective of my work was to assess the nature of the R6G:silica interaction to determine the origin of the nanosecond decay component, and ultimately validate the model used to fit the TRFA data and gain further insight into the physical meaning of the anisotropy decay parameters. Our results show the origin of the nanosecond decay component (ϕ_2) is due to the presence of a subpopulation of small nanoparticles in the Ludox sol.

With the correct physical model in place, we have been able use TRFA of R6G in aqueous Ludox to monitor peptide adsorption onto the silica particles *in situ.* Steady-state anisotropy and TRFA of R6G in Ludox sols were measured to characterize the extent of the ionic binding of the probe to silica particles in the presence of varying levels of tripeptides of varying charge, including Lys-Trp-Lys (KWK), N-acetylated Lys-Trp-Lys (Ac-KWK), Glu-Trp-Glu (EWE) and N-acetylated Glu-Trp-Glu (Ac-EWE). R6G showed significant decreases in anisotropy in the presence of cationic peptides, consistent with the addition of cationic peptides blocking the adsorption of the dye to the silica surface. The study shows that the competitive binding method can be used to assess the binding of various biologically

relevant compounds onto silica surfaces, and demonstrates the potential of TRFA for probing peptide:silica and protein:silica interactions.

We have also extended the application of TRFA to monitor protein adsorption onto plain and modified silica particles using a recently reported cationic long-lifetime quinolinium dye, CG437, which strongly binds to anionic silica particles through electrostatic interactions. In this case, alterations in the rotational correlation time of Ludox particles resulting from increases in the diameter of the rotating body upon binding of protein to the silica surface were monitored. The study shows that TRFA analysis of long-lived cationic probes such as CG437 can provide an effective method to investigate interactions between proteins and modified silica surfaces, extending the utility of the TRFA method.

ACKNOWLEDGEMENTS

I would like to thank my supervisor Dr. John D. Brennan for his guidance and support over the last two years. I am greatly indebted to Dr. Dina Tleugabulova for answering a lot of questions about my research and helping get my project moving.

I would like to thank my current and former labmates, for their invaluable support, interesting conversations throughout this project. Thanks to my committee members Dr. Philip Britz-McKibbin and Dr. Paul W. Ayers for the time to read the thesis and provide revision advices.

Last but not least, I would like to thank my parents, my husband and my friends for their moral support during the course of my study.

TABLE OF CONTENTS

Abstract	iii
Acknowledgements	v
Table of Contents	vi
List of Tables	ix
List of Figures	xi
List of Abbreviations	xv

Chapter 1 Introduction **1**

1.1 Sol-Gel Based Biomolecule Encapsulation 1
1.2 Methods to Evaluate Protein: Silica Interactions 4
1.3 Model System for TRFA Analysis of Protein: Silica Interactions 5
1.4 Goals of this Thesis 7
1.4.1 Evaluation of TRFA Decay Parameters 7
1.4.2 Direct and Indirect Evaluation of Peptide:Silica Interactions 8
1.4.3 Extension of TRFA to Protein:Silica Interactions 8
1.5 Thesis Overview 10
1.6 References 11

Chapter 2 Theory **17**

2.1 Basic Concepts in Fluorescence 17
2.1.1 The Fluorescence Process 18
2.1.2 Intrinsic and Extrinsic Fluorescence 18
2.1.3 Fluorescence Anisotropy 19
2.2 Fluorescence Anisotropy Measurements and Data Analysis 21
2.2.1 Steady-state Fluorescence Anisotropy 21
2.2.2 Time-resolved Fluorescence Anisotropy 22
2.2.3 TRFA Data Analysis 25
2.2.3.1 Free Dynamics In Non-Interacting Environments 26
2.2.3.2 Restricted Dynamics in the Presence of Probe-Ludox Silica Interactions 27
2.2.3.3 TRFA Analysis of Surface Modification of Ludox 28
2.3 References 28

Chapter 3 Evidence for Rigid Binding of Rhodamin 6G to Silica Surfaces in Aqueous Solution based on Fluorescence Anisotropy Decay Analysis **30**

3.1 Introduction 32
3.2 Theory 35

3.2.1 R6G-Ludox as a Mixture of Rotating Spheres 35
3.2.2 Local Probe Motion 38
3.3 Experimental Section 39
3.3.1 Chemicals 39
3.3.2 Procedures 39
3.4 Results and Discussion 42
3.4.1 TRFA of R6G in Aqueous Silica Sols 42
3.4.2 Ludox-R6G System as a Model of Rigid Spheres 50
3.4.3 Theoretical Analysis of R6G-Silica Interaction from Structural Considerations 53
3.5 Conclusions 57
3.6 References and Notes 58

Chapter 4 Direct and Indirect Monitoring of Peptide-Silica Interactions using Time-Resolved Fluorescence Anisotropy **62**

4.1 Introduction 64
4.2 Experimental Section 66
4.2.1 Chemicals 66
4.2.2 Procedures 67
4.2.2.1 Sample Preparation 67
4.2.2.2 Fluorescence Measurements 67
4.2.2.3 Atomic Force Microscopy 68
4.3 Results and Discussion 68
4.3.1 Direct Monitoring of Peptide Adsorption via Intrinsic Trp Fluorescence 68
4.3.2 Indirect Monitoring of Peptide Adsorption via R6G Anisotropy 71
4.3.3 Time-Resolved Anisotropy of R6G in Peptide/R6G/Ludox Mixtures 75
4.3.4 Atomic force microscopy 85
4.4 Conclusions 89
4.5 References 90

Chapter 5 Using a Long-lived Fluorescence Quinolinium Dye to Probe Protein Adsorption on Plain and Modified Colloidal Silica Nanoparticles **92**

5.1 Introduction 94
5.2 Experimental Section 96
5.2.1 Chemicals 96
5.2.2 Procedures 97
5.2.2.1 Synthesis and Characterization of CG437 97
5.2.2.2 Labeling of HSA 97

5.2.2.3 Sample Preparation 98
5.2.2.4 Modified Colloidal Silica 98
5.2.2.5 Silica Flocculation Study 98
5.2.2.6 Fluorescence Measurements 99
5.3 Results and Discussion 100
5.3.1 Characterization of Synthesized Probe 100
5.3.2 Silica Flocculation 105
5.3.3 Monitoring of Protein Adsorption via Trp Steady-State Anisotropy 108
5.3.4 TRFA of CG437 Protein/Ludox Mixtures 112
5.3.5 TRFA of CG437 in APTES modified Ludox 114
5.4 Conclusions 119
5.5 References 120

Chapter 6 Conclusions and Future Outlook **124**

6.1 Summary and Conclusions 124
6.2 Future Outlook 126

LIST OF TABLES

Table 3.1: TRFA decay parameters for R6G-DGS (0.25 wt % SiO_2), R6G-Ludox and R6G-SS. 45

Table 3.2: Fitting parameters resulting from analysis of TRFA decays for R6G in aqueous solutions of DGS (0.25 wt % SiO_2), Ludox (3 wt % SiO_2), polyacrylic acid (PAA) and polyglutamic acid (PGA). 52

Table 4.1: Effect of adding R6G and peptides in varying order on TRFA parameters. 73

Table 4.2: Time-resolved fluorescence anisotropy decay parameters of R6G in 10 mM, pH=7.4 Tris buffer solution and in 0.75 wt % SiO_2 in the presence of varying levels of tripeptides. 78

Table 4.3: Time-resolved fluorescence anisotropy decay data of R6G in 10 mM, pH=7.4 Tris buffer solution and in 0.75 wt % SiO_2 in the presence of varying levels of KWK. 79

Table 4.4: Time-resolved fluorescence anisotropy decay data of R6G in 10 mM, pH=7.4 Tris buffer solution and in 0.75 wt % SiO_2 in the presence of varying levels of Ac-KWK. 80

Table 4.5: Time-resolved fluorescence anisotropy decay data of R6G in 10 mM, pH=7.4 Tris buffer solution and in 0.75 wt % SiO_2 in the presence of varying levels of EWE. 81

Table 4.6: Time-resolved fluorescence anisotropy decay data of R6G in 10 mM, pH=7.4 Tris buffer solution and in 0.75 wt % SiO_2 in the presence of varying levels of Ac-EWE. 82

Table 5.1: Time-resolved fluorescence anisotropy decay parameters of CG437 in 10 mM, pH=7.5 HEPES buffer solution and in 1.5wt% SiO_2 in the presence of varying levels of proteins. 115

Table 5.2: Time-resolved fluorescence anisotropy decay parameters of CG437 in 10 mM, pH=7.5 HEPES buffer solution and in 1.5 wt % SiO_2, 0.0475% APTES, in the presence of varying levels of proteins. 116

LIST OF FIGURES

Figure 1.1: Methods Used to Entrap Biomolecules into Inorganic, Organic and Nanocomposite Sol–gel-derived Materials 2

Figure 1.2: Structure of Rhodamine 6G 6

Figure 2.1: Structures of Aromatic Amino Acids 18

Figure 2.2: Absorption Spectra of Aromatic Amino Acids (The extinction coefficient at pH 6) 18

Figure 2.3: Experimental setup of fluorescence anisotropy 21

Figure 2.4: Experimentally obtained I_{VH} (t) and I_{VV} (t) curves in time-resolved fluorescence anisotropy 23

Figure 2.5: S(t) and D(t) curves obtained from I_{VH} (t) and I_{VV} (t) curves in time-resolved fluorescence anisotropy 24

Figure 2.6: A typical fluorescence anisotropy decay curve 25

Figure 3.1: Structures of R6G and Ludox. 33

Figure 3.2: TRFA decay of R6G-DGS in 20 mM borate buffer, pH 9.2. SiO_2, 0.35 wt %; R6G, 1 μM. 43

Figure 3.3: TRFA decay of R6G-SS in 5 mM Tris-HCl, pH 9.2. SiO_2, 3 wt %; R6G, 1 μM. 46

Figure 3.4: TRFA decay of R6G-Ludox in water 47

Figure 3.5: A) Transmission electron microscopy image of Ludox particles.

B) Particle size distribution of Ludox particles imaged by TEM. 49

Figure 3.6: Resonance structures of R6G. 54

Figure 3.7: Graphical representation of interactions involved in rigid binding of R6G to the surface of Ludox. Note: The dashed lines indicate hydrogen bonds or ionic bonds to the surface. 57

Figure 4.1: Steady-state fluorescence anisotropy of rhodamine 6G (■, lex = 495 nm, lem = 551 nm) and KWK (●), Ac-KWK (○), EWE (▼) and Ac-EWE (▽) at λex = 295 nm, λem = 335 nm as a function of silica concentration. 69

Figure 4.2: Steady-state R6G anisotropy as a function of peptide concentration at 0.75 wt% SiO_2 for KWK (●), Ac-KWK (○), EWE (▼) and Ac-EWE (▽). 72

Figure 4.3: Time-resolved fluorescence anisotropy decays of R6G in Ludox silica sols (10 mM Tris-buffer, pH = 7.4, 0.75 wt % SiO2) at different concentrations of (A) KWK, (B) Ac-KWK, (C) EWE and (D) Ac-EWE. 0 mM (black); 0.6 mM (red); 1 mM (green); 2 mM (yellow); 5 mM (blue). The pink decay trace refers to 6 mM Ac-KWK (Panel B) or 10 mM EWE (Panel D). 76

Figure 4.4: Degree of adsorption of KWK (●), Ac-KWK (○), EWE (▼) and Ac-EWE (▽) on the surface of Ludox particles as a function of peptide concentration as determined by indirect monitoring of R6G anisotropy decay parameters. 84

Figure 4.5: Height and phase contrast atomic force microscopy images of Ludox silica particles (0.75 wt % SiO_2). a) Height image of unmodified particles; b) phase image of unmodified particles; c) height image of Ludox particles exposed to 2 mM KWK; d) phase image of Ludox particles exposed to 2 mM KWK; e) height image of Ludox particles exposed to 5 mM KWK; f) phase image of Ludox particles exposed to 5 mM KWK, g) height image of Ludox particles exposed to 5 mM EWE; f) phase image of Ludox particles exposed to 5 mM EWE. 87

Figure 5.1: CG437 Structure 100

Figure 5.2: ^1H NMR (D_2O) of 6-methoxyquinoline and CG437 101

Figure 5.3: IR spectra of 6-methoxyquinoline and CG437 102

Figure 5.4: MASS Spectrum of CG437 103

Figure 5.5: Absorption spectra of 40μM CG437 104

Figure 5.6: Emission spectra of 40μM CG437 105

Figure 5.7: Absorption changes to monitor the flocculation of Ludox (1.5 wt%) by HSA, melittin, PG (MW 17,000), RNAse T1, lysozyme, monellin, PL (MW 41,000) and PL (MW 2,500) 107

Figure 5.8: Steady-state fluorescence anisotropy of HSA (●), Monellin (○) and F-HSA (▼) at λex = 295 nm, λem = 335 nm and for F-HSA at λex = 495 nm, λem = 552 nm as a function of silica concentration. Samples contained 100 μM of the Monellin, HSA and 20 μM F-HSA. 109

Figure 5.9: Steady-state fluorescence anisotropy of HSA (●) and Monellin (○) at λex = 295 nm, λem = 335 nm as a function of APTES concentration. Samples contained 100μM of the proteins and 1.5 wt% silica. 111

Figure 5.10: CG437 time-resolved fluorescence anisotropy rotational correlation time changes in Ludox silica sols (10 mM HEPES buffer, pH = 7.5, 1.5 wt % SiO_2) at different concentrations of HSA (●) and Monellin (○). 117

LIST OF ABBREVIATIONS

Cys	Cysteine
Da	Dalton (g/mol)
DGS	Diglyceryl Silane
ESI	Electrospray Ionization
ESI-MS	Electrospray Ionization Mass Spectrometry
F-HSA	Fluorescein Labeled Human Serum Albumin
HEPES	4-(-2hydroxyethyl)-1-piperazineethanesulfonic acid
HSA	Human Serum Albumin
HPLC	High Performance Liquid Chromatography
Lys	Lysine
M	Molar (mol/liter)
MW	Molecular Weight
NaCl	Sodium Chloride
NATA	N-acetyl-tryptophanylamide
NMR	Nuclear Magnetic Resonance
Phe	Phenylalanine
pI	Isoelectric Point
R6G	Rhodamine 6G
RNASe T1	Ribonuclease T1
SEM	Scanning Electron Microscopy
SS	Steady State (Fluorescence Anisotropy)
TCSPC	Time-Correlated Single Photon Counting
TEOS	Tetraethyl orthosilicate
TRFA	Time Resolved Fluorescence Anisotropy
TRIS	Tris(hydroxymethyl)aminomethane hydrochloride
Trp	Tryptophan
E	Glutamate (1 letter code)
K	Lysine (1 letter code)
UV	Ultraviolet
W	Tryptophan (1 letter code)
WWW	World Wide Web

Chapter 1

Introduction

1.1 Sol-Gel Based Biomolecule Encapsulation

The development of sol–gel derived materials used for biomolecule encapsulation has been an area of intense interest in the past decade.[1,2] Typical applications of these sol-gel biomaterials include selective coatings for optical and electrochemical biosensors,[3-8] stationary phases for affinity chromatography,[9,10,11] immunoadsorbent and solid-phase extraction media,[12,13] controlled release agents[14-22] and development of solid-phase biosynthesis platforms.[23-26]

Encapsulation involves the trapping of biological species such as enzymes, antibodies and other proteins in a functional state within a nanoporous silica network where the analytes can diffuse into the matrix while the protein remains entrapped. The standard protocol for preparation of sol-gel-derived materials involves the partial or complete acid-catalyzed hydrolysis and condensation of alkoxysilane precursors.[27] The typical alkoxysilane precursors, either tetraethylorthosilicate (TEOS) or tetramethylortho- silicate (TMOS), undergo nucleophilic attack by the oxygen in water causing the alkoxide groups (OR) to be substituted by hydroxy groups (OH), as shown in Figure 1.1. Subsequently, in the condensation reaction, the silanol groups (Si-OH) are converted into siloxane bonds (Si-O-Si) with the water or alcohol are formed. During the whole process, the sol may be used immediately or may be stored for several weeks following hydrolysis to allow continued evolution of the sol particles. During this time, further hydrolysis and condensation reactions occur, resulting in a wide range of linear, branched and colloidal polysilicates. The hydrolysed precursor is then mixed with a buffered aqueous solution containing the biomolecule.

Aging of the wet silica network over a period of days to months promotes further condensation and strengthens the network. During this stage, entrapped alcohol and water resulting from the initial hydrolysis and condensation reactions will mostly evaporate from the matrix, causing the matrix to shrink by 10–30%, the pore diameters to decrease by about 25%, and the relative proportion of siloxane to silanol groups to increase owing to coarsening of the material.[28] Finally, the aged material is partially dried, resulting in the loss of most of the interstitial water, further cross-linking of the matrix, shrinkage of the pores to the range of 2–20 nm, and overall shrinkage of the material by up to 85% of its initial volume.

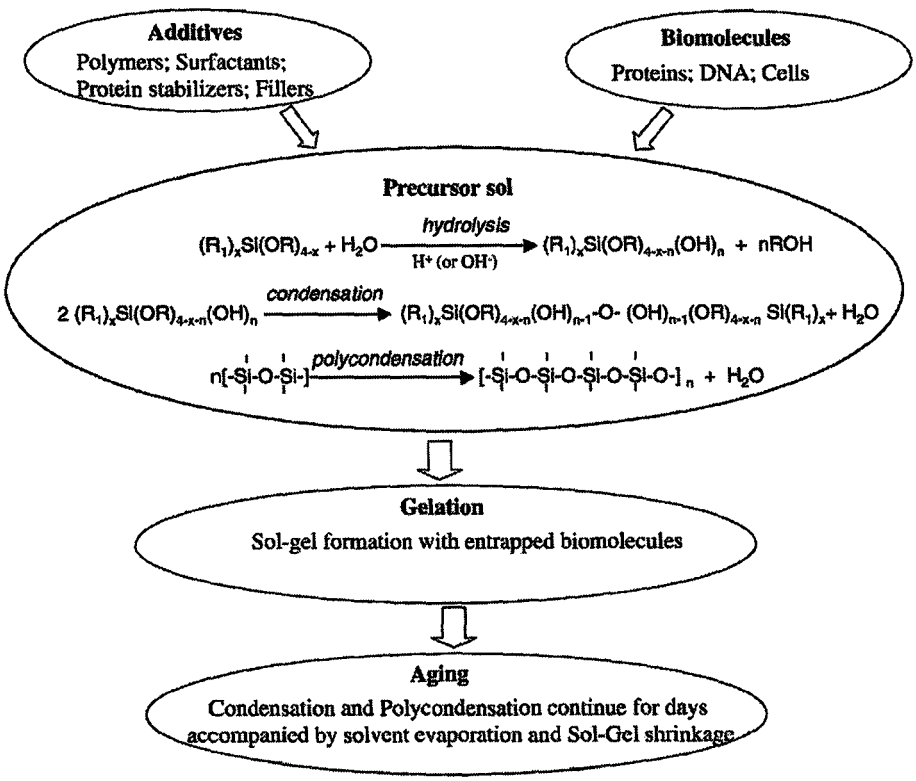

Figure 1.1 Methods Used to Entrap Biomolecules into Inorganic, Organic and Nanocomposite Sol–gel-derived Materials

One of the most important requirements for immobilization of proteins in sol-gel derived materials is that the entrapped proteins remain a functional state. However, the interactions (electrostatic interaction, hydrophobic interaction, H-bonding, etc) of entrapped proteins with the internal silica surfaces can cause protein adsorption, significantly decrease protein dynamics, and may lead to protein denaturation. Methods to control protein adsorption have included the addition of polymers to the silica matrix to passivate the pore wall,[29] and the inclusion of organically modified silanes to reduce the surface charge of the silica matrix.[30] However, the addition of these reagents not only altered the silica surface, but also changed the morphology of the material and the nature of the internal solvent, making it difficult to interpret what factors were responsible for altering protein dynamics.

Aside from sol-gel based biomolecule encapsulation systems, protein adsorption also plays an important role in a variety of other important technological and biological processes.[31,32] A large number of biotechnological devices require surface-bound proteins, including biosensors,[33] immonoaffinity supports[34] and bioreactors.[35] Separation of proteins by chromatography also involves the competitive adsorption of proteins onto the packed particles inside particulate or monolithic columns. [36] Protein adsorption can also cause problems, particularly in cases where such a process could cause surface fouling, such as protein adsorption to contact lenses[37] or implants[38, 39]. It is also well known that interactions between proteins and the capillary wall by means of ionic, hydrophobic and/or other mechanisms of interaction area detrimental to capillary electrophoresis (CE).[40,41] Development of methods for *in situ* analysis of protein-silica interactions is therefore required to improve our ability to design biocompatible materials, biotechnological devices and to modify silica surfaces in order to avoid unwanted protein adsorption. [42,43]

1.2 Methods to Evaluate Protein:Silica Interactions

A number of methods have been used to study the interactions of proteins with planar surfaces. These include x-ray photoelectron spectroscopy,[44] elliposometry,[45] attenuated total reflection FTIR,[46] total internal reflection fluorescence,[47,48] surface plasmon resonance,[49,50] and various interferometry methods.[51] Imaging methods such as confocal florescence microscopy and atomic force microscopy[52,53,54] have also been utilized to examine the spatial distribution of adsorbed proteins.[55] Frontal mode chromatography has also been widely used to evaluate interactions between proteins of interest and columns of varying types, especially for ion-exchange columns.[56,57,58,59] Capillary electrophoresis has also been used to study protein:silica interactions[60] and interaction of proteins with modified capillary surfaces.[61] In addition, methods such as NMR have been used to evaluate the nature of protein adsorption on silica using high surface area controlled pore glass materials.[62]

In the case of sol-gel derived biomaterials, protein:silica interactions are typically evaluated using time-resolved fluorescence anisotropy (TRFA), which can assess the rotational dynamics of fluorescently labeled proteins after entrapment in sol-gel derived materials.[29,63-68] Unlike NMR, it can be applied to study the dynamics of proteins at low concentrations or when entrapped in silica sol-gels. While such studies have provided useful insights into the dynamics of entrapped proteins, the size and complexity of proteins results in a wide array of different motions that occur on different timescales. Furthermore, proteins may be entrapped in a range of different environments within a sol-gel derived material, making the overall dynamics of the system highly complex. This situation can make the anisotropy decay complicated and very difficult to interpret. Moreover, the deconvolution of the intensity decay of a protein can be done into no more than three major components, and can be

complicated by alteration of protein conformation upon labeling. Thus, there is a need to develop more appropriate model systems that display reliable and easily interpretable dynamic motions, and yet provide sufficient complexity to allow insights into the parameters that affect protein-silica interactions.

1.3 Model System for TRFA Analysis of Protein: Silica Interactions

In the past few years, Geddes and Birch [69-73] introduced a new theoretical framework that describes the relationship between the rotational characteristics of entrapped fluorescent probes and the evolution of particle growth in silica-based sols. According to this theory, short (ps timescale) rotational correlation times correspond to probe that is free in solution, long (ns scale) rotational correlation times, which are often observed in the anisotropy decays of cationic probes such as rhodamine 6G (R6G) in silica sols, correspond to dye molecules that are electrostatically bound to anionic primary silica nanoparticles, while residual anisotropy (r_∞) values correspond to dye molecules that are bound to large silica structures existing in the medium that rotate too slowly to cause fluorescence depolarization during the 1-10 ns emission lifetime of a typical fluorescent probe (e.g. R6G). The chemical structure of R6G is shown in Figure 1.2. R6G has a molar extinction coefficient of 116,000 $M^{-1}cm^{-1}$ at 530 nm[74] and a quantum yield of 0.95.[75] R6G also has well understood single-lifetime photophysics with an excited-state lifetime independent of solvent of ~4 ns. R6G is a small cationic probe, 5.6 ± 0.1Å in radius and has a high experimental limiting anisotropy (r_0 = 0.38). [69-73] All of these properties make R6G an ideal probe for assessing the rotational dynamics of silica nanoparticles.

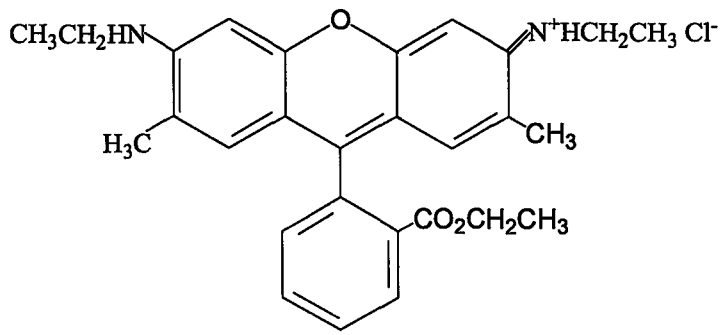

Figure 1.2: Structure of Rhodamine 6G

Provided that the viscosity of the surrounding solution is known, the nanosecond anisotropy decay component for a silica sol containing R6G can be related to the hydrodynamic radius (R) of the primary particles by applying the Stokes-Einstein-Debye (SED) equation,[76]

$$\eta = \frac{3\phi kT}{4\pi R^3}$$

where ϕ is the rotational correlation time on the nanosecond scale, η is the microviscosity of the sol solution, k is the Boltzmann constant and T is the temperature.

Our research group has applied the nanoparticle metrology approach to follow the evolution of aqueous and glycerol-doped sodium silicate sols through the sol-to-gel transition.[77] The possibility of differentiating between the free molecular rotation of the probe and the slow motion of silica-probe complexes led us to hypothesize that the nanosize metrology approach may be appropriate for testing the efficiency of silica surface modification. This was demonstrated using both polymers[78] and covalently coupled silanes such as aminopropyltriethoxysilane,[79] with changes in the proportions of the rotational decay components being used to assess the degree of surface modification of Ludox particles.

1.4 Goals of this Thesis

1.4.1 Evaluation of TRFA Decay Parameters

The first objective of my work was to assess the nature of the R6G:silica interaction to determine the dynamics of adsorbed R6G and ultimately validate the model used to fit the TRFA data and gain further insight into the physical meaning of the anisotropy decay parameters. The binding of R6G to larger particles, such as Ludox, leads to significant residual anisotropy, $r_\infty > 0$, in the TRFA decay. The degree of rotation of such particles on the time scale of the R6G intensity decay is insignificant and addressed as a "non-decaying" component.[79,82] This removes the ability to measure the mean particle radius, since much of the particle motion is hidden due to r_∞. However, the fractional contribution from the non-decaying component can be calculated as $g = r_\infty/r_0$, where r_0 is the limiting anisotropy, and can be used to estimate the degree of silica surface modification.[79,82] Besides the g value, two correlation times in a range 0.2 – 6 ns can be measured with the excited R6G probe.[79] The faster correlation time, ϕ_1, of ~ 0.2 ns corresponds to the rotation of free R6G molecules in solution and is therefore attributed to the fraction of free, non-adsorbed R6G molecules in silica sols. The interpretation of the second, slower component (ϕ_2) is less straightforward and has been subjected to different explanations, such as the presence of a subpopulation of small nanoparticles in silica sols and gels,[78,79] the wobbling motion of R6G on the silica surface,[79,80,82] association-dissociation reactions that occur on the timescale of the fluorescence emission of the dye or a fitting artifact caused by the presence of a particle size distribution in the case of Ludox sols. Whether this component arises solely from the overall rotation of the R6G-Ludox particles or experiences some contribution from the local motion of the R6G dipole relative to the silica surface will influence the choice of a physical model

for interpretation of the TRFA parameters. With the correct physical model in place, the practical applications of TRFA can be extended from particle growth kinetics measurements[69,70,71,72,73, 80] and the calculation of the degree of silica surface modification [79,78] to studies of more complex phenomena, such as silica-peptide and silica-protein interactions.

1.4.2 Direct and Indirect Evaluation of Peptide:Silica Interactions

The second objective was to extend the TRFA approach to allow the monitoring of the electrostatic binding of four model peptides to the silica surface, and to compare the results obtained by indirect measurements based on R6G reparitioning to those obtained by directly monitoring the changes in anisotropy of the peptides upon adsorption. Four peptides were chosen for this study: the cationic tripeptides Lys-Trp-Lys (KWK) and N-acetyl-Lys-Trp-Lys (Ac-KWK) and the anionic peptides Glu-Trp-Glu (EWE) and N-acetyl-Glu-Trp-Glu (Ac-EWE). The number of positively charged ammonium groups in these tripeptides vary from 0 (Ac-EWE) to 3 (KWK) and in the case of EWE and Ac-EWE there are also carboxylate groups of the Glu side chains, which should be repelled from the anionic surface of Ludox. The relatively small size of the tripeptides provides a higher flocculation limit than larger cationic peptides such as polylysine,[81] and thus is likely to lead to greater coverage of the silica surface, while the tryptophan residue provides a spectroscopic handle to allow direct observation of peptide adsorption via Trp fluorescence anisotropy.

1.4.3 Extension of TRFA to Protein:Silica Interactions

The third objective of this work was to extend our studies from the realm of small peptides toward larger biomolecules such as proteins, and to extend the Ludox system

to allow examination of interactions between proteins and surface-modified silica. To achieve these goals, it was necessary to redevelop the assay method to move beyond the use of R6G as a probe. The key drawback of this probe is that it is unable to assess slow rotational motions (ϕ > 60 ns), and thus particles larger than about 2 nm radius simply result in high residual anisotropy. Secondly, if a surface is highly modified with a species such as APTES, then there will be little space available for binding of the probe, and more importantly, binding of the protein to the modified surface will not displace the probe, since it will be bound to the unmodified portion of the surface. Hence, it is not possible to use change in the fractional values of decay components to measure adsorption. To overcome the problems with short lived probes and to extend our studies to modified surfaces, we have to use long-lived fluorescent probes, such as quinolinium type dyes.

Over the past 20 years quinolinium type dyes, especially those based on the 6-methoxyquinoline nucleus, have had various applications, including their use to probe polymer and sol-gel materials and as a sensor for halide ions.[82-90] Recently, Geddes et al. synthesized four new 6-methoxyquinoline-based fluorescent dyes containing cationic groups and applied one of these dyes, CG437 (6-methoxy-1-(3-propanol) quinolinium bromide), to TRFA analysis of nanoparticle sizing.[90] In this thesis, the adsorption of cationic and anionic proteins to native, polymer and APTES modified silica surfaces is examined using time-resolved fluorescence anisotropy of CG437, and compare the results to those obtained by flocculation studies and by directly monitoring Trp steady-state anisotropy from the proteins. The results demonstrate that TRFA of the CG437/Ludox system provides a useful new tool for probing the interactions of proteins with both native and modified silica surfaces.

1.5 Thesis Overview

In Chapter 2 of the thesis some of the key theoretical issues related to the use of TRFA for the examination of surface modification are introduced. This is intended to provide the reader with sufficient background to understand both the experimental protocols used to obtain TRFA data, and the models used to interpret the data.

Chapter 3 focuses on a study of the nature of binding of R6G to silica surfaces. The TRFA decay of R6G was examined in several silica systems, including Ludox, sodium silicate (SS) and diglycerylsilane (DGS), to provide a framework for interpreting the TRFA decay parameters, and in particular the origin of the nanosecond decay component. Supporting information from transmission electron microscopy studies and theoretical modeling of the R6G-silica interaction are used to develop a physical model for the origin of the ϕ_2 component, which provides new insight into the interpretation of TRFA data for R6G-silica systems.

In Chapter 4, tripeptide adsorption onto silica surfaces is examined both directly, via Trp steady-state anisotropy, and indirectly, using both steady-state and time-resolved fluorescence anisotropy of R6G. Both assays were done using different peptide:silica molar ratios and the data obtained from direct and indirect assay methods are compared. The results demonstrate that the competitive binding assay using TRFA of the RG6/Ludox system should provide a useful new tool for probing peptide:silica or protein:silica interactions, and should be amenable to adsorption measurements even for non-fluorescent biomolecules.

In Chapter 5, the long-lived cationic quinolinium probe CG437 was used to directly measure the rotational correlation times of Ludox particles and conditions were optimized so that the dye could bind to both unmodified and APTES modified Ludox particles without causing flocculation. Using the long lifetime of the probe, the

binding of cationic and anionic proteins to native and modified silica surfaces was examined, and compared to data obtained through both flocculation studies and by direct observation of Trp anisotropy of the proteins. The results demonstrate that TRFA of the CG437/Ludox system provides a useful new tool for probing protein: silica and protein: modified silica interactions.

Finally, chapter 6 provides an overall summary of the thesis work in the context of both the utility of the TRFA method for surface analysis and the potential drawbacks of this method. A suggestion for future work is also provided.

1.6 References

1. Jin, W; Brennan, J.D. *Anal. Chim. Acta* **2002**, *461*, 1.
2. Gill, I. *Chem. Mater.* **2001**, *13*, 3404.
3. Dave, B.C.; Dunn, B.; Valentine, J.S.; Zink, J.I. *Anal. Chem.* **1994**, 66, 1120A.
4. Lev, O.; Tsionsky, M.; Rabinovich, L.; Glezer, V.; Sampath, S.; Pankratov, I.; Gun, J. *Anal. Chem.* **1995**, 67, 22A.
5. MacCraith, B.D.; McDonagh, C.; McEvoy, A.K.; Butler, T.; O'Keeffe, G.; Murphy, V. *J. Sol–Gel Sci. Technol.* **1997**, 8, 1053.
6. Brennan, J.D., *Encyclopedia of Analytical Chemistry*; John Wiley and Sons, Ltd., Chichester, **2000**, pp. 383-403.
7. Lin, J.; Brown, C.W. *Trends Anal. Chem.* **1997**, 16, 200.
8. Wu, X.J.; Choi, M.F. *Analytica Chimica Acta* **2004**, 514, 219.
9. Tanaka, N.; Kobayashi, H.; Nakanishi, K.; Minakuchi, H.; Ishizuka, N. *Anal. Chem.* **2001**,73, 420A.

10. Tanaka, N.; Nagayama, H.; Kobayashi, H.; Ikegami, T.; Hosoya, K.; Ishizuka, N.; Minakuchi, H.; Nakanishi, K.; Cabrera, K., D. ; Lubda, D. *J. High Resol. Chromatogr.* **2000**, 23, 111.

11. Hodgson, R.; Chen, Y.; Zhang, Z.; Tleugabulova, D.; Long, H.; Zhao, X.; Organ, M. G.; Brook, M. A.; Brennan, J. D. *Anal. Chem.*, **2004**, 76, 2780.

12. Arthur, C.L.; Pawliszyn J. *Anal. Chem.* **1990**, 62 , 2145.

13. Schedl, M.; Wilharm, G.; Achatz, S.; Kettrup, A.; Niessner R.; Knopp D. *Anal. Chem.* **2001**,73, 5669.

14. Sieminska, L.; Ferguson M.; Zerda, T.W.; Couch, E. *J. Sol–Gel Sci. Technol.* **1997**, 8, 1105.

15. Kortesuo, P., Ahola, M., Kangas, M., Yli-Urpo, A., Kiesvaara, J., Marvola, M. *Int. J. Pharm.* **2001**, 221,107.

16. Radin, S.; Ducheyne, P.; Kamplain, T.; Tan, B.H. *J. Biomed. Mater. Res.* **2001**, 57, 313.

17. Aughenbaugh, W.; Radin, S.; Ducheyne, P. *J. Biomed. Mater. Res.* **2001**, 57, 321.

18. Ahola, M.S.; Sailynoja, E.S.; Raitavuo, M.H.; Vaahtio, M.M.; Salonen, J.I.; Yli-Urpo, A.U.O.; *Biomater.* **2001**, 22, 2163.

19. Böttcher, H.; Slowik, P.; Suss, W. *J. Sol–Gel Sci. Technol.* **1998**, 13, 277.

20. Nicoll, S.B.; Radin, S.; Santos, E.M.; Tuan, R.S.; Ducheyne, P. *Biomater.* **1997**, 18, 853.

21. Santos, E.M.; Radin, S.; Ducheyne, P. *Biomater* **1999**, 20, 1695.

22. Böttcher H.; Jagota, C.; Trepte, J.; Kaiiles, K.H.; Haufe, H. *J. Control Release* **1999**, 60, 57.

23. Obert, R.; Dave, B.C. *J. Am. Chem. Soc.* **1999**, *121*, 12192.

24. Gill,I.; Ballesteros, A. *J. Am. Chem. Soc.* **1998**, 120, 8587.

25. Reetz, M.T.; Wenkel, R.; Avnir, D. *Synthesis* **2000**, 6, 781.

26. Badjic, J.D.; Kadnikova, E.N.; Kostic, N.M. *Org. Lett.* **2001**, 3, 2025

27. Brennan, J.D. *Applied Spectroscopy*, **1999**, 53, 106A

28. C.J. Brinker, G.W. Scherer, Sol–Gel Science: The Physics and Chemistry of Sol–Gel Processing, Academic Press, San Diego, 1990.

29. Baker, G.A.; Jordan, J.D.; Bright, F.V. *J. Sol-Gel Sci. Technol.* **1998**, *11*, 43.

30. Sui, X.; Cruz-Aguado, J.A.; Chen, D.Y.; Zhang, Z.; Brook, M.A.; Brennan, J.D. *Chem. Mater.* **2005**, *17*, 1174.

31. Clerc, D., and W. Lukosz. *Biosens. Bioelectron.* **1997**, 12,185.

32. Shi, H. Q., and B. D. Ratner. *J. Biomed. Materials Res.* **2000**, 49,1.

33. Nyquist, R. M., A. S. Eberhardt, L. A. Silks, Z. Li, X. Yang, and B. I. Swanson. *Langmuir.* **2000**,16,1793.

34. Hage, D. S. *J. Chromatog. B* **1998**, *715*, 3.

35. Prazeres, D.; Miguel F.; Cabral, J. M. S. in: *Multiphase Bioreactor Design*, Cabral, J. M. S.; Mota, M.; Tramper, J. (Eds.) Taylor & Francis Ltd., London, UK, 2001, pp. 135-180.

36. Pawel Szabelski, Alberto Cavazzini, Krzysztof Kaczmarski, Xiaoda Liu and Georges Guiochon. *J. Chromatogr. A,* **2002**, 950, 41.

37. St. John, H.A.W. et al.; *Polymeric Materials Science and Engineering.* **1997**, 78,83

38. Bohnert JL, Horbett TA. *Journal of Colloid and Interface Science.* **1986**, 111, 363.

39. Tang L *et al. Biomaterials.* **1999**, 20, 1365.

40. J.K.Towns and F.E. Regnier, *Anal. Chem.*, **1992**, 64, 2473.

41. F.E. Regnier and D. Wu, in N.A. Guzman (Editor) Capillary Electrophoresis Technology, Marcel Dekker, New York, 1993, pp. 287-309

42. S. Hjertén, *J. Chromatogr.*, **1985,** 347, 191.

43. L. Capelli, S. Ermakov and P.G. Righetti, *J. Biochem. Biophys. Methods.* **1996,** 32, 109.

44. Gail E. Fanucci and Daniel R. Talham. *Langmuir* **1999,** 15, 3289.

45. Jana Jass, Torbjörn Tjärnhage, and Gertrud Puu. *Biophys J*, **2000**, 79, 3153.

46. Chen, Y.; Iroh, J. O. *Chem. Mater.* **1999**, 11, 1218.

47. J.D. Andrade, ed., Protein Adsorption, Plenum Press, N.Y., **1985**.

48. V. Hlady, Interfacial Behavior of Bioproducts, Dekker, **1994**.

49. B. Liedberg, C. Nylander and I. Lundstrom, *Sensors and Actuators*, **1983**,4, 299

50. Terry T. Goodrich, Hye Jin Lee, and Robert M. Corn, *J. Am. Chem. Soc.*, **2004,** 126, 4086.

51. Su, T.J., Lu, J.R., Thomas, R.K., Cui, Z.F. and Penfold, J., *J. Phys. Chem. B.* , **1998**, 102, 8100.

52. Jean Jacques Bonvent, Riccardo Barberi, Roberto Bartolino, Laura Capelli, Pier Giorgio Righetti. *Journal of Chromatogr. A.* **1996,** 756, 233.

53. J. J. Valle-Delgado, J. A. Molina-Bolívar, F. Galisteo-González, M. J. Gálvez-Ruiz, A. Feiler and M. W. Rutland. *Jounal of Physics: Condensed Matter.* **2004,** 16, S2383.

54. A. M. Moulin, S. J. O'Shea, R. A. Badley, P. Doyle, and M. E. Welland, *Langmuir.* **1999,** 15, 8775.

55. J. N. Lin, B. Drake, A. S. Lea, P. K. Hansma, and J. D. Andrade, *Langmuir*, **1990**, 6, 509.

56. Tsou, H.S., and Graham, E. E. *AIChE J.* **1985,** 31, 1959

57. Johnston, A., and Hearn, M. T. W., *J. Chromatogr.* **1990,** 512, 101

58. Bowen, W. R., and Hughes, D. T., *J. Colloid Interface Sci.* **1993,** 158, 395

59. Hunter AK, Carta G. *J. Chromatogr. A.* **2001,** 937:13-9.

60. Barbara Verzola; Cecilia Gelfi; Pier Giorgio Righetti. *Journal of Chromatography A.* **2000,** 874, 293.

61. Barbara Verzola , Cecilia Gelfi, Pier Giorgio Righetti. *Journal of Chromatography A.* **2000,** 894, 281.

62. V. M. Gun'ko, V. V. Turov, V. I. Zarko, V. V. Dudnik, V. A. Tischenko, O. A. Kazakova, E. F. Voronin, S. S. Siltchenko, V. N. Barvinchenko and A. A. Chuiko *Journal of colloid and interface science.* **1997,** 192, 166.

63. R. Wang, U. Narang, P.N. Prasad, F.V. Bright. *Anal. Chem.* **1993,** 65, 2671.

64. K. Flora, J.D. Brennan. *Chem. Mater.* **2001,** 13, 4170.

65. D. S. Gottfried, A. Kagan, B. M. Hoffman, J.M. Friedman. *J. Phys. Chem. B.* **1999,** 103, 2803.

66. J. D. Jordan, R.A. Dunbar, F.V. Bright. *Anal. Chem.* **1995,** 67, 2436.

67. M. A. Doody, G.A.Baker, S.Pandey, F. V. Bright. *Chem. Mater.* **2000,** 12, 1142.

68. I. Khan, C. F. Shannon, D. Dantsker, A.J. Friedman, J. P.-G.-de-Apodaca, J.M. Friedman. *Biochemistry.* **2000,** 39, 16099.

69. Geddes, C. D.; Birch, D. J. S. *J. Non-Cryst. Solids* **2000,** 270, 191.

70. Birch, D. J. S.; Geddes, C. D. *Phys. Rev. E.* **2000,** 62, 2977.

71. Geddes, C. D.; Karolin, J.; Birch, D. J. S. *J. Fluoresc.* **2002,** 12, 113

72. Geddes, C. D.; Karolin, J.; Birch, D. J. S. *J. Fluoresc.* **2002,** 12, 135

73. Geddes, C. D. *J. Fluoresc.* **2002,** 12, 343.

74. R. R. Birge. Kodak Laser Dyes. 1987

75. R. F. Kubin and A. N. Fletcher. *J. Luminescence* **1982,** 27, 455.

76. Debye, P. *Polar Molecule*; Chemical Catalog Co.: New York, 1929

77. Tleugabulova, D.; Chen, Y.; Zheng, Z.; Brook, M.; Brennan, J. D. *J. Phys. Chem. B* **2003**, , *107*, 10127.

78. Tleugabulova, D.; Duft, A.M.; Brook, M.A.; Brennan, J. D. *Langmuir* **2004**, *20*, 101.

79. Tleugabulova, D.; Chen, Y.; Zheng, Z.; Brook, M.; Brennan, J.D. *Langmuir*, **2004**, 20, 848.

80. Tleugabulova, D.; Duft, A. M.; Zhang, Z.; Chen, Y.; Brook, M. A.; Brennan, J. D. *Langmuir* **2004**, *20*, 5924.

81. Coradin T., Durupty O., Livage J. *Langmuir*, **2002**, *18*, 2331.

82. Geddes CD, Douglas P, Moore C, Wear T, Egerton P. *J. Fluorescence* **1999**, 9, 163.

83. Geddes CD, Douglas P, Moore C, Wear T, Egerton P. J. *Dyes and Pigments* **1999**, 43, 59.

84. Jiwan HJ-L, Soumillion J-Ph. *J Non Cryst Solids* **1997**, 220, 316.

85. Urbano E, O.enbacher H, Wolfbeis OS. A*nal Chem* **1984**, 56, 427.

86. Wolfbeis OS, Hochmuth P. *Mikrochimica Acta* **1984**, 3, 129.

87. Schulman SG, Threatte RM, Capamacchia AC. *J Pharm Sci.* **1974**, 63, 876.

88. Chris D. Geddes, Kathleen Apperson, Jan Karolin and David J. S. Birch. *Analytical Biochemistry.* **2001**, 293, 60.

89. Chris D Geddes. *Meas. Sci. Technol.* **2001**, 12, R53.

90. Chris D. Geddes, Kathleen Apperson, David J.S. Birch. *Dyes and Pigments* **2000**, 44, 69.

Chapter 2

Theory

2.1 Basic Concepts in Fluorescence

2.1.1 The Fluorescence Process

The absorption of a photon of ultraviolet, visible or infrared radiation by a molecule leads to the promotion of an electron to the first (or higher) excited singlet state. Following excitation, the molecule can undergo a number of excited state processes, including vibrational relaxation, intersystem crossing to a triplet state, and variations in excited state energy owing to changes in the local solvent microenvironment. After a few nanoseconds, the excited electron can return to the ground state, either by a non-radiative process termed internal conversion, or by the emission of a photon. The latter process, involving movement from the singlet excited state to the ground state, is termed fluorescence. Emission from the triplet state, on the other hand, is termed phosphorescence, and typically has a much longer excited state lifetime and a longer emission wavelength than fluorescence.[1,2]

Given that the excited state exists for several nanoseconds, the nature of the fluorescence emission is highly dependent on processes that occur on this timescale. This can include solvent reorientation, collisions with other molecules, transfer of energy to nearby "acceptor" molecules, and overall rotational motion of the excited fluorescent molecule. In this thesis, it is the effects of molecular rotation on fluorescence that are of importance, and thus this process will be described in further detail. The nature of the fluorescent probes that can be used in such studies is also briefly described to provide insight into the types of systems that can be used to examine molecular dynamics and, ultimately, biomolecule:surface interactions.

2.1.2 Intrinsic and Extrinsic Fluorescence

Molecules capable of undergoing electronic transitions that ultimately result in fluorescence are known as fluorescent probes, fluorophores or simply dyes. In general, fluorophores are divided into two broad classes, termed intrinsic and extrinsic.

Intrinsic fluorophores are any probe that is inherently part of the system under study. In proteins, intrinsic fluorophores include three naturally occurring aromatic amino acids: phenylalanine (Phe), tyrosine (Tyr) and tryptophan (Trp). These three residues are responsible for the characteristic absorption of proteins and polypeptides in the wavelength region between 260 and 300 nm. The structures and absorption spectra of the aromatic amino acids are presented in Figures 2.1 and 2.2, respectively.

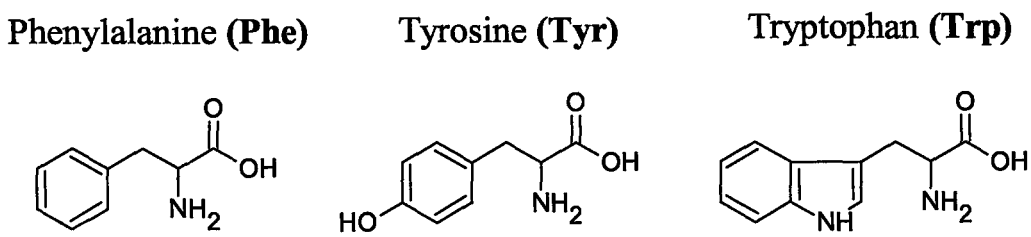

Figure 2.1: Structures of Aromatic Amino Acids

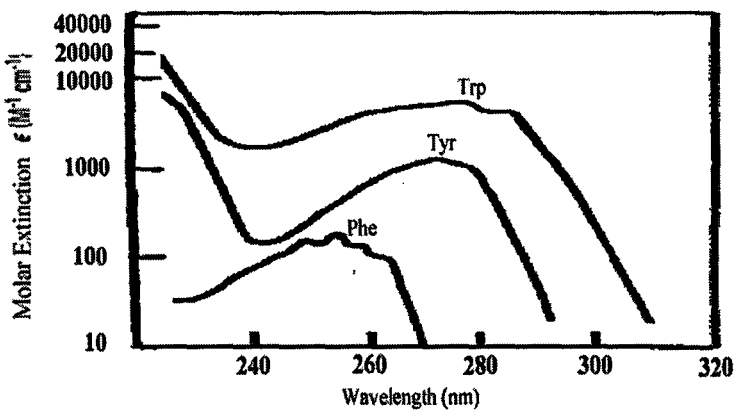

Figure 2.2: Absorption Spectra of Aromatic Amino Acids

(The extinction coefficient at pH 6)[3]

Trp and Tyr have stronger absorption than Phe, making them better suited to spectroscopic studies. More importantly, Trp has a red extended absorption spectrum and the highest extinction coefficient relative to either Phe or Tyr, and thus one can selectively excite Trp in the presence of other amino acids at $\lambda_{ex} > 295$nm, allowing one to observe the fluorescence originating solely from the Trp residues within the protein. The Trp emission spectrum is moderately sensitive to the external environment, shifting from an emission maximum of ~310 nm in hydrophobic environments to 350 nm in polar solvents. The Trp residue will also display anisotropic emission when excited with polarized light (see below), making it amenable to studies of molecular rotation.

Extrinsic fluorophores are typically synthetic dyes or modified biochemicals that are added to a specimen such as proteins to produce fluorescence with specific spectral properties. The characteristics of fluorescence (excitation and emission spectrum, quantum yield, lifetime, limiting anisotropy, solvent sensitivity, excited state behaviour), can be selected by choosing the appropriate dye, which then allows one to monitor specific excited state processes involving interactions of the excited molecule with its close environment. The choice of a fluorescent probe is crucial for obtaining an unambiguous interpretation of a particular property of the microenvironment in which the probe is located.

2.1.3 Fluorescence Anisotropy [1, 2]

Light is an electromagnetic wave consisting of an electric field **E** and a magnetic field **B** perpendicular both to each other and to the direction of propagation, and oscillating in phase. For natural light, these fields have no preferential orientation, but for linearly polarized light, the electric field oscillates along a given direction.

In the quantum mechanical approach, a transition moment is introduced for characterizing the transition between the initial and final state of a molecule. The transition moment represents the transient dipole resulting from the displacement of charges during the transition; therefore, it is not strictly a dipole moment. In most cases, the transition moment can be drawn as a vector in the coordinate system defined by the location of the nuclei of the atoms; therefore, the molecules whose absorption transition moments are parallel to the electric vector of a linearly polarized incident light are preferentially excited. This probability is maximized when the two vectors are parallel to each other and zero when they are perpendicular.

When a population of fluorophores is illuminated by linearly polarized incident light, those molecules whose transition moments are oriented in a direction close to that of the electric vector of the incident beam are preferentially excited. This is called photoselection. Because the distribution of excited fluorophores has a preferred orientation parallel to the electric vector of the excitation beam, the resulting distribution of excited fluorophores is anisotropic. Thus, in the absence of molecular motion during the excited state lifetime, the emitted fluorescence will also be anisotropic. However, any change in direction of the transition moment during the lifetime of the excited state will cause this anisotropy to decrease, i.e., it will induce a partial (or total) depolarization of fluorescence.

Depolarization of fluorescence can result from a number of phenomena such as internal conversion to a lower energy state with a different dipole direction, energy to another molecule with a different orientation, or rotational diffusion of the fluorophores. In the absence of internal conversion and energy transfer, the fluorescence anisotropy can provide useful information on molecular mobility, size,

shape and the flexibility of molecules, and on the microviscosity of the surrounding medium.

2.2 Fluorescence Anisotropy Measurements and Data Analysis

2.2.1 Steady - state Fluorescence Anisotropy [1,2]

The basic experimental setup for measuring fluorescence anisotropy is shown in Figure 2.3:

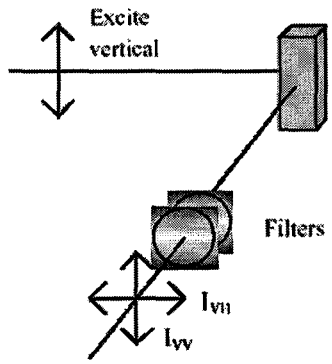

Figure 2.3: Experimental setup of fluorescence anisotropy [4]

Steady-state fluorescence anisotropy involves measurement of the intensity of parallel and perpendicularly polarized emission from a sample after continuous excitation parallel polarized light. The steady-state anisotropy r is given by:

$$r = \frac{I_{VV} - I_{VH}}{I_{VV} + 2I_{VH}} \tag{1}$$

where I_{VV} is the intensity of parallel polarized emission and I_{VH} is the intensity of perpendicularly polarized emission after excitation with a parallel polarized excitation beam. The relationship between the average rotational correlation time of the fluorescent species (ϕ) and the steady-state anisotropy is given by:

$$r = \frac{r_0}{1 + \phi/\tau} \tag{2}$$

where r_0 is the limiting anisotropy in the absence of rotational motion and τ is the mean lifetime of the probe. Based on equation (2) it is clear that the ratio of the fluorescence lifetime to the rotational correlation time determines the average anisotropy. The anisotropy value is sensitive to changes in the ratio of ϕ/τ over the range from ~1/15 to 15. Thus, probes with short lifetimes will be best suited to report on rapid rotational motions, while those with long lifetimes will be better suited for reporting slower rotational motions. Given this relationship, it is important to know both r_0 and τ, and to ensure that these do not change as a result of a given perturbation to the fluorescent system, if one wishes to quantitatively evaluate changes in ϕ from steady-state anisotropy measurements.

The steady-state anisotropy value is averaged over all rotational motions of the fluorescent species, and is not able to monitor the underlying rotational components that go into producing the average value. On the other hand, steady-state fluorescence anisotropy measurements can be done considerably faster than time-resolved fluorescence anisotropy, which allows for more measurements of a given sample per unit time, which is useful to following kinetic processes, or for analysis of more samples per unit time, increasing throughput.

2.2.2 Time-Resolved Fluorescence Anisotropy[1,2]

To evaluate the underlying rotational components that do into the steady-state anisotropy value, it is necessary to measure the temporal evolution of I_{VV} and I_{VH}. This can be done in a number of ways, however for the purposes of this work only the time-domain measurement method will be described. In this case, the sample is excited with a series of extremely short pulses of vertically polarized light and the intensity of the resulting emission is monitored as a function of time after the

excitation pulse in both the vertical and horizontal polarization planes to yield $I_{VV}(t)$ and $I_{VH}(t)$. These curves will display both the inherent decay of fluorescence intensity, which will occur with the characteristic lifetime of the fluorophore (τ), and the additional alterations in fluorescence intensity owing to rotation of the fluorescent species. Typical $I_{VV}(t)$ and $I_{VH}(t)$ curves are shown in Figure 2.4.

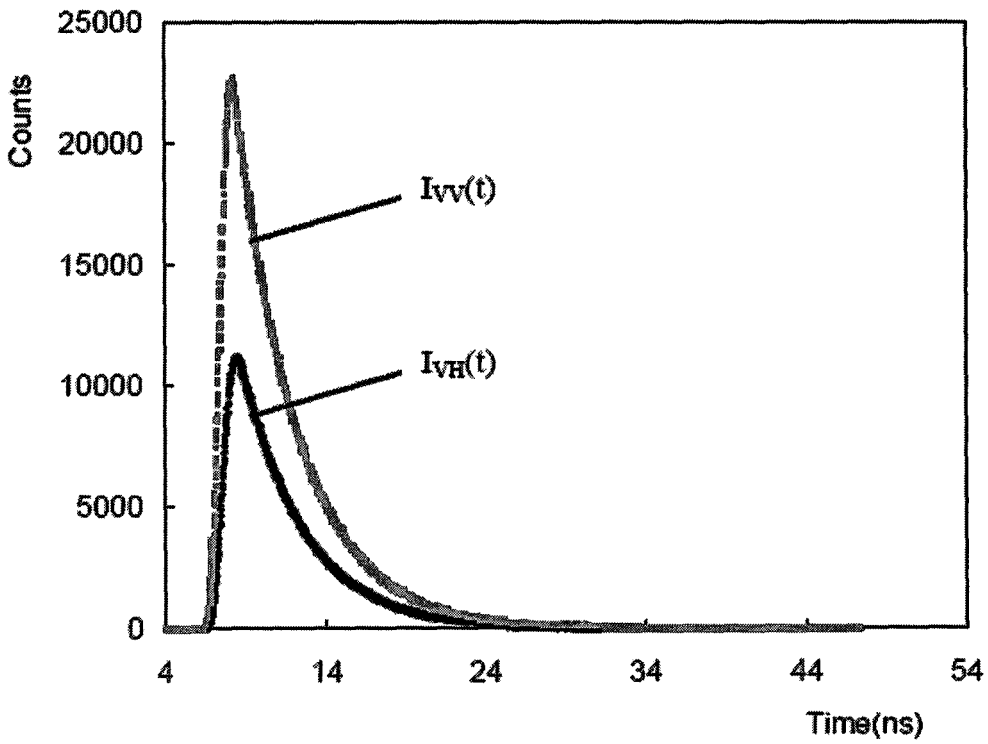

Figure 2.4: Experimentally obtained I_{VH} (t) and I_{VV} (t) curves in time-resolved fluorescence anisotropy

The $I_{VV}(t)$ decay curve shows an more rapid initial decay profile owing to the rotation of vertically polarized fluorophores out of the vertical plane, while the $I_{VH}(t)$ curve shows an initial rising portion owing to rotation of such molecules into the horizontal plane.

By summing the decay traces (noting that the decay can occur into two mutually independent orthogonal directions), one obtains the sum $S(t)= I_{VV}(t)+2I_{VH}(t)$, which cancels the rotational contributions and thus results in a normal intensity decay, and can therefore be used to extract the excited state lifetime of the probe. The difference $D(t)=I_{VV}(t)-I_{VH}(t)$ gives the decay owing to rotational components only, but this curve is still scaled to the intensity in any given channel, which decreases with time, as shown in Figure 2.5.

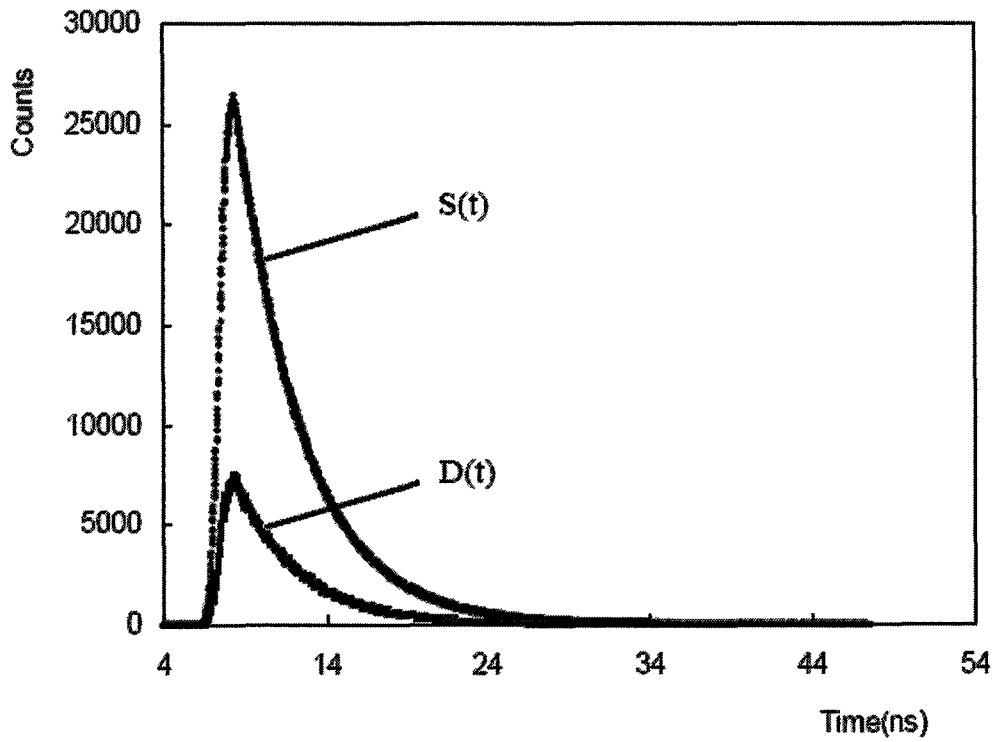

Figure 2.5: S(t) and D(t) curves obtained from I_{VH} (t) and I_{VV} (t) curves in time-resolved fluorescence anisotropy

By dividing the difference function by the sum function, the intensity variations are normalized across all channels, canceling the contributions from the intensity decay and leaving only the time resolved fluorescence anisotropy r(t) decay data:

$$r(t) = \frac{D(t)}{S(t)} = \frac{I_{VV}(t) - I_{VH}(t)}{I_{VV}(t) + 2I_{VH}(t)} \tag{3}$$

A typical fluorescence anisotropy decay curve calculated by software based on experimentally obtained decays $I_{VV}(t)$ and $I_{VH}(t)$ is shown below:

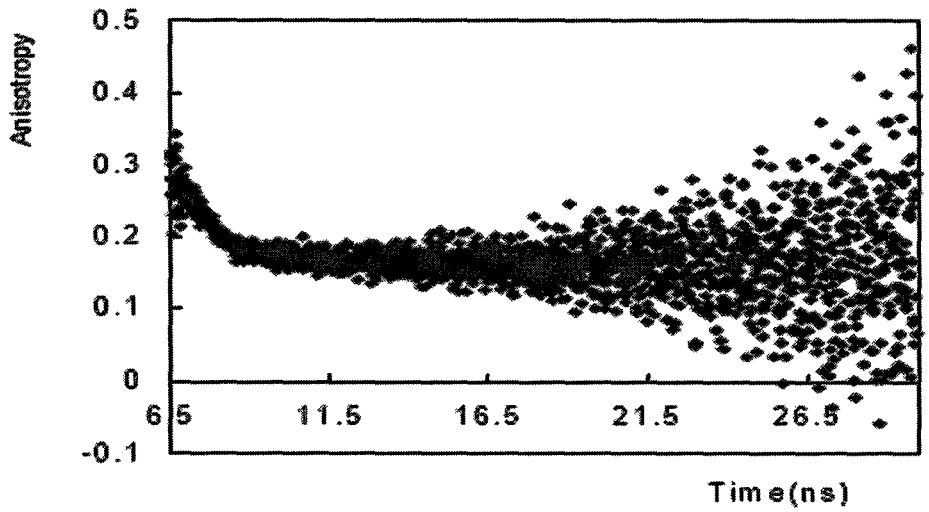

Figure 2.6: A typical fluorescence anisotropy decay curve

2.2.3 TRFA Data Analysis

The measured $r(t)$ decay contains information about the probe motion through its relationship to the Fourier transform of the orientational time correlation function $P_2(t)$ of a rotating emission dipole [5,6]

$$r(t) = P_2(t) = \frac{3}{2} < \cos^2 \alpha(t) > -\frac{1}{2} \tag{4}$$

where α is the displacement angle between the absorption and emission dipole moments of the probe. Depending on the probe structure, shape and its environment, several mathematical models have been developed to describe $P_2(t)$.[5,6] The fit of a particular model to the experimental r(t) decay is usually achieved via an algorithm[6,7]

that minimizes the difference between the experimental and simulated data and finds the global minimum in the fitting function. The acceptance criteria for goodness of the fit include a satisfactory reduced chi-squared value (χ_R^2) and a random distribution of weighted residuals. Since more than one mathematical solution can potentially exist that will fit the experimental r(t) data equally well, a statistically good fit may generate meaningless decay parameters.[8] Hence, the fulfillment of the statistical requirements by itself cannot be regarded as a definitive proof of the rotational diffusion model. Rather, the validity of the model is judged by its physical significance in describing the system under study.

2.2.3.1 Free Dynamics In Non-Interacting Environments

The rotation of a fluorescent probe in water is usually taken as a reference point. The probe molecule is approached as a small rigid body (sphere, ellipsoid or rod) and its motion in water is modeled as isotropic Brownian rotation in an unhindered environment. In the case of a probe in buffer containing other species such as small peptides, the motion of the probe molecule is also unhindered provided there are no interactions between probe molecule and the second species in the solution. The simplest model for this free motion is that of the rigid sphere[9], which describes as a single-exponential function

$$r(t) = r_0 \exp(-t/\phi) \tag{5}$$

where r_0 is the limiting anisotropy at time zero and ϕ is the rotational correlation time. The r_0 value indicates the initial anisotropy after internal conversion and vibrational relaxation, prior to probe rotation, and should nearly correspond to the steady-state anisotropy of the fluorescent probe in a glassy frozen solvent. The theoretical value of

r_0 depends upon the nature of the excitation process: maximum values are $r_0 = 0.4$ using one-photon excitation.[10]

The rotational correlation time (ϕ) indicates how fast the initially polarized emission is randomized due to Brownian diffusion. Provided that the viscosity of the surrounding solution is known, the nanosecond anisotropy decay component can be related to the hydrodynamic radius (R) of the primary particles by applying the Debye-Stokes-Einstein equation,[11]

$$\phi = \frac{\eta V}{kT} = \frac{4\eta\pi R^3}{3kT} \tag{6}$$

where η is the microviscosity of the sol solution, k is the Boltzmann constant and T is the temperature.

2.2.3.2 Restricted Dynamics in the Presence of Probe-Ludox silica Interactions

The anisotropy decay in R6G:Ludox systems can be fit to a two-component hindered rotor model according to the following equation (7):

$$r(t) = \beta_1 \exp(-t/\phi_1) + \beta_2 \exp(-t/\phi_2) + r_\infty = r_0 f_1 \exp(-t/\phi_1) + r_0 f_2 \exp(-t/\phi_2) + g r_0 \tag{7}$$

where β_1 and β_2 are the pre-exponential terms ($0 \leq \beta \leq r_0$, $\beta_1 + \beta_2 = r_0$) representing the extent to which the probe emission is depolarized by each correlation time; $r_0 = (\beta_1 + \beta_2)$ is the experimental initial anisotropy at $t = 0$; r_∞ is the residual anisotropy due to hindered motion of species with $\phi > 15\tau$; ϕ_1 reflects rapid rotational motions associated with rotation of free probes in solution, ϕ_2 reflects slow rotational motions of the probes bound to small silica nanoparticles, $f_1 = \beta_1 \phi_1/(\beta_1 \phi_1+\beta_2 \phi_2)$ is the fractional fluorescence associated with ϕ_1, and $f_2 = \beta_2 \phi_2/(\beta_1 \phi_1+\beta_2 \phi_2)$, is the fractional fluorescence corresponding to ϕ_2, and $g = r_\infty/r_0$ is the fraction of fluorescence

originating from probe that is rigidly bound to larger particles that rotate more slowly than can be measured with the probe. In cases where the quantum yield does not change upon binding of probe to the silica particle, the fractional fluorescence of each component is directly proportional to the fraction of probe in each environment.

2.2.3.3 TRFA Analysis of Surface Modification of Ludox

Using the anisotropy decay data it is possible to obtain an estimate of the degree of adsorption of the peptide onto the Ludox particles as a function of peptide concentration. Since the emission properties of R6G do not change upon adsorption,[12] it can be assumed that the total fluorescence from the nanosecond and residual anisotropy components ($g + f_2$) corresponds to the fraction of bound dye. The degree of adsorption of peptide (D) can be found from the equation:

$$D = 1 - \frac{(g + f_2)_P}{(g + f_2)_0} \tag{8}$$

where $(g + f_2)_0$ is obtained in the absence of the adsorbate and $(g + f_2)_P$ is obtained in the presence of a given concentration of absorbate.

2.4 REFERENCES

1 . Bernard Valeur. *Molecular Fluorescence: An Introduction: Principles and Applications.* Canada: John Wiley & Sons, 2002

2. Joseph R. Lakowicz. *Principles of Fluorescence Spectroscopy.* New York: Kluwer Academic/Plenum, c1999.

3. D. B. Wetlaufer. *Adv. Protein Chem.* **1962,** 17, 303.

4. www.fki.uu.se/education/MATNAT/LASER/laser/PDF_filer/FA-manual.PDF

5. J. R. Lakowicz, *Principles of Fluorescence spectroscopy* (Klüwer Academic Plenum Publishers, New York, 1999)

6. J. M. Beechem, J. R. Knutson and L. Brand, *Biochem. Soc. Trans.* **1986**, 14, 832.

7. B. Imhof, *Decay Analysis Software Support Manual*, (IBH Consultants Ltd, Glasgow, 1989).

8. D. Tleugabulova, J. Sui, P. W. Ayers and J. D. Brennan, *J. Phys. Chem. B.* **2005**, 109,7850.

9. F. Perrin, Ann. *Phys. Paris.* **1929**, 12, 169.

10. J. R. Lakowicz, *Principles of Fluorescence spectroscopy* (Klüwer Academic Plenum Publishers, New York, 1999).

11. Debye, P. Polar Molecule; Chemical Catalog Co.: New York, 1929

12. Tleugabulova, D.; Duft, A.M.; Brook, M.A.; Brennan, J. D. *Langmuir* **2004**, *20*, 101.

Chapter 3

Evidence for Rigid Binding of Rhodamine 6G to Silica Surfaces in Aqueous Solution based on Fluorescence Anisotropy Decay Analysis

The following chapter was published in the *Journal of Physical Chemistry B* under the citation:

D. Tleugabulova, J. Sui, P. Ayers and J.D. Brennan*. Evidence for Rigid Binding of Rhodamine 6G to Silica Surfaces in Aqueous Solution based on Fluorescence Anisotropy Decay Analysis. *Journal of Physical Chemistry B*, **2005**, *109*, 7850-7858.

This project was a team work involving myself, Dr. Tleugabulova and Dr. Ayers. Dr. Tleugabulova was the primary person involved in reference search and writing for the theory part. Experiments involved in this project were designed and performed by her and myself. Specifically, she did the experiments involving R6G in DGS, Sodium Silicate; I did the experiments involving R6G in Ludox, PAA and PGA. In addition, I also made the particle size distribution of Ludox particles imaged by TEM using software. The figures involved in theoretical analysis of R6G-silica interaction were also made by me. Dr. Ayers provided theoretical analysis of R6G-silica interaction from structural considerations. Dr. Tleugabulova wrote the first draft of the manuscript and Dr. Brennan provided editorial input to generate the final draft of the paper.

Abstract

Strong ionic binding of the cationic probe rhodamine 6G (R6G) to the anionic surface of silica particles in water provides a convenient labeling procedure to study both particle growth kinetics and surface modification by time-resolved fluorescence anisotropy (TRFA). The decays for R6G dispersed in diluted Ludox silica sols usually fit to a sum of picosecond and nanosecond decay components, along with a significant residual anisotropy component. The origin of the nanosecond decay component (ϕ_2) is not fully understood, and has been ascribed to wobbling of the probe on the silica surface, the presence of a subpopulation of small nanoparticles in the Ludox sol, or rapid exchange between free and bound R6G. In order to elucidate the physical meaning of ϕ_2, measurements were performed in various silica-based colloidal systems using different concentrations of silica. We found that the fraction of ϕ_2 was generally higher in Ludox than in aqueous sodium silicate and decreased with increasing silica concentration; ϕ_2 vanished upon gelation of sodium silicate at pH 7 leading to a total loss of R6G depolarization ($r(t) = const$). These results rule out the presence of local R6G wobbling when bound ionically to the colloidal silica and support the rigid sphere model to describe the TRFA decays for R6G-Ludox. This conclusion is entirely supported by steady-state anisotropy data and structural considerations for the R6G molecule and the silica surface.

3.1 Introduction

The use of time-resolved fluorescence anisotropy (TRFA) techniques for measuring the dynamic properties of macromolecules relies upon the assumption that the rotation of the fluorescent probe is a good indicator of the overall rotational diffusion of the probe-macromolecule complex. This is true only in cases when the local probe motion, which is independent of the rotation of the macromolecule, has a minimal contribution to the anisotropy decay.[1,2,3,4,5] The presence of local probe motion and the internal flexibility of macromolecules are the most significant problems,[6,7,8,9,10,11,12,13] which make it difficult and often misleading to assign physical significance to the TRFA decay parameters. Vast experimental work is currently in progress to design fluorescent probes, which bind rigidly to biomolecules.[14,15,16,17] Despite these efforts, the problem of the local probe motion is not completely solved,[18] suggesting that it may be an intrinsic property of the covalent bond.[16]

There has recently been significant interest in using TRFA to probe the growth[19,20,21,22,23,24] and surface modification[25,26] of colloidal silica particles. The rigidity of silica particles removes the problem of internal flexibility found in previous experimental work with biomolecules[6-9] while the ionic labeling of silica with cationic probes seems to overcome the problem of the local probe motion.[23,24] Although this latter aspect has not been rigorously tested, the experimental TRFA decays of ionically labeled silica particles are well described by the rigid spherical rotor model developed by Debye[27] and Perrin,[28] and the rotational correlation time measured by TRFA using long-lifetime fluorescent probes is in excellent agreement with the mean particle radius of silica particles present in the silica sol.[23]

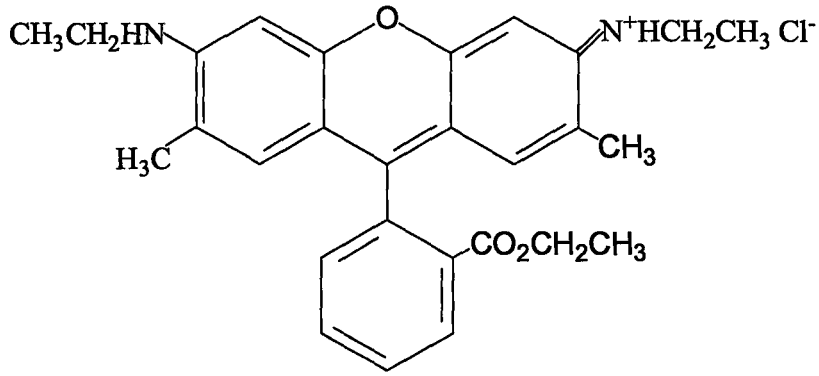

R6G

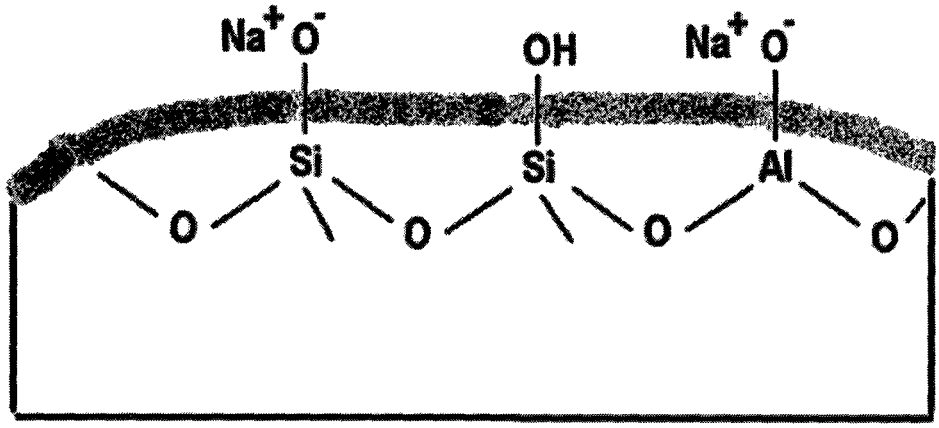

surface of Ludox particle

Figure 3.1: Structures of R6G and Ludox. The thick line denotes the particle surface.

This suggests that the TRFA decay reports on the average diffusional information when applied to a mixture of particles with a normal size distribution.

The most common probe for examination of silica systems by TRFA is rhodamine 6G (R6G, Figure 3.1), since it has well understood single-lifetime photophysics and a high experimental limiting anisotropy ($r_0 = 0.38$).[29] Since its emission properties do not change upon ionic binding to silica particles,[23-25,30] R6G can be used for

monitoring the free and the silica-bound fractions of probe from the same TRFA decay. An issue with the use of short-lifetime probes, such as rhodamine 6G (R6G), for silica labeling is that it restricts the TRFA measurement to the rotational diffusion of particles less than 2.5 nm-radius.[24] The binding of R6G to larger particles, such as Ludox, leads to significant residual anisotropy $r_\infty > 0$ in the TRFA decay. The degree of rotation of such particles on the time scale of the R6G intensity decay is insignificant and addressed as a "non-decaying" component.[25,26] This removes the ability to measure the mean particle radius, since much of the particle motion is hidden due to r_∞. However, the fractional contribution from the non-decaying component can be calculated as $g = r_\infty/r_0$,[23] where r_0 is the limiting anisotropy, and can be used to estimate the degree of silica surface modification.[25,26] Besides the g value, two correlation times in a range 0.2 – 6 ns can be measured with the excited R6G probe.[25,26] The faster correlation time, ϕ_1, of ~ 0.2 ns corresponds to the rotation of free R6G molecules in solution and is therefore attributed to the fraction of free, non-adsorbed R6G molecules in silica sols. The interpretation of the second, slower component (ϕ_2) is less straightforward and has been subjected to different explanations, such as the presence of a subpopulation of small nanoparticles in silica sols and gels,[24,26] the wobbling motion of R6G on the silica surface,[25,26,31] association-dissociation reactions that occur on the timescale of the fluorescence emission of the dye[29] or a fitting artifact caused by the presence of a particle size distribution in the case of Ludox sols.[23] Whether this component arises solely from the overall rotation of the R6G-Ludox particles or experiences some contribution from the local motion of the R6G dipole relative to the silica surface will influence the choice of a physical model for interpretation of the TRFA parameters. With the correct physical model in place, the practical applications of TRFA can be extended

from particle growth kinetics measurements[19-24] and the calculation of the degree of silica surface modification[25,26] to studies of more complex phenomena, such as silica-protein interactions.

In the present paper, we examine the nature of binding of R6G to silica surfaces using experimental TRFA data from several silica systems, including Ludox, sodium silicate (SS) and diglycerylsilane (DGS), and provide supporting data from steady-state anisotropy, transmission electron microscopy and the theoretical modeling of the R6G-silica interaction to develop a physical model for the origin of the ϕ_2 component, which provides new insight into the interpretation of TRFA data for R6G-silica systems.

3.2 Theory

3.2.1 R6G-Ludox as a Mixture of Rotating Spheres

The fundamentals of TRFA analysis are described in detail in the book of Lakowicz.[2] Herein, we provide only specific details of rotational models that apply to the silica systems under study.

In the absence of independent motion of R6G, the time decay of anisotropy *r(t)* for the probe dipole attached to the surface of silica particles can be modeled as isotropic rotation of *k* silica spheres of different sizes

$$r(t) = \sum_{i=1}^{i=k} b_i \exp(-t/\phi_i) + r_\infty = r_0^{\exp} \sum_{i=1}^{i=k} f_i \exp(-t/\phi_i) + g r_0^{\exp} \qquad (1)$$

where b_i $(0 \le b_i \le r_0)$ and ϕ_i, are the pre-exponential constant and rotational correlation time, respectively, corresponding to the rotation of the *i*th particle, $f_i = \dfrac{b_i \phi_i}{\sum_{i=1}^{i=7} b_i \phi_i}$ $(\sum_i f_i = 1,\ 0 \le f_i \le 1)$ is the fractional contribution from ϕ_i to *r(t)*,

$r_0^{exp} = \sum_{i=1}^{i=7} b_i$ is the experimental initial anisotropy at t = 0 and $g = r_\infty / r_0^{exp}$,[23] is the fractional contribution from the non-decaying component. The r_0^{exp} value indicates the anisotropy after internal conversion and vibrational relaxation, prior to probe rotation, and should nearly correspond to steady state anisotropy of R6G in a glassy frozen solvent ($r_0^{exp} = r_0^{R6G} = 0.38$).[30] The reasons for $r_0^{exp} < 0.38$ have previously been discussed.[24]

If the particles are normally distributed around the mean radius R, the experimental decay $r(t)$ is biexponential[23]

$$r(t) = f_1 r_0^{exp} \exp(-t/\phi_1) + f_g r_0^{exp} \exp(-t/\phi_g) \quad (2)$$

where ϕ_1 is the rotational correlation time of free R6G molecule and ϕ_g ($\phi_g > \phi_1$) reflects the global ("g") tumbling of labeled silica spheres and is related to R by the equation

$$\phi_g = \frac{4\pi R^3 \eta}{3kT} \quad (3)$$

where k is the Boltzmann constant, T is the temperature and η the viscosity of the solution.

In Ludox AM-30, the particles are size-distributed around the mean particle radius R = 6 nm.[32] The labeling of Ludox with the long-lived probe CG437 followed by the TRFA measurement and the fitting of $r(t)$ to the equation (2) gives ϕ_g = 375 ns, which corresponds to the mean radius of hydrated particles of 7 nm, as calculated from the equation 3.[23] The global tumbling of Ludox spheres cannot be measured by using R6G for labeling because of restrictions imposed on measurable ϕ values by the duration of the excited state ($0.1\tau < \phi < 15\tau$, where τ is the fluorescence lifetime of the probe). As a result, the labeling with R6G is feasible for measuring mean particle

sizes less than 2.5 nm.[24] In Ludox, the binding of R6G to large particles ($R > 2.5$ nm) leads to significant residual anisotropy, $r_\infty > 0$, and $r(t)$ is described as

$$r(t) = b_1 \exp(-t/\phi_1) + b_2 \exp(-t/\phi_2) + r_\infty = f_1 r_0^{exp} \exp(-t/\phi_1) + f_2 r_0^{exp} \exp(-t/\phi_2) + g r_0^{exp} \quad (4)$$

where $f_1 + f_2 + g = 1$. The global tumbling of Ludox is hidden by r_∞ ("non-decaying" component) and contributes to $r(t)$ with $g = r_\infty/r_0$.[23] In this equation, ϕ_1, b_1 and f_1 account for a possible presence of free R6G molecules in solution, whereas ϕ_2, b_2 and f_2 remain to be attributed to a meaningful motional mode of R6G in Ludox. Noteworthy in this situation is the fact that the upper part of the normal distribution of particles is "hidden" in the non-decaying component, and thus ϕ_2 reflects only the lower part of the distribution, and thus does not provide the average rotational motion of the overall distribution, but only the average of the rotational motions of the lower part of the distribution.

For a rigid sphere,[27,28] the originally polarized emission decays monoexponentially and the time-averaged value of $r(t)$, denoted as the steady-state anisotropy r, is given by the Perrin equation[28]

$$\frac{1}{r} = \frac{1}{r_0}(1 + \frac{3\tau}{\phi}) \quad (5)$$

where τ is the emission lifetime.

For a mixture of isotropic spheres of different sizes labeled with the same probe with emission lifetime, τ, Weber[33] introduced a relationship between the reduced measure of fluorescence polarization and the spectrum of relaxation processes with rotational correlation times ϕ_i

$$\frac{1/P + 1/3}{1/P_0 + 1/3} = \frac{r_0}{r} = \frac{1}{\sum_i [f_i/(1 + 3\tau/\phi_i)]} \quad (6)$$

where P is the degree of fluorescence polarization and P_0 is the degree of fluorescence polarization for a completely immobile fluorophore determined by its electronic structure. Assuming that only ϕ_1, ϕ_2 and g (equation 4) can be accurately extracted from the anisotropy decay of R6G-Ludox, the equation (6) can be re-written as:

$$\frac{r}{r_0^{exp}} = \frac{1}{f_1/(1+3\tau/\phi_1) + f_2/(1+3\tau/\phi_2) + g/(1+3\tau/\phi_3)} \tag{7}$$

Rearranging, and noting that $3\tau/\phi_3 \approx 0$

$$r = r_0^{exp}(f/(1+3\tau/\phi_1) + (1-f-g)/(1+3\tau/\phi_2) + g) \tag{8}$$

This equation is valid only if ϕ_1, ϕ_2 and g correspond to independent and isotropic rotations of the rigid spheres.

3.2.2 Local Probe Motion

The physical model of the mixture of isotropic spheres, presented above, assumes the absence of local probe motion, which is independent on the global rotation taken by the Ludox particle. According to this model, ϕ_2 would be attributed to isotropic motion of small silica spheres, which rotate with correlation times on the scale of the intensity decay of R6G. However, if R6G undergoes free rotational diffusion within a cone of semiangle θ, ϕ_2 would be attributed to this wobbling motion. According to the wobble-in-cone model, [34] the order parameter S, which in our case is equal to the g value from equation 4, is related to θ_0

$$S = g = \frac{1}{2}\cos\theta_0(1+\cos\theta_0) \tag{9}$$

According to equation (9), $g < 1$ in the presence of local probe motion and thus the condition $g = 1$ ($\theta_0 = 0°$) would rule out the local wobbling of the probe. In R6G-silica systems, the fraction f_1 corresponding to the fast component ϕ_1 is too small

($f_1 \leq 0.01$) to reduce the order parameter significantly ($1\text{-}g = f_1 + f_2$) and thus $g < 1$ is mostly due to the presence of f_2.[25,26,31] Thus, in cases where $f_1 = f_2 = 0$, $g = 1$ and there can be no local probe motion.

3.3 Experimental Section

3.3.1 Chemicals

Rhodamine 6G (R6G), poly(acrylic acid) (sodium salt) of $M_w \sim 78\ 400$ and poly-L-glutamic acid of $M_w \sim 17\ 000$ were purchased from Sigma (St. Louis, MO). Ludox AM-30, (average particle radius of 6 nm, specific surface area of 220 $m^2.g^{-1}$)[32] was obtained from DuPont. Sodium silicate solution (27 wt % SiO_2, 14 wt % NaOH) and Dowex 50WX8-100 ion-exchange resin of analytical grade were purchased from Aldrich (Milwaukee, WI). Diglycerylsilane (DGS) was prepared from TMOS as described elsewhere.[35] All water was distilled and deionized using a Milli-Q Synthesis A10 water purification system. All other reagents were used without further purification.

3.3.2 Procedures

All samples were made immediately before the analysis. Ludox samples containing 0.75-3 wt % SiO_2 were prepared by diluting Ludox (AM-30; 30 wt % SiO_2; nominal particle radius $\geq$ 6 nm[32]) in water. DGS sols containing 0.25 wt % SiO_2 were prepared by dissolving 0.21 g of finely ground DGS powder in 20 ml of borate buffer (20 mM, pH 9.2) that was previously cooled to 4 °C. After ~ 1 min of strong vortexing or sonication, the DGS suspension was filtered through a 0.45 μm-membrane filter and the filtrate was doped with R6G to a final concentration of 1μM. The sample was immediately used for steady state and time-resolved anisotropy measurements, which were repeated at different time intervals. Sodium

silicate stock solution (6.4 wt % SiO_2) was prepared by acidification of sodium silicate via reaction with Dowex resin.[36] Sodium silicate samples containing 0.75-3.0 wt % SiO_2 were prepared by diluting the sodium silicate stock solution in 5 mM Tris-HCL, pH 9.2. After mixing, the pH of sodium silicate sols was 7.2. All samples were filtered through a 0.45 μm Acrodisc filter and R6G (1 μM) was added.

Steady-state fluorescence anisotropy measurements were performed at 25°C using a SLM 8100 spectrofluorimeter (Spectronic Instruments, Rochester, NY) as described elsewhere[37] using λ_{ex} = 495 nm, λ_{em} = 551 nm.

Time-resolved fluorescence intensity and anisotropy decays were collected in the time domain mode using an IBH 5000U time-correlated single photon counting fluorimeter (Edinburgh, UK). The measurements were done using a 495-nm NanoLED™ source run at 1 MHz and an IBH model TBX-04 photon counting PMT detector. The vertically (I_{VV}) and horizontally (I_{VH}) polarized emission components were collected by exciting samples with vertically polarized light while orienting the emission polarizer (Polaroid HNPNB dichroic film) in either a vertical or horizontal direction. Excitation and emission bands were selected with a 500-nm short-pass interference filter (Andover Corporation, AM-49672) and a 515-nm long-pass filter (Andover Corporation, AM-46370). Typically, 1 x 10^4 counts were collected into the peak channel when the emission polarizer was vertically oriented. The decay histograms were collected over 4096 channels at 22 ps per channel. The horizontal emission decay profile $I_{VH}(t)$ was generated over the same time interval that was used to generate the vertical emission decay profile $I_{VV}(t)$. Samples were held at 25 °C during the measurements. To minimize convolution artifacts, the instrument response profiles were recorded by removing the emission filter and monitoring light scatter from a suspension of Ludox particles in the absence of R6G. The data analysis

software corrected the wavelength-dependent temporal dispersion of the photoelectrons by the photomultiplier. The polarization bias (G) of the detection instrumentation was determined by measuring the intensity profiles while the samples were excited with horizontally polarized light and the emission was monitored with a polarizer oriented in the vertical and horizontal directions ($G = 0.65$).

The anisotropy decays were analyzed using the IBH DAS analysis software package, which involves the formation of two related experimental decay curves, $S(t)$ (the "sum" function) and $D(t)$ (the "difference" function)

$$S(t) = I_{VV}(t) + 2GI_{VH}(t) \tag{10}$$

$$D(t) = I_{VV}(t) - GI_{VH}(t) \tag{11}$$

and the experimental anisotropy function is defined as

$$r(t) = \frac{D(t)}{S(t)} = \frac{I_{VV}(t) - GI_{VH}(t)}{I_{VV}(t) + 2GI_{VH}(t)} \tag{12}$$

The $r(t)$ decay curve (equation 11) is then analyzed by the reconvolution fitting program for the biexponential hindered rotor model (equation 3) using nonlinear least-squares regression.[38] Attempts were also made to fit the anisotropy decay data to other models, including distributed rotational correlation time models, using Globals WE. However, it was not possible to obtain adequate fits using any of the distribution models provided by Global WE, likely because the use of R6G resulted in sampling of a non-symmetric distribution of motions, since slower motions associated with large particles is not detected by this probe. Therefore, in all cases the TRFA data was fit to the two-component hindered rotor model provided in the IBH software.

3.4 Results and Discussion

3.4.1 TRFA of R6G in aqueous silica sols

In the present work, we studied three aqueous colloidal silica systems: the diglycerylsilane (DGS) sol (0.25 wt % SiO_2) composed of stable primary silica nanoparticles (R = 1.7 nm),[24] the sodium silicate (SS) sol, which undergoes continuous polymerization in water[39] and the Ludox sol composed of stable secondary silica particles (R = 6-7 nm).[32] For each of these systems labeled ionically with R6G, the experimental $r(t)$ data are fitted to the equation (4), in which ϕ_1 and f_1 are attributed to the correlation time and the fraction, respectively, of free R6G molecules present in the silica sol, ϕ_2 and f_2 to the mean correlation time and the fraction, respectively, of silica particles, which rotate on the time scale of the R6G intensity decay, and g, which corresponds to the fraction of larger particles, whose correlation times are significantly larger than the R6G lifetime. We show how the fitting to equation (4) leads to the different equations, which reflect the *in situ* colloidal state of the system under study.

The TRFA decay of R6G-DGS is shown in Figure 3.2, and the fits to the decay are provided in Table 3.1. For R6G-DGS, the fit of $r(t)$ to the equation (4) leads to $g \approx 0$ (Table 3.1). This suggests the absence of large secondary particles and inter-particle aggregates in the DGS sol, as is indeed the case, as shown by AFM analysis.[24] Hence, based on the fitted results, the equation (4) can be re-written as

$$r(t) = f_1 r_0^{exp} \exp(-t/\phi_1) + (1-f_1) r_0^{exp} \exp(-t/\phi_2) \qquad (13)$$

As shown in Table 3.1, the main contribution to $r(t)$ comes from the ϕ_2 component. The value of 4.78 ± 0.02 ns measured 30 min after DGS dissolution corresponds to the mean particle radius of 1.73 ± 0.05 nm,[24] according to equation 3. At longer time

intervals, the increase in ϕ_2 is due to further particle growth until a radius of 2.27 ± 0.05 nm is reached after 96 h of aging.

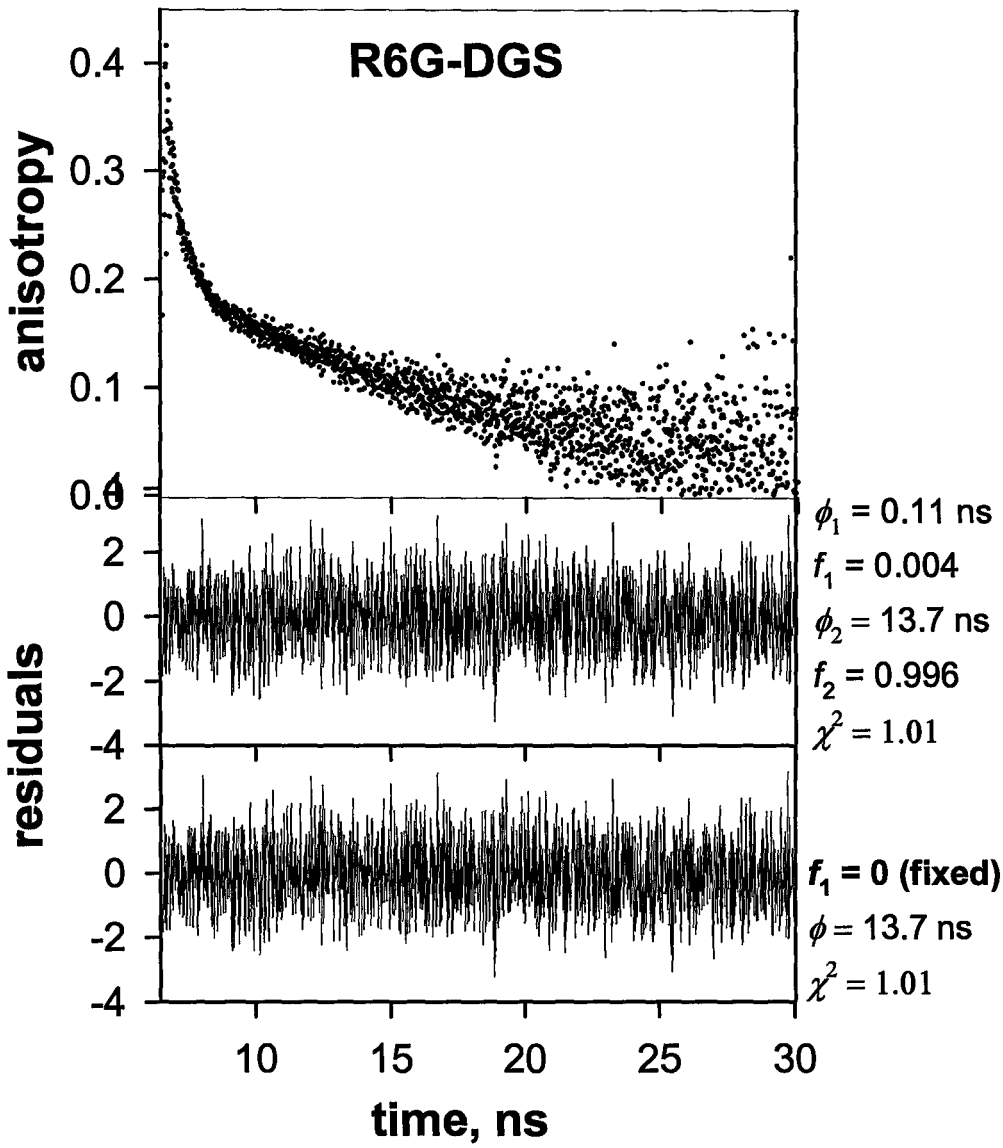

Figure 3.2: TRFA decay of R6G-DGS in 20 mM borate buffer, pH 9.2. SiO_2, 0.35 wt %; R6G, 1 μM. The upper panel shows the experimental *r(t)* decay curve generated by using equation (12). The middle panel shows the distribution of weighted residuals obtained by the fitting *r(t)* to equation (4). The lower panel shows the distribution of

weighted residuals obtained by the forced fitting to the equation (14) (f_1 fixed to 0, g = 0), indicating that in this system there is essentially no free rotation of R6G.

At a higher DGS concentration (0.35 wt % SiO_2), the fit of the experimental *r(t)* data to equation (4) gives $g \approx 0$ and $f_1 < 0.01$ (Figure 3.2). Hence, most R6G molecules are bound to the silica particles and the decay of r(t) is essentially monoexponential:

$$r(t) = r_0^{exp} \exp(-t/\phi) \qquad (14)$$

Figure 3.3 shows the TRFA decay for the R6G-SS system. For R6G-SS (Table 3.1), the fit to equation (4) leads to a significant r_∞ value and the absence of correlation times on the picosecond scale ($f_1 = 0$). This is in good agreement with the fact that the SS sol is composed of polymerized silica particles[40] and R6G is thus adsorbed to the large silica structures. Since these structures are not expected to reorient on the time scale of the excited state of R6G, the high r_∞ value is well justified. Based on the results of the fit (Table 3.1), equation (4) can be re-written as

$$r(t) = (1-g)r_0 \exp(-t/\phi_2) + gr_0 \qquad (15)$$

The absence of ϕ_1 indicates that all R6G molecules are adsorbed to the silica. In this system, ϕ_2 was previously attributed to rotation of single silica nanoparticles entrapped into the pores of the polymerized silica network, whereas the non- decaying component was attributed to the fraction of R6G molecules that were immobilized on the surface of silica walls.[31] As shown in Table 3.1, the fraction f_2 (f_2 = 1-g) decreases with increasing the silica concentration in the sol. This decrease in f_2 occurs under experimental conditions (SiO_2 > 1.5 wt %; pH = 7.2) that promote fast silica particle growth and polymerization,[31] and for the gelled SS the R6G decay becomes time-independent $r(t) = r_0^{exp}$ (Table 3.1).

Table 3.1: TRFA decay parameters for R6G-DGS (0.25 wt % SiO_2), R6G-Ludox and R6G-SS[a].

Sample	Condition	τ, ns	ϕ_1, ns	ϕ_2, ns	r_0^{exp}	r_∞	χ_R^2	g	f_1	f_2
R6G-DGS	30 min[b]	3.95 ± 0.01	0.17 ± 0.02	4.78 ± 0.02	0.366	0.001	1.01	0.003	0.156	0.841
	1 h	3.95 ± 0.01	0.13 ± 0.03	5.32 ± 0.02	0.361	0.001	0.99	0.003	0.021	0.977
	6 h	3.95 ± 0.01	0.16 ± 0.02	6.40 ± 0.02	0.358	0.001	1.00	0.003	0.012	0.985
	48 h	3.95 ± 0.01	0.17 ± 0.01	9.50 ± 0.02	0.367	0.003	0.98	0.009	0.010	0.981
	72 h	3.95 ± 0.01	0.29 ± 0.07	11.50 ± 0.02	0.375	0.001	0.98	0.003	0.009	0.988
	96 h	3.95 ± 0.01	0.17 ± 0.03	11.20 ± 0.02	0.358	0.001	1.03	0.003	0.011	0.986
R6G-SS	0.3 wt % SiO_2 (sol)	3.95 ± 0.01	-	3 ± 1	0.347	0.329	0.99	0.919	0	0.081
	0.7 wt % SiO_2 (sol)	3.94 ± 0.01	-	2.7 ± 0.3	0.360	0.332	0.98	0.923	0	0.077
	1.5 wt % SiO_2 (sol)	3.97 ± 0.01	-	4 ± 1	0.355	0.334	0.98	0.940	0	0.060
	3.0 wt % SiO_2 (gel)	3.96 ± 0.01	-	-	0.350	0.348	1.01	>0.998	0	< 0.002
R6G-Ludox	0.3 wt % SiO_2	3.92 ± 0.01	0.4 ± 0.1	4 ± 1	0.358	0.286	1.01	0.798	0.019	0.183
	0.7 wt % SiO_2	3.92 ± 0.01	0.3 ± 0.2	3.0 ± 0.4	0.350	0.300	1.01	0.856	0.008	0.136
	1.5 wt % SiO_2	3.93 ± 0.01	-	3.0 ± 0.4	0.360	0.328	0.98	0.915	0	0.085
	3.0 wt % SiO_2	3.92 ± 0.01	-	2.5 ± 0.3	0.361	0.332	0.99	0.921	0	0.079
	6.0 wt % SiO2	3.94± 0.01	-	1.9 ± 0.2	0.350	0.312	0.99	0.891	0	0.011

[a] R6G, 1 μM. Solvent, 20 mM borate buffer, pH 9.2 (R6G-DGS), distilled water (R6G-Ludox) and 5 mM Tris-HCl, pH 9.2 (R6G-SS). Excitation, 495 nm; emission, 551 nm.
[b]Different time periods after DGS dissolution in 20 mM borate buffer, pH 9.2.

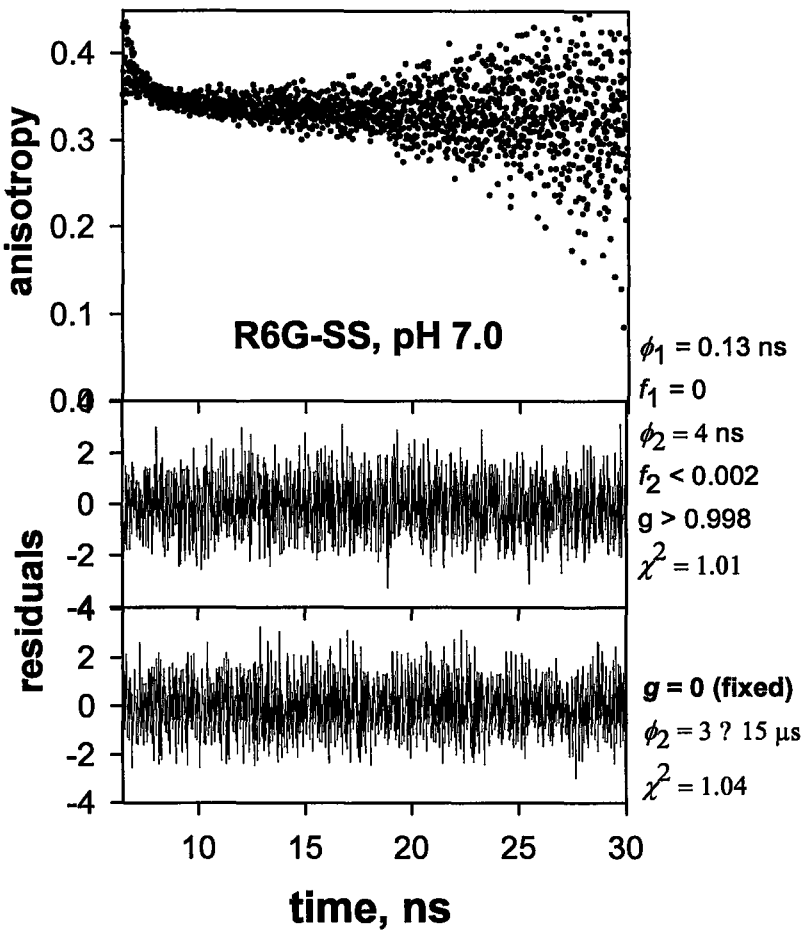

Figure 3.3: TRFA decay of R6G-SS in 5 mM Tris-HCl, pH 9.2. SiO_2, 3 wt %; R6G, 1 µM. The upper panel shows the experimental *r(t)* decay curve generated by using equation (12). The middle panel shows the distributions of weighted residuals obtained by fitting *r(t)* to the equation (4). The lower panel shows the distribution of weighted residuals obtained by the forced fit of the data to equation (14) (f_1 = 0, r_∞ forced to 0). The recovered correlation time of 3 ± 15 µs is statistically insignificant, and is well outside of the range of correlation times measurable using R6G.

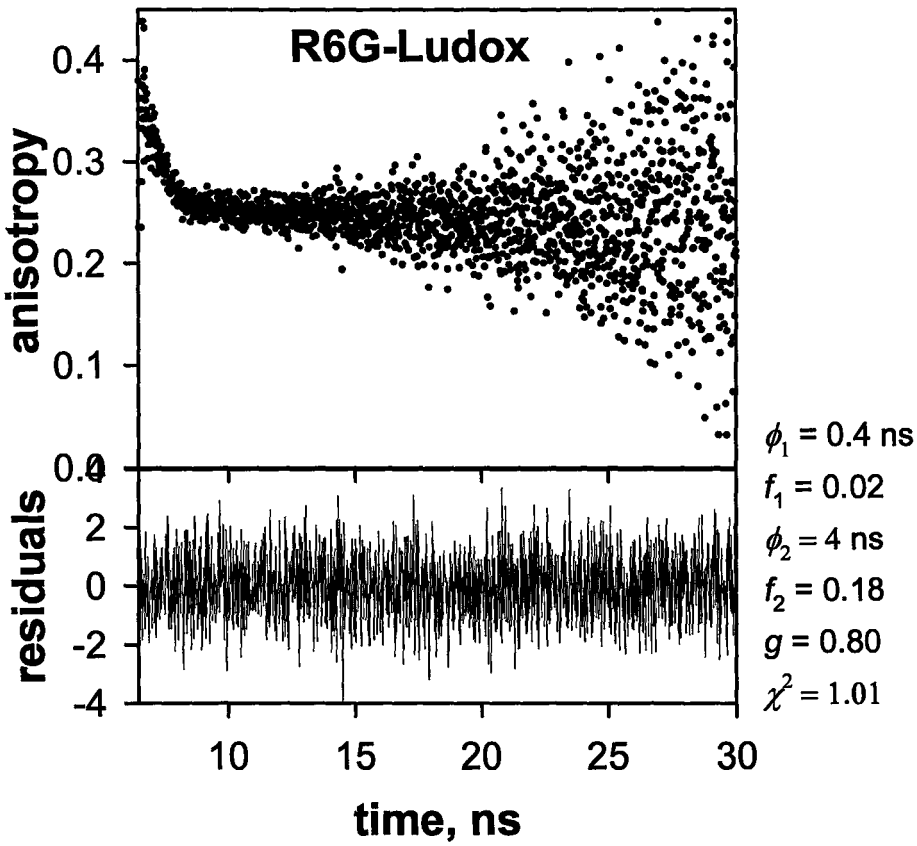

Figure 3.4: TRFA decay of R6G-Ludox in water. SiO_2, 0.3 wt %; R6G, 1 μM. The upper panel shows the experimental *r(t)* decay curve generated by using equation (12). The lower panel shows the distribution of weighted residuals obtained by fitting *r(t)* to the equation (4). All parameters were allowed to float freely during the fitting.

This result indicates that when the amount of free silica particles is decreased due to the polymerization process, the condition $g = 1$ (equation 8) is reached. Importantly, this condition rules out the possibility of ϕ_2 being due to local motion, or "wobbling" of the probe on the silica surface. Figure 3.4 shows a typical TRFA decay for the R6G-Ludox system, along with residuals obtained upon fitting of the decay to Equation (4). For R6G-Ludox (0.3-0.7 wt % SiO_2), the fit to the equation (4) reveals the presence of all three components, ϕ_1, ϕ_2 and g. However, the ϕ_1 component is lost

with increasing silica concentration (Table 3.1) and equation (4) takes the form of equation (15). We relate this effect to the increased uptake of free R6G molecules by silica particles with increasing silica concentration. The non-decaying component is the major contributor to the decay, which is in good agreement with the mean particle radius of 7 nm in water.[23]

The main difference between the decay parameters for R6G in Ludox and in the gelled SS, under the same silica concentration, is the absence of ϕ_2 in SS samples (Table 3.1). The surface area is expected to be larger in the SS gel[31] than in the suspension of non-porous Ludox particles. In SS the probe is adsorbed to the walls of the silica network whereas in Ludox it is bound to the surface of discrete particles. If ϕ_2 reflects the local probe motion on the silica surface, it should be present in the decay independent of the physical state or concentration of the silica, provided that in the concentration range 0.3-3 wt % SiO_2 the sol microviscosity is not significantly altered.[26] In this case, the presence of ϕ_2 would result in $g \neq 0$ (equation 9) and the f_2 value would be constant or higher at increased particle concentrations. Since our results are in disagreement with these expectations, we must attribute ϕ_2 to isotropic rotation of small nanoparticles present in Ludox. According to this conclusion, ϕ_2 and f_2 depend on the fraction of small particles in the silica sol. Particle polymerization would clearly decrease f_2, which is indeed the case for R6G in the gelled SS samples (Table 3.1).

To better support the interpretation of ϕ_2 being related to small particles, we sought to provide direct evidence for the presence of small silica particles in the Ludox sol. Toward this end, we performed transmission electron microscopy (TEM) on diluted Ludox sols that were cast onto a suitable surface. Dilute sols were utilized to minimize the possibility of aggregation of small particles with radii less

than 2 nm during sample preparation. It should also be noted that such particles are near the detection limit of TEM as an imaging method. Nevertheless, we were able to detect particles of ~ 2 nm radius, as shown in Figure 3.5a.

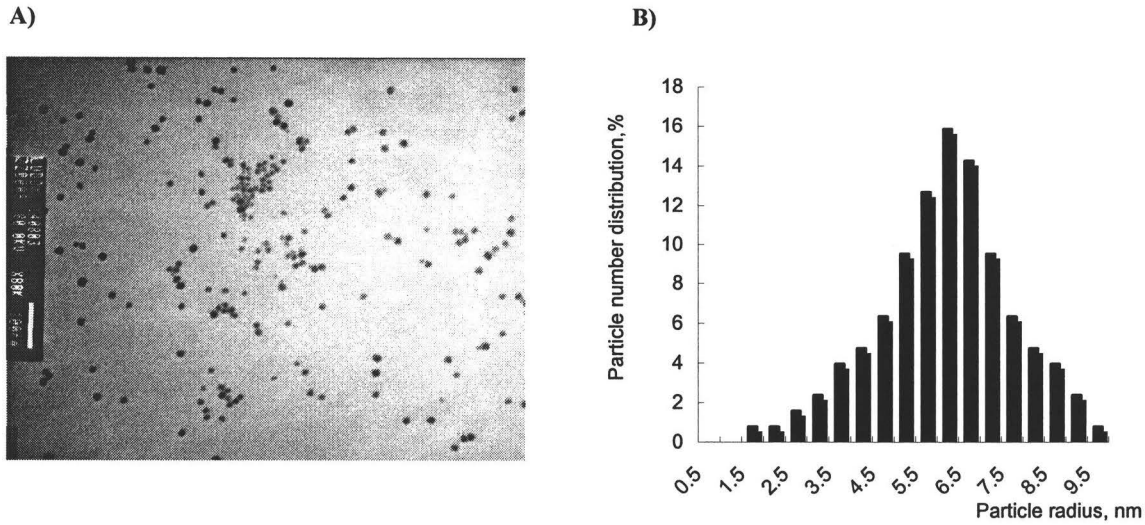

Figure 3.5: A) Transmission electron microscopy image of Ludox particles.

B) Particle size distribution of Ludox particles imaged by TEM.

These small particles were often seen as single particles, attached to the surface of larger particles or forming particle aggregates. As shown in Figure 3.5b, the Ludox sample was actually composed of a range of particles sizes, covering the region from 1.5 to 9.5 nm radius. The polydispersity of Ludox particles has been previously corroborated by small-angle X-ray scattering techniques,[40,41,42,43] and independent studies have reported the presence of small particles (radius, < 5 nm).[42,43] Hence, it is likely that the fit to the TRFA measurement collapses the normal particle distribution into two categories; particles that are too large to be observed by TRFA ($R > 2.5$ nm) and those that are sufficiently small to be observable by TRFA ($R < 2.5$ nm). Since the distribution of observable particles is intrinsically non-Gaussian, it is

understandable why the fits of R6G-Ludox to distributed correlation times did not give any statistical improvement over the fits to the equation (4) (data not shown).

3.4.2 Ludox-R6G system as a model of rigid spheres

The use of Ludox-R6G as the model of the rigid sphere is based on the following assumptions: 1) Ludox particles are uniform, rigid and stable, with no internal surface and no detectable crystallinity; 2) in diluted Ludox sols (≤ 3 wt % SiO_2 in water), silica particles rotate independently on each other and the effects of inter-particle collisions and repulsions on the rotation are negligible; 3) when dispersed in the diluted Ludox sol, R6G randomly binds to particles of different size; 4) at the probe/particle ratio used, one of every ten particles is labeled with one R6G molecule; 5) the adsorption of R6G does not modify particle rotation. In the absence of local probe motion, there is a straightforward relationship (equations 5-8) between the steady-state anisotropy value r and the TRFA parameters. Hence, for R6G-Ludox, we expect a good agreement between experimental r values and those calculated from TRFA data using the equation (8). For this comparison, we used TRFA data measured for R6G-Ludox containing different additives, such as diallyldimethylammonium chloride (DADMAC), N-(3-triethoxysilylpropyl) gluconamide (GLTES), N-(3-triethoxysilylpropyl)maltonamide (MLTES) and 3-aminopropyltriethoxysilane (APTES).[26] Depending on their affinity towards the silica surface, these compounds bind to varying degrees, blocking the sites potentially available for R6G adsorption. The competition for the silica surface causes drastic changes in the f_1 and g, but not in ϕ_1 and ϕ_2. These changes in f_1 and g are thus primarily responsible for the decrease in the steady-state anisotropy value due to the modification process (Table 3.2). As a result, there was a close agreement between experimental r values and those

calculated from the TRFA data using equation (7), which supports our assumption that the Ludox-R6G system can be modeled as a collection of rigid spheres. The ϕ_2 component thus reflects the rotation of silica nanoparticles of ~ 1.2-1.5 nm in radius, which are rigidly labeled with R6G. There was also the close agreement between experimental *r* values and those calculated from the TRFA data for R6G-DGS (Table 3.2), which represents a different colloidal system than Ludox and is described by a different *r(t)* equation (equation 13). This justifies the use of TRFA for the calculation of the mean particle radius of DGS.[24]

The model of the rigid sphere also requires the rigidity of the labeled host. If R6G is bound to a flexible macromolecule, instead of the Ludox particle, the treatment of such a system as a rigid sphere would be inadequate and thus the Weber equation would not be applicable. In order to prove this, we added R6G to aqueous solutions of random-coil anionic polymers, such as polyacrylic acid and polyglutamic acid, and measured TRFA decays for the R6G-polymer complexes. The ionic binding of R6G to surfactants and random-coil polyelectrolytes has been reviewed in several recent reports.[44,45,46] The TRFA decay for R6G-polyglutamic acid was monoexponential (Table 3.2), showing only the ϕ_1 component. Probably, the binding through a relatively long alkyl side chain does not significantly restrict the mobility of the R6G dipole. The TRFA decay of R6G-polyacrylic acid was biexponential with ϕ_2 as a major component. The low *g* values probably indicate the absence of rigidity in the polymer chain. As shown in Table 3.2, there is poor agreement between

Table 3.2: Fitting parameters resulting from analysis of TRFA decays for R6G in aqueous solutions of DGS (0.25 wt % SiO_2), Ludox (3 wt % SiO_2), polyacrylic acid (PAA) and polyglutamic acid (PGA)[a].

Sample	conditions	ϕ_1, *ns*	ϕ_2, *ns*	f_1	f_2	g	r_{calc}	r_{exp}	r_{calc}/r_{exp}
R6G-Ludox	H_2O	0.29	2.88	0.015	0.137	0.848	0.332	0.336	0.99
	0.07 wt % DADMAC	0.18	2.54	0.111	0.300	0.589	0.244	0.240	1.02
	0.15 wt % DADMAC	0.19	2.11	0.395	0.346	0.259	0.120	0.113	1.06
	0.30 wt % DADMAC	0.19	2.01	0.550	0.310	0.140	0.073	0.066	1.11
	2.5 wt % GLTES	0.15	2.31	0.224	0.289	0.487	0.204	0.200	1.02
	2.0 wt % MLTES	0.16	2.10	0.164	0.292	0.544	0.224	0.200	1.12
	0.005 wt % APTES	0.20	2.20	0.725	0.093	0.182	0.079	0.074	1.07
	0.01 wt % APTES	0.17	1.70	0.804	0.110	0.086	0.042	0.040	1.05
R6G-DGS	30 min[b]	0.17	4.61	0.156	0.841	0.003	0.085	0.085	1.00
	1 h	0.13	5.32	0.021	0.977	0.003	0.116	0.115	0.99
	6 h	0.16	6.40	0.012	0.985	0.003	0.135	0.138	1.02
	48 h	0.17	9.50	0.010	0.981	0.009	0.174	0.176	1.01
	72 h	0.29	11.50	0.009	0.988	0.003	0.189	0.185	0.98
	96 h	0.17	11.20	0.011	0.986	0.003	0.189	0.187	0.99
R6G-PAA	0.02 wt %	0.56	3.38	0.193	0.742	0.065	0.090	0.042	2.14
	0.12 wt %	0.83	4.64	0.084	0.848	0.068	0.118	0.090	1.31
R6G-PGA	0.02 wt %	0.19	-	0.974	0	0.026	0.016	0.025	0.64
	0.12 wt %	0.23	-	0.964	0	0.036	0.021	0.026	0.80

[a]R6G concentration, 1 μM. Excitation, 495 nm; emission, 551 nm. TRFA parameters: r_0^{exp}, 0.35-0.38; ϕ_1, ± 0.01 ns; ϕ_2, ± 0.05 ns; χ_R^2, 0.96-1.05. r_{calc} is calculated using τ = 4 ns and equation (8). r_{exp} (± 0.001) is measured experimentally using continuous excitation at 495 nm. [b]Different time periods after DGS dissolution in 20 mM borate buffer, pH 9.2.

experimental r values and those calculated from the TRFA parameters, which is consistent with the intrinsically dynamic polymers being improperly described by the model of rigid spheres. Hence, the ability to model silica particles as rigid spheres provides strong evidence that such particles show no internal motion.

3.4.3 Theoretical Analysis of R6G-Silica Interaction from Structural Considerations

The two physical models for the interpretation of TRFA decays assume two different binding modes of the R6G molecule to the silica particle. The wobbling model[34] (equation 9) assumes that the probe dipole is not completely fixed relative to the particle, but rotates with some degree of independence about a bond linking it to the particle. Such partial rotation is to be expected for single-point covalent and ionic conjugates. The model of the rigid sphere is based on the assumption that the R6G dipole maintains constant orientation relative to the particle axes. This binding mode is expected for probe-particle complexes formed by multiple bonds and several delocalized forces.

From structural considerations, the R6G molecule (Figure 3.1) has one esterified phenylcarboxyl group and two basic monoethylamino groups, which are formally identical and capable of protonating when they interact with a protic solvent. Hence, in the bulk aqueous phase, the cationic form $(R6G)^+$ is dominant. The phenylcarboxyl and xanthene rings intersect each other with an angle near 90°.[47,48] The main adsorption band of R6G in the visible region corresponds to a transition moment largely parallel to the long axis of the xanthene ring due to a $\pi \rightarrow \pi^*$ transition. Calculation of the atom electron density of R6G using the MOPAC program with a BFGS gradient minimization routine and the MNDO and AM1 Hamiltonians shows

that the maximum negative charges in the R6G molecule are on N and O atoms of the ethylamine and COOEt groups, respectively.[49] Hence, R6G interacts with other molecules via either N atoms of the ethylamine group or O atoms of the COOEt group. Assuming that, when using excitation in visible region, the direction of the transition dipole moment of R6G does not change, it is evident that by using TRFA, we are actually probing the interaction between the xanthene moiety of R6G and the silica surface.

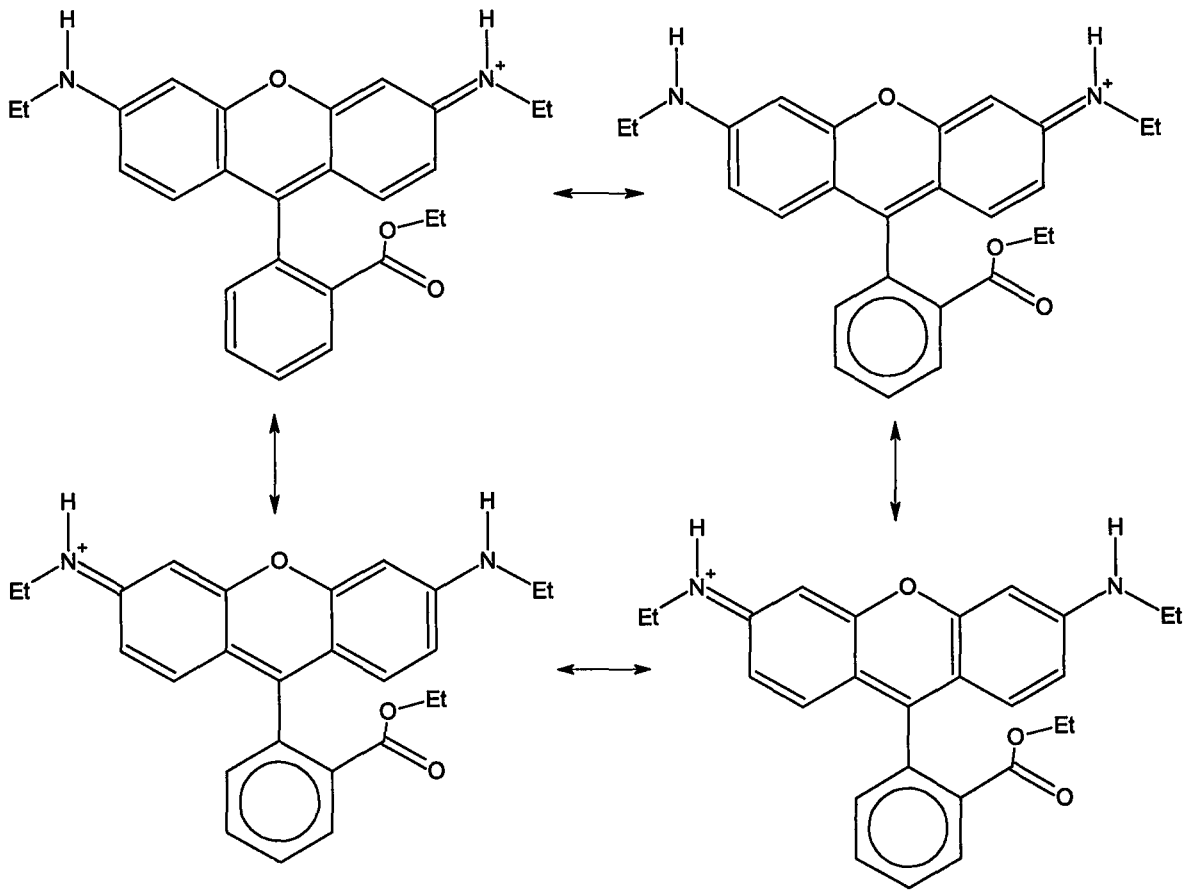

Figure 3.6: Resonance structures of R6G.

In both resonance structures of R6G (Figure 3.6), the pK_a of the amine group would resemble that of ammonia (pK_a = 36) while in the other two one would predict

it to be somewhere between that of pyrrole (pK_a = 0.6) and aniline (pK_a = 4.6). In crystal structures of R6G,[50,51] however, both nitrogens have substantial sp_2 character, with the nitrogen lone pair partly delocalized onto the xanthene rings, leaving nitrogen with a partial positive charge. Consequently, the amine/imine hydrogen atoms should be more positively charged than those in most amines, and thus ideally suited for hydrogen bonding.

Possible chemical forms having a potentially higher fluorescence quantum yield than $(R6G)^+$ are a fluorescent dimer[52] and a contact ion-pair of the form $(R6G)^+$-A^-.[53] At the concentration of R6G used in the present study (1 μM), the formation of dimers is negligible in bulk solution.[54] From the adsorption spectra (data not shown), we can infer that the relative intensity of the 498-527 nm bands, corresponding to the dimer adsorption, does not change appreciably in the presence of Ludox. This observation rules out any significant increase in aggregation of the dye molecules due to formation of dimers or higher aggregates on the silica surface.

The structures of R6G and Ludox (Figure 3.1) can be used to rationalize the experimentally observed rigidity of the R6G-Ludox complex. If the positive charge on the imine group is stabilized by the negatively charged silica surface, the symmetry is broken and as a result, the structure in Figure 3.1 becomes a more accurate representation than its resonance hybrids shown in Figure 3.6. To support this hypothesis, it is worth noting that the symmetry of the crystal structure of R6G is broken due to hydrogen bonding with the co-crystallized water molecules.[50,51] Examination of the structure of R6G reveals five groups that are available for hydrogen bonding: the two amine/imine groups, the central oxygen, and the ester. If the R6G molecule adsorbs with the xanthene moiety perpendicular to the Ludox surface, the amine/imine hydrogens and the central oxygen atom can all participate in

the hydrogen bonding network of the Ludox particle and/or its solvation shell. Unlike ionic bonds, hydrogen bonds are highly directional, and so these interactions will tend to constrain R6G to a rigid geometry relative to the Ludox surface. Nonetheless, the R6G molecule might still "rock" or "wobble" back and forth, rotating about the axis that contains the two amine/imine groups and the central oxygen atom, although the amplitude of the motion will be constrained by the directionality of the interactions tethering these atoms to the surface. For this reason, it seems favorable to tip the xanthene ring system at an angle to the surface and bring the ester moiety towards the Ludox particle, so that the ester can join the hydrogen-bonding network solvating the Ludox particle (Figure 3.7). If just two of the other three groups formed hydrogen bonds to the surface, then this would totally immobilize the R6G molecule, explaining the experimentally observed results.

The crystal structures seem to indicate that one of the ethylamine groups has more imine character than the other.[50,51] It is useful to ensure, then, that the essential details of the discussion of the previous paragraph would not change even in the extreme case where R6G resembles the structure in Figure 3.1, rather than a resonance hybrid thereof. Clearly the amine, central oxygen, and ester are still capable of forming hydrogen bonds to the Ludox surface. The imine can also form hydrogen bonds (through the hydrogen), but the nitrogen atom can also interact directly with water in the solvation shell or, more favorably, the OH or O^- termini of the Ludox surface. Interactions between the imine nitrogen and O^- termini will be especially strong. These interactions may lead to a partial charge transfer from O^- to N^+; if so, one expects the interaction between the imine nitrogen and the surface to be partly ionic and partly covalent.[50,51] Combining this analysis with that of the resonance structures of R6G, it seems that whatever the status of the amine/imine

resonance is (and different surface geometries probably favor different structures), there are interactions of sufficient strength, number, and directionality to ensure that motion of R6G is rigidly coupled to that of Ludox particles.

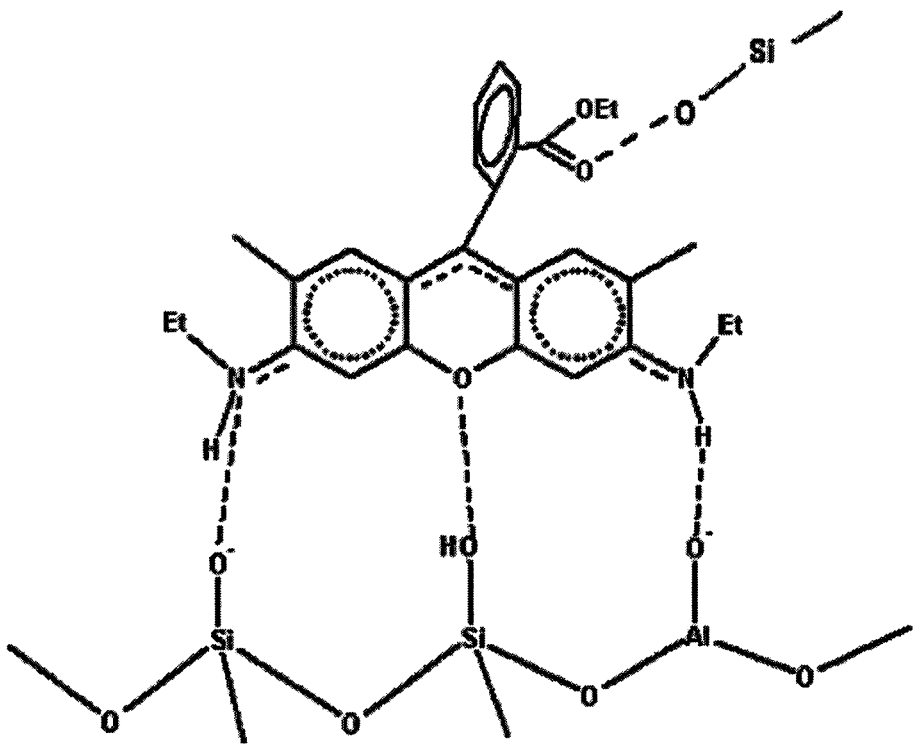

Figure 3.7: Graphical representation of interactions involved in rigid binding of R6G to the surface of Ludox. Note: The dashed lines indicate hydrogen bonds or ionic bonds to the surface.

3.5 Conclusions

The recent applications of TRFA for the analysis of silica colloids include the nanoparticle metrology approach developed by Geddes[19,20,21,22,23] and the analysis of silica surface modifications developed in our group. Both approaches are based on the assumption that the orientation of the probe dipole relative to the axes of the silica

nanoparticle is constant during the measurement. However, this assumption has not been rigorously inspected. The contribution of wobbling motion of R6G on the silica surface or exchange equilibria would be likely reflected by the nanosecond component ϕ_2. Here we show that the fraction of this component is sensitive to the physical state of the sol and the silica concentration. The fact that ϕ_2 vanishes after gelation of SS is the strongest argument against the wobbling of R6G dipole on the silica surface. In addition, a close agreement between experimental steady-state anisotropy values and those calculated from TRFA parameters, as well as structural considerations, further support the applicability of the model of the rigid spherical rotor to R6G-silica systems. The ϕ_2 component in the decay of R6G-Ludox can thus be attributed to R6G bound to small nanoparticles, and their presence in Ludox was confirmed by TEM analysis.

The present paper also shows that even if the fit of experimental *r(t)* data to equation (4) is done in a model-independent way, the final form of this equation varies depending on the physical state of the colloidal silica. This is the most powerful demonstration of the versatility of TRFA approach to the *in situ* analysis of nanosize colloids.

3.6 References and Notes

1. Liu, B. M.; Cheung, H. C.; Mestecky, J. *Biochemistry* **1981,** *20*, 1997.

2. Lakowitcz, J. R. *Principles of Fluorescence spectroscopy*, 2nd ed.; Kluwer Academic Plenum Publishers: New York, **1999**.

3. Palmer, A. G.; Hochstrasser; R.; Millar, D. P.; Rance, M.; Wright, P. E. *J. Am. Chem. Soc.* **1992,** *115*, 6333.

4. Kemple, M. D.; Buckley, P.; Yuan, P.; Prendergast, F. G. *Biochemistry* **1997**, *36*, 1678.

5. Damberg, P.; Jarvet, J.; Allard, P.; Mets, U.; Rigler, R.; Graslund, A.. *Biophys J.* **2002**, *83*, 2812.

6. Kinosita, K., Jr., A. Ikegami, and S. Kawato. *Biophys. J.* **1982**, 37, 461.

7. Vogel, H., and F. Jaehnig. *Proc. Natl. Acad. Sci. USA.* **1984**, 82, 2029.

8. Restall, C. J., R. E. Dale, E. K. Murray, C. W. Gilbert, and D. Chapman. *Biochemistry* **1989**, 23, 6765.

9. Stein, R. A., R. D. Ludescher, P. S. Dahlberg, P. G. Fajer, R. L. H. Bennett, and D. D. Thomas. *Biochemistry* **1990**, 29, 10023.

10. Van der Heide, U. A., M. A. M. J. Zandvoort, E. van Faassen, G. van Ginkel, and Y. K. Levine. *J. Fluorescence* **1993**, 3, 271.

11. Engelborghs Y. *Spectrochim Acta A Mol Biomol Spectrosc.* **2001**, *57*, 2255.

12. Phillips D. *Analyst* **1994**, *119*, 543.

13. Berman, H. A.; Yguerabide, J.; Taylor, P. *Biochemistry* **1985**, *24*, 7140.

14. Girouard, S.; Houle, M.-H.; Grandbois, A.; Keillor, J. W.; Michnick, S. W. *J. Am. Chem. Soc.* **2004**; ASAP Article.

15. Adams, S. R.; Campbell, R. E.; Gross, L. A.; Martin, B. R.; Walkup, G. K.; Yao, Y.; Llopis, J.; Tsien, R. Y. *J. Am. Chem. Soc.* **2002**, *124*, 6063.

16. Dattelbaum, J. D.; Abugo, O. O.; Lakowicz, J. R. *Bioconjugate Chem.* **2000**; *11*, 533.

17. Corrie JE, Craik JS, Munasinghe VR. *Bioconjug Chem.* **1998**, 9,160.

18 Mercier, P., Ferguson, R.E., Irving, M., Corrie, J.E., Trentham, D.R., Sykes, B.D. *Biochemistry* **2003**, *42*, 4333.

19. Geddes, C. D.; Birch, D. J. S. *J. Non-Cryst. Solids* **2000**, *270*, 191.

20. Birch, D. J. S.; Geddes, C. D. *Phys. Rev. E.* **2000**, *62*, 2977.

21. Geddes, C. D.; Karolin, J.; Birch, D. J. S. *J. Fluoresc.* **2002**, *12*, 113.

22. Geddes, C. D.; Karolin, J.; Birch, D. J. S. *J. Fluoresc.* **2002**, *12*, 135.

23. Geddes, C. D. *J. Fluoresc.* **2002**, *12*, 343.

24. Tleugabulova, D.; Duft, A. M.; Zhang, Z.; Chen, Y.; Brook, M. A.; Brennan, J. D. *Langmuir* **2004**, *20*, 5924.

25. Tleugabulova, D.; Duft, A. M.; Brook, M. A.; Brennan, J. D. *Langmuir* **2004**, *20*, 101.

26. Tleugabulova, D.; Zhang, Z.; Chen, Y.; Brook, M. A.; Brennan, J. D. *Langmuir* **2004**, *20*, 848.

27. Debye, P. Polar molecules; Dover: New York, 1929.

28. Perrin F. *J. Phys. Radium* **1934**, V, 497; **1936**, VII, 1.

29. Narang, U.; Wang, R.; Prasad, P. N.; Bright, F. V. *J. Phys. Chem.* **1994**, *98*, 17.

30. Tleugabulova, D.; Zhang, Z.; Brennan, J. D. *J. Phys. Chem. B.* **2003**, *107*, 10127.

31. Geddes, C. D.; Karolin, J.; Birch, D. J. S. J. *Phys. Chem. B* **2002**, *106*, 3835.

32. Du Pont. *Ludox Colloidal Silica, Properties, Uses, Storage and Handling*, Data sheet. 1987

33. Weber, G. *Biochem. J.* **1952**, *51*, 145.

34. Kinosita, K., Jr., A. Ikegami, and S. Kawato. *Biophys. J.* **1982**,37,461

35. M.A. Brook, Y. Chen, K. Guo, Z. Zhang, J.D. Brennan, *J. Mater. Chem.* **2004**, *14*, 1469.

36. Bhatia, R.B.; Brinker, C. J.; Gupta, A.K.; Singh, A.K. *Chem. Mater.* **2000**, *12*, 2434.

37. Zheng, L.; Reid, W.R.; Brennan, J.D. *Anal. Chem.* **1997**, *69*, 3940.

38. Imhof, B. *Decay Analysis Software Support Manual.* Version 4. IBH Consultants Ltd, 1989.

39. Brill, O. L., Weil, C. G., Schmidt, P. W. *J. Colloid Interface Sci.* **1968**, *27*, 479.

40. Brill, O. L., Weil, C. G., Schmidt, P. W. *J. Colloid Interface Sci.* **1968**, *27*, 479.

41. Janosi, A., Kratky, O., Sekora, A. *Monatsh. Chem.* **1969**, 100, 1973.

42. Walter, G., Kranold, R., Baldrian, J., Steinhart, M. *J. Appl. Cryst.* **1985**, 18, 205.

43. Axelos, M. A. V., Tchoubar, D., Bottero, J. Y. *Langmuir* **1989**, *5*, 1186.

44. Hamai, S., Sasaki, K. Microchem. J. **2001**, 69, 27.

45. DeLaCruz, J. L., Blanchard, G. L. *J. Phys. Chem. B* **2004**, ASAP paper.

46. Deshpande, A. V., Namdas, E. B. *Appl. Phys. B* **1997**, 64, 419.

47. Abrahams, M. J.; Picher, D. H.; Fackler, P. H.; Lock, C. J.; Howard-Lock, H. E.; Faggiani, R.; Teher, B. A.; Richmond, R. C. *Inorg. Chem.* **1986**, 25, 3980.

48. Kvick, A.; Vaughan, G. B. M.; Wang, X.; Sun, Y.; Long, Y. *Acta Cryst.* **2000**, *C56*, 1232.

49. Saini, G. S. S., Kaur, S., Tripathi, S. K., Mahajan, C. G., Thanga, H. H., Verma, A. L. *Spectrochimica Acta Part A* **2005**, *61*, 653.

50. Adhikesavalu, D. N., Mastropaolo, D., Camerman, A., Camerman, N. *Acta Cryst.* **2001**, *C57*, 657.

51. Fun, H-K., Chinnakali, K., Sivakumar, K., Lu, C. M., Xiong, R. G., You, X. Z. *Acta. Cryst.* **1997**, *C53*, 1619.

52. Kemnitz, K., Yoshihara, K. *J. Phys. Chem.* **1991**, *95*, 6095.

53. Ferreira, J.A.B., Costa, S.M.B. *Chem. Phys. Lett.* **1999**, *307*, 139.

54. Tapia Estevez, M. J., Lopez Arbeloa, F., Lopez Arbeloa, T., Lopez Arbeloa, I., *Langmuir* **1993**, *9*, 3629.

Chapter 4

Direct and Indirect Monitoring of Peptide-Silica Interactions using Time-Resolved Fluorescence Anisotropy

The following chapter was published in the journal *Langmuir* under the citation:

J. Sui, D. Tleugabulova and J.D. Brennan*. Direct and Indirect Monitoring of Peptide-Silica Interactions using Time-Resolved Fluorescence Anisotropy. *Langmuir*, **2005**, *21*, 4996-5001.

I was responsible for all data collection and TRFA data analysis. Dr. Tleugabulova and Dr. Brennan assisted me in the analysis of steady-state anisotropy data. I wrote the first draft of the manuscript and Dr. Brennan provided editorial input to generate the final draft of the paper.

Abstract

The present work extends the application of time-resolved fluorescence anisotropy (TRFA) of a cationic probe rhodamine 6G (R6G) in aqueous Ludox to in situ monitoring of peptide adsorption onto the silica particles. Steady-state anisotropy and TRFA of R6G in Ludox sols were measured to characterize the extent of the ionic binding of the probe to silica particles in the presence of varying levels of tripeptides of varying charge, including Lys-Trp-Lys (KWK), N-acetylated Lys-Trp-Lys (Ac-KWK), Glu-Trp-Glu (EWE) and N-acetylated Glu-Trp-Glu (Ac-EWE). The results were compared to those obtained by direct observation of peptide adsorption using the steady-state anisotropy of the intrinsic tryptophan residue. Ionic binding of the peptides to Ludox particles produced an increase in the steady-state Trp anisotropy that was dependent on the number of cationic groups present, but the limiting anisotropy values were relatively low, indicating significant rotational freedom of the indole residue in the adsorbed peptides. On the other hand, R6G showed significant decreases in anisotropy in the presence of cationic peptides, consistent with the addition of cationic peptides blocking the adsorption of the dye to the silica surface. Thus, R6G is able to indirectly report on the binding of peptides to Ludox particles. It was noteworthy that while there were similar trends in the data obtained from steady-state anisotropy and TRFA studies of R6G, the use of steady-state anisotropy to assess binding of peptides overestimates the degree of peptide adsorption relative to the value obtained by TRFA. The study shows that the competitive binding method can be used to assess the binding of various biologically relevant compounds onto silica surfaces, and demonstrates the potential of TRFA for probing peptide:silica and protein:silica interactions.

4.1 Introduction

The development of sol–gel derived materials used to encapsulate biological species such as enzymes, antibodies and other proteins in a functional state has been an area of intense interest in the past decade.[1,2] One of the most important requirements for immobilization of proteins in sol-gel derived materials is that the entrapped proteins remain a functional state. However, the interaction of entrapped proteins with the internal silica surfaces can cause significant decreases in protein dynamics and may lead to protein denaturation.[1] Such interactions are typically evaluated using time-resolved fluorescence anisotropy (TRFA), which can assess the rotational dynamics of fluorescently labeled proteins after entrapment in sol-gel derived materials.[3-9] While such studies have provided useful insights into the dynamics of entrapped proteins, the size and complexity of proteins results in a wide array of different motions that occur on different timescales. Furthermore, proteins may be entrapped in a range of different environments within a sol-gel derived material, making the overall dynamics of the system highly complex. This situation can make the anisotropy decay complicated and very difficult to interpret. To overcome such issues, it is necessary to develop appropriate model systems that display reliable and easily interpretable dynamic motions, and yet provide sufficient complexity to allow insights into the parameters that affect protein-silica interactions.

Recently, Geddes and Birch[10-14] showed that the use of a cationic probe, such as rhodamine 6G (R6G), could allow for the measurement of the rotational times of silica particles. Based on their studies, it was shown that short (ps timescale) rotational correlation times correspond to probe that is free in solution, long (ns scale) rotational correlation times correspond to dye molecules that are electrostatically bound to primary anionic silica nanoparticles, while residual anisotropy (r_∞) values

correspond to dye molecules that are rigidly bound to larger (> 4.5 nm radius) particles, and thus rotate too slowly to cause fluorescence depolarization during the emission lifetime of R6G.[14] More recently, our group has demonstrated that such a method can be used to assess the degree of surface modification of colloidal silica particles in aqueous systems.[15,16] It was shown that the modification of silica particles with either polymers[15] or organosilanes[16] caused a higher proportion of R6G to be in solution relative to that adsorbed to unmodified surfaces (i.e., higher fraction of the ps decay component), indicating that adsorption of the dye could be blocked using appropriately modified surfaces.

In this work, we are extending the previous work with the R6G:Ludox system to the area of peptide:silica interactions. Ludox particles are discrete, uniform, negatively charged spheres of silica that have no internal surface area or detectable crystallinity. R6G, being a cationic probe, adsorbs strongly to the surface of Ludox particles and under such conditions will rotate with the correlation time of the silica particle.[14] Four peptides were chosen for this study: the cationic tripeptides Lys-Trp-Lys (KWK) and N-acetyl-Lys-Trp-Lys (Ac-KWK) and the anionic peptides Glu-Trp-Glu (EWE) and N-acetyl-Glu-Trp-Glu (Ac-EWE). The number of positively charged ammonium groups in these tripeptides vary from 0 (Ac-EWE) to 3 (KWK) and in the case of EWE and Ac-EWE there are also carboxylate groups of the Glu side chains, which should be repelled from the anionic surface of Ludox. The relatively small size of the tripeptides provides a higher flocculation limit than larger cationic peptides such as polylysine,[17] and thus is likely to lead to greater coverage of the silica surface, while the tryptophan residue provides a spectroscopic handle to allow direct observation of peptide adsorption via Trp fluorescence anisotropy.

Herein, we examine the tripeptide adsorption both directly, via Trp steady-state anisotropy, and indirectly, using both steady-state and time-resolved fluorescence anisotropy of R6G, by monitoring the competition of the peptide with R6G for binding to the silica surface. Both assays were done using different peptide:silica molar ratios and the data obtained from direct and indirect assay methods are compared. The TRFA results are also considered in light of atomic force microscopy (AFM) images of Ludox particles in the presence of different mole ratio of silica to KWK or Ac-EWE. The results demonstrate that the competitive binding assay using TRFA of the R6G/Ludox system should provide a useful new tool for probing peptide:silica or protein:silica interactions, and should be amenable to adsorption measurements even for non-fluorescent biomolecules.

4.2 Experimental Section

4.2.1 Chemicals

Lys-Trp-Lys acetate salt (KWK), rhodamine 6G and Tris(hydroxymethyl)aminomethane hydrochloride were obtained from Sigma (St. Louis, MO). Glu-Trp-Glu (EWE), N-acetyl-Glu-Trp-Glu (Ac-EWE) and N-acetyl-Lys-Trp-Lys (Ac-KWK) were synthesized by ANASpec (San Jose, CA). Ludox AM-30, 30 wt% SiO_2 in water (d=1.210, average particle radius of 6 nm, specific surface area of 220 $m^2 \cdot g^{-1}$) was purchased from Aldrich (Milwaukee, WI). All water was distilled and deionized using a Milli-Q Synthesis A10 water purification system. All other reagents were of analytical grade and were used as received.

4.2.2 Procedures

4.2.2.1 *Sample Preparation*

All samples were prepared daily and contained Ludox (0-14 wt% SiO_2) and 0-20 mM peptide diluted with 10 mM Tris-HCl buffer, pH 7.4. In cases where the peptide induced flocculation of Ludox particles, a lower peptide concentration was used to assure optical transparency and sample stability during the measurement. The samples for R6G anisotropy contained 1μM R6G, in addition to the peptide and Ludox.

The samples for TRFA experiments contained 0 - 5 mM peptide, 0.75 wt% SiO_2 and 1μM R6G. Under these conditions, we estimate that there is one R6G molecule bound for every 7 Ludox particles (in the absence of peptide), based on the specific surface area, density and the radius of Ludox particles and assuming complete adsorption of R6G molecules to the silica particles.

4.2.2.2 *Fluorescence Measurements*

Steady-state fluorescence anisotropy measurements were performed using a SLM 8100 spectrofluorimeter (Spectronic Instruments, Rochester, NY) as described elsewhere.[15,18] Single point fluorescence anisotropy measurements were made at λ_{ex} = 495 nm, λ_{em} = 551 nm for R6G and at λ_{ex} = 295 nm, λ_{em} = 335 nm for Trp. The values reported represent the average of 5 measurements each on three different samples.

Time-resolved fluorescence intensity and anisotropy decays were acquired in the time-domain using an IBH 5000U time-correlated single photon counting fluorimeter with a TBX-04 PMT detector, as described elsewhere.[15,16,19] The anisotropy decay was fit to a two-component hindered rotor model according to the following equation:[20]

$$r(t) = f_1 r_0 \exp(-t/\phi_1) + f_2 r_0(-t/\phi_2) + g r_0 \quad (1)$$

where r_0 is the limiting anisotropy at $t = 0$, ϕ_1 ($\phi_1 < \phi_2$) reflects isotropic rotation of free R6G in solution, ϕ_2 reflects slower reorientation of R6G bound to silica particles (1.2 – 1.5 nm in radius)[21], f_1 is the fraction of fluorescence originating from ϕ_1, f_2 is the fraction of fluorescence originating from ϕ_2, g is the fraction of fluorescence due to R6G that is rigidly bound to larger particles (> 3 nm in radius) that rotate more slowly than can be measured with the R6G probe (ϕ > 60 ns) and thus is assessed as "non-motion".[21] It should be noted that the value of gr_0 is equivalent to the residual anisotropy, r_∞, which is the anisotropy at $t \rightarrow \infty$. Fits were considered acceptable if the reduced chi-squared (χ_R^2) was close to 1.0 and the residuals showed a random pattern.

4.2.2.3 *Atomic Force Microscopy*

AFM imaging was performed using a NanoScope IIIa Multimode instrument from Digital Instruments Inc., USA. The Ludox samples were prepared with 0, 0.4 or 1 mol% of peptide present, corresponding to the mole ratios obtained using 0 mM, 2 mM or 5 mM peptide. The samples were then diluted (1/100 v/v) with distilled water, while maintaining the same peptide:Ludox ratio, and one drop of the diluted Ludox samples was placed onto an electronics grade silicon substrate (mean roughness < 0.150 nm over a 5mm x 5mm area) and allowed to dry. Height and phase data were collected from a 250 nm x 250 nm scan area in tapping mode using an Olympus silicon tapping probe (tip radius < 10 nm) operated at a 2.44 Hz scan rate.

4.3 Results and Discussion

4.3.1 Direct Monitoring of Peptide Adsorption via Intrinsic Trp Fluorescence

Since all peptides possess the intrinsically fluorescent Trp residue, the steady-state Trp anisotropy was measured for each tripeptide solution (2 mM) as a function of the amount of Ludox, expressed as the wt% SiO_2. To avoid interferences, the measurements of Trp anisotropy were done in the absence of R6G. As shown in Figure 4.1, all peptides containing cationic groups showed increases in anisotropy as a function of the silica concentration, consistent with the peptide binding to silica particles and a more restricted rotational freedom of the indole ring in the adsorbed peptide relative to the soluble one. The slope of the binding curve and the maximum anisotropy both increased with the number of cationic groups, and interestingly, adsorption was observed even for EWE, which has a net negative charge, indicating that the adsorption of anionic peptides onto the silica can occur through the N-terminal group even when no cationic side chains are present in the peptide.

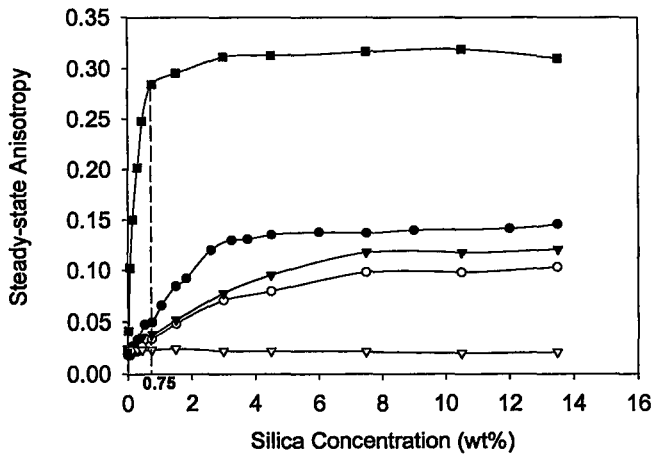

Figure 4.1 Steady-state fluorescence anisotropy of rhodamine 6G (■, λ_{ex} = 495nm, λ_{em} = 551 nm) and KWK (●), Ac-KWK (○), EWE (▼) and Ac-EWE (▽) at λ_{ex}= 295 nm, λ_{em} = 335 nm as a function of silica concentration. Samples contained either 1μM R6G or 2 mM of the peptide. The dashed line indicates the experimental conditions chosen for indirect measurements of peptide adsorption. Typical error in anisotropy values is 0.01.

The limiting values on the anisotropy curves correspond to the point at which the peptide is essentially fully adsorbed to the Ludox surface and the amount of free peptide in solution is negligible. The limiting anisotropy of KWK in Ludox (0.146) is relatively close to the limiting anisotropy (r_0 = 0.174) measured for KWK in 1,2-propanediol at -58°C,[22] suggesting significant restriction of the backbone motion in the adsorbed KWK. This is consistent with the formation of three ionic bonds between the peptide and the silica surface, which would cause severe damping of backbone motion. For Ac-KWK, the maximum anisotropy in Ludox is 0.121, which indicates that blocking of the N-terminal amine leads to a reduction in the number of ionic bonds between the peptide and silica, and hence increases backbone motion relative to KWK. The differences in maximum anisotropy for KWK and Ac-KWK highlight the importance of the N-terminal amine in promoting peptide adsorption. This is further demonstrated by the non-zero limiting anisotropy of EWE in Ludox (r_{max} = 0.103). However, it should be noted that the maximum anisotropy for EWE adsorbed on Ludox is much lower than its anisotropy in the absence of rotational diffusion (r_0 = 0.171),[22] and also lower than the value for KWK. This suggests the presence of significant backbone motion for the adsorbed EWE, which reflects the ability of the peptide to undergo significant motion as a result of binding to the silica through only one site. Finally, Ac-EWE shows essentially no change in anisotropy in the presence of Ludox (r_{max} = 0.021), showing that cationic groups are required to cause peptide adsorption to the silica surface.

Overall, while the differences in maximum Trp anisotropy appear to correlate well to the number of bonds to the silica surface, the dependence of Trp anisotropy on both the degree of adsorption and the binding geometry of the peptide makes it difficult to use Trp anisotropy for quantitative assessment of the extent of peptide binding, since

one must know *a priori* the maximum anisotropy and slope of the binding curve. In addition, the relatively low value of the maximum anisotropy leads to a narrow dynamic range for measurement of changes in steady-state anisotropy.

4.3.2 Indirect Monitoring of Peptide Adsorption via R6G Anisotropy

To overcome issues with Trp fluorescence, we examined the use of R6G for indirect measurement of peptide adsorption based on competition between the peptide and R6G for binding to the silica surface. The positively charged probe R6G adsorbs strongly and rigidly to the silica surface, causing complete damping of isotropic rotation of the R6G dipole.[21] As a result, there is a sharp increase in the steady-state anisotropy of R6G with increasing amounts of Ludox (Fig. 3.1) until reaching a value of 0.34, which is slightly lower than the R6G anisotropy in the absence of rotational diffusion ($r_0 = 0.38$).[23] The binding of peptides to Ludox will decrease the free silica surface area available for R6G binding. Since more R6G molecules will reside in solution, the R6G anisotropy is expected to decrease.[17,21,23]

An essential requirement for anisotropy measurements in colloidal systems is the optical transparency of a sample. We found that the diluted Ludox sol (0.75 wt% SiO_2) is stable and does not flocculate over a broad range (0-5 mM) of peptide concentrations. Sensitivity to peptide adsorption is another important requirement, particularly when using TRFA for surface adsorption studies. At 1μM R6G and 0.75 wt% SiO_2, R6G anisotropy approaches, but does not reach the plateau value (Fig. 3.1), indicating that under these conditions, the addition of relatively small amounts of a peptide is expected to produce large decreases in R6G anisotropy.

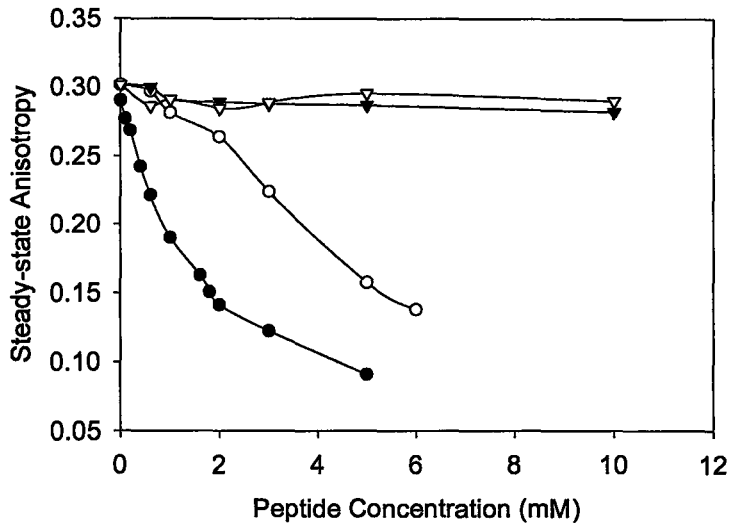

Figure 4.2. Steady-state R6G anisotropy as a function of peptide concentration at 0.75 wt% SiO_2 for KWK (●), Ac-KWK (○), EWE (▼) and Ac-EWE (▽). R6G concentration is 1 μ M. Typical error in anisotropy values is ± 0.01.

Figure 4.2 shows the changes in R6G steady-state anisotropy as the concentration of each tripeptide was increased with constant concentrations of R6G and Ludox present in solution. It is clear that R6G anisotropy values decrease dramatically as the concentration of either KWK or Ac-KWK increases, and both the concentration range and the overall changes in R6G anisotropy were dependent on the nature of the peptide. The measurements of R6G anisotropy led to the same results, regardless of whether R6G was added to Ludox before, after or with the peptide (Table 4.1). Thus, the data obtained by measurement of R6G anisotropy reflect equilibrium conditions. In general, the range over which anisotropy decreases is smaller and the overall change in anisotropy was larger as the number of binding sites in the peptide increased. The decreases in R6G anisotropy upon addition of Lys-containing peptides are consistent with these peptides adsorbing to the Ludox particles and thus decreasing the surface area available for the binding of R6G. This blockage of adsorption indirectly reflects the interactions between Lys-containing peptides and

Table 4.1 Effect of adding R6G and peptides in varying order on TRFA parameters.

	R6G in Ludox		
	A	B	C
τ, *ns*	3.89 ± 0.005 (93.9%) 1.79 ± 0.01 (6.1%)	3.86 ± 0.005 (95.4%) 1.94 ± 0.02 (4.6%)	3.87 ± 0.005 (96.5%) 1.94 ± 0.03 (3.5%)
χ_R^2	1.07	1.10	1.09
ϕ_1, *ns*	0.16 ± 0.02	0.19 ± 0.04	0.17 ± 0.04
ϕ_2, *ns*	3.3 ± 0.7	3.7± 0.4	3.9 ± 0.3
r_0	0.40	0.39	0.38
r_∞	0.16	0.16	0.16
g	0.40	0.41	0.42
f_1	0.22	0.20	0.20
f_2	0.38	0.39	0.38
χ_R^2	1.00	1.02	0.99

A. 0.6mM KWK+Ludox, 1h, +R6G
B. R6G +Ludox, 1h, +0.6mM KWK
C. 0.6mM KWK+R6G, 1h, +Ludox

silica surface, and importantly does not rely on the presence of any tag on the peptide, indicating that the method should be applicable to monitoring adsorption of even non-fluorescent peptides or polymers. The differences in adsorption of the four peptides follow the trend of stronger adsorption with larger numbers of amino groups. This shows that the binding of the peptides is purely electrostatic in nature, and that there are minimal hydrophobic or hydrogen bonding interactions between the indole ring and the Ludox surface. The key differences between the peptides are the minimum R6G anisotropy that is attainable for each peptide (corresponding to maximum surface coverage of silica by the peptide), and the amount of peptide required to achieve maximum adsorption. As is evident from Figure 4.2, the highly cationic KWK peptide achieves maximum surface coverage, prior to flocculation, at a peptide concentration of 5 mM. Ac-KWK causes R6G anisotropy to decrease more gradually

and the final anisotropy (0.157) is much higher than that for KWK (0.091) under identical experimental conditions, indicative of a lower association constant. EWE did not cause significant changes in R6G anisotropy at low peptide concentrations, but did result in moderate changes in R6G steady-state anisotropy at higher levels (r = 0.282 at 10 mM). Ac-EWE had no effect on R6G anisotropy, even at a concentration of 10 mM (the solubility limit of the peptide in 10 mM Tris buffer), consistent with the absence of cationic groups in the Ac-EWE molecule and thus no adsorption to Ludox.

If we attribute the observed decreases in R6G steady-state anisotropy values to less binding of R6G to the silica particles, as a result of peptide adsorption, the minimum in the anisotropy curves (Figure 4.2) should correspond to maximum adsorption of the peptide to the silica surface. Since the quantum yield of R6G is the same in the bound and free states,[15] one can estimate the fractional coverage of the surface by comparing the minimum and maximum steady-state anisotropy values for R6G (r_{max} = 0.301) as (1- (r_{min}/r_{max})), where r_{min} is the anisotropy prior to flocculation the peptide. The ratio r_{min}/r_{max} is proportional to the fraction of R6G that is adsorbed to the silica surface under conditions of maximum peptide adsorption, and thus 1-(r_{min}/r_{max}) is the fraction of sites that are inaccessible to R6G, and thus assumed to be associated with the peptide. Based on this simple equation, the coverage values are thus estimated to be on the order of 70% for KWK (5 mM), 60% for Ac-KWK (6 mM), ~6% for EWE (10 mM) and ~ 3% for Ac-EWE (10 mM). These values show the trend of higher adsorption as the number of cationic groups increases. However, in the case of EWE, the extent of adsorption appears to be low relative to that obtained from Trp anisotropy when using high silica concentrations. This reflects a large difference in available silica surface area in the two experiments. In the case of

Trp anisotropy, the plateau anisotropy value was obtained at 8 wt% SiO_2, while in the R6G experiment there was only 0.75 wt% SiO_2, and the peptide must compete against R6G, which binds much more strongly to silica, for adsorption sites.

4.3.3 Time-Resolved Anisotropy of R6G in Peptide/R6G/Ludox Mixtures

To obtain more detailed information on the extent of binding of the peptides to the Ludox particles, time-resolved fluorescence anisotropy was used to assess the individual rotational motions of R6G in the peptide/R6G/Ludox system. Time-resolved fluorescence anisotropy provides accurate information on the relative ratio of R6G molecules adsorbed to Ludox particles versus free R6G molecules in solution.[15,16] This ratio depends exclusively on the free silica surface available for R6G adsorption and thus indirectly reflects the extent of peptide binding to Ludox. Similar information cannot be obtained using Trp fluorescence for several reasons. First, at the given peptide concentrations the intensity of Trp fluorescence is too low when using a flashlamp for excitation. Second, the limiting anisotropy of Trp in short peptides is ~0.17,[22] which is significantly lower than the theoretical value of 0.4. Hence, the range of r values available for the reconvolution of $r(t)$ function into different exponential terms (equation 1) is dramatically reduced and this will affect the quality of fitted data. Third, considerable backbone flexibility in the adsorbed Ac-KWK and EWE will influence the rotational correlation times and their fractions in a complex way. Under these conditions, attributing specific anisotropy decay components to free and silica-bound probes become meaningless.

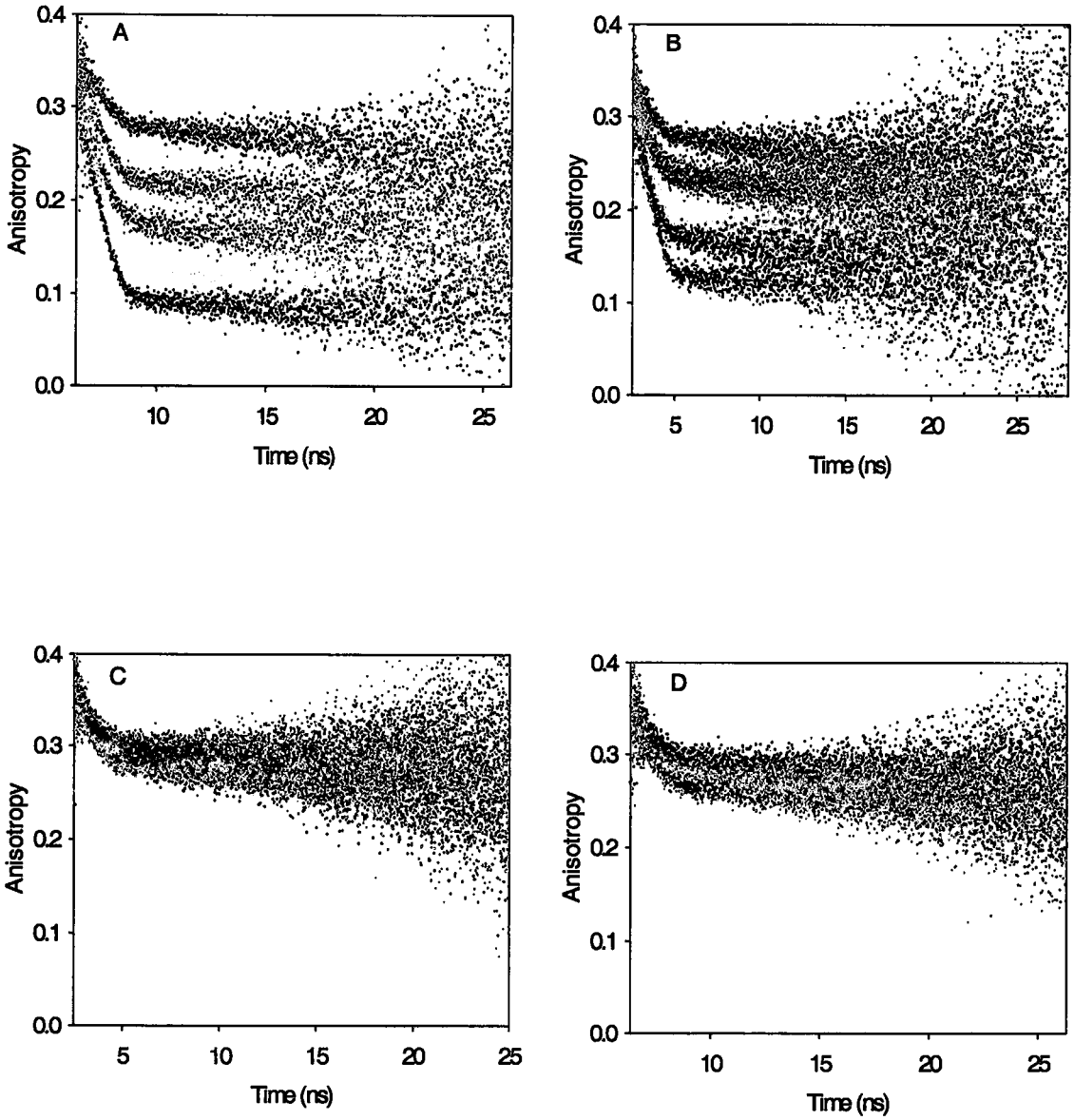

Figure 4.3 Time-resolved fluorescence anisotropy decays of R6G in Ludox silica sols (10 mM Tris-buffer, pH = 7.4, 0.75 wt % SiO_2) at different concentrations of (A) KWK, (B) Ac-KWK, (C) EWE and (D) Ac-EWE. 0 mM (black); 0.6 mM (red); 1mM (green); 2 mM (yellow); 5 mM (blue). The pink decay trace refers to 6 mM Ac-KWK (Panel B) or 10 mM EWE (Panel D).

Figure 4.3 shows typical decays of fluorescence anisotropy for 1 μ M R6G in 10 mM Tris buffer solution containing varying levels of KWK (Panel A), Ac-KWK (Panel B), EWE (Panel C) and Ac-EWE (Panel D) in the presence of 0.75 wt% of Ludox. Table 4.2 shows the fits to the R6G anisotropy decays as a function of peptide concentration (Table 4.3-3.6 show all fitting parameters). It should be noted that the intensity decays of R6G in Ludox and Ludox/peptide mixtures were essentially monoexponential, with a lifetime of ~ 4 ns, although in some cases a minor component (< 7%) of a ~ 2 ns component was present in the fits, the origin of which is not clear. It is evident from Figure 4.3 that in the Ludox/R6G system without peptide present, the anisotropy of R6G does not decay to a value of zero, indicative of a significant fraction of dye that is rigidly bound to silica structures that do not rotate on a timescale of at least 15τ (*ca.* 60 ns), in agreement with previous studies of the R6G:Ludox system.[14] Furthermore, a second rotational correlation time appears in the nanosecond time range, which we attribute to binding of R6G to small particles present in the Ludox sol.[21] Taken together, the percentage of bound dye, given by (f_2 + g), is on the order of 95%, and thus it is likely that the majority of R6G molecules are bound to the silica surface in the Ludox sample. It should be noted that the extent of R6G binding is somewhat lower than reported for earlier studies of polymer and organosilanes modification of Ludox (>99%),[15,16] which we attribute to the presence of 10 mM Tris buffer in the present study.

Table 4.2 Time-resolved fluorescence anisotropy decay parameters of R6G in 10 mM, pH=7.4 Tris buffer solution and in 0.75 wt % SiO_2 in the presence of varying levels of tripeptides.[a]

Sample		r_0	ϕ_1, ns	ϕ_2, ns	f_1	f_2	g
R6G in buffer		0.38	0.17± 0.01	-	0.97	0	0.03
R6G in Ludox		0.38	0.18 ± 0.05	3.9 ± 0.5	0.05	0.28	0.67
R6G in Buffer	KWK 0.6 mM	0.38	0.17 ± 0.01	-	0.98	0	0.02
	1 mM	0.38	0.17 ± 0.01	-	0.97	0	0.03
	2 mM	0.39	0.17 ± 0.01	-	0.98	0	0.02
	5 mM	0.38	0.18 ± 0.01	-	0.98	0	0.02
R6G in Ludox	KWK 0.6 mM	0.38	0.17 ± 0.04	3.9 ± 0.3	0.20	0.38	0.42
	1 mM	0.38	0.18 ± 0.03	4.1± 0.4	0.24	0.39	0.37
	2 mM	0.39	0.16 ± 0.02	3.0± 0.4	0.33	0.41	0.26
	5 mM	0.38	0.19± 0.02	3.4± 0.5	0.44	0.54	0.02
	Ac-KWK 0.6 mM	0.39	0.21 ± 0.04	4.9 ± 0.8	0.08	0.36	0.56
	1 mM	0.37	0.20 ± 0.04	4.5± 0.6	0.10	0.31	0.59
	2 mM	0.39	0.16 ± 0.03	3.1± 0.7	0.27	0.29	0.44
	5 mM	0.40	0.20 ± 0.03	3.0± 0.7	0.35	0.25	0.40
	6 mM	0.40	0.19 ± 0.03	3.3± 0.9	0.43	0.27	0.30
	EWE 0.6 mM	0.38	0.18 ± 0.09	4.6 ± 0.7	0.07	0.22	0.71
	1 mM	0.40	0.16 ± 0.09	4.5 ± 0.4	0.07	0.23	0.70
	2 mM	0.38	0.19 ± 0.05	4.3± 0.9	0.08	0.26	0.66
	5 mM	0.40	0.14 ± 0.05	4.5 ± 0.9	0.06	0.26	0.68
	10 mM	0.36	0.23± 0.7	14.0 ± 7.0	0.05	0.23	0.72
	Ac-EWE 0.6 mM	0.37	0.21 ± 0.06	4.1 ± 0.5	0.02	0.28	0.70
	1 mM	0.37	0.18 ± 0.04	4.0 ± 0.4	0.02	0.33	0.64
	2 mM	0.37	0.19 ± 0.02	4.9 ± 0.9	0.04	0.35	0.61
	5 mM	0.38	0.19 ± 0.01	5.1 ± 1.3	0.02	0.27	0.71
	10 mM	0.39	0.17 ± 0.01	3.9 ± 0.3	0.05	0.29	0.66

a) ϕ_1, ϕ_2, rotational correlation times; f_1, fractional contribution to anisotropy decay owing to ϕ_1; f_2, fractional contribution to anisotropy decay owing to ϕ_2; g, fraction of fluorescence arising from slow motion of probes corresponding to limiting anisotropy ($g = r_\infty/r_0$). Typical errors in r_∞, r_0, f_1 and f_2 are ± 0.02, error in g is ± 0.03.

Table 4.3 Time-resolved fluorescence anisotropy decay data of R6G in 10 mM, pH=7.4 Tris buffer solution and in 0.75 wt % SiO_2 in the presence of varying levels of KWK.[a]

R6G in Ludox					
	0 mM KWK	0.6 mM KWK	1 mM KWK	2 mM KWK	5 mM KWK
τ, *ns*	3.93 ± 0.002	3.87 ± 0.005 (96.5%) 1.94 ± 0.03 (3.5%)	3.89 ± 0.004 (96.4%) 1.91 ± 0.006 (3.6%)	3.87 ± 0.005 (95.4%) 1.91 ± 0.009 (4.6%)	3.82± 0.006 (96.9%) 1.82 ± 0.009 (3.1%)
χ_R^2	1.14	1.09	1.12	1.13	1.10
ϕ_1, *ns*	0.18 ± 0.05	0.17 ± 0.04	0.18 ± 0.03	0.16 ± 0.02	0.19± 0.02
ϕ_2, *ns*	3.9 ± 0.5	3.9 ± 0.3	4.1± 0.4	3.0± 0.4	3.4± 0.5
r_0	0.38	0.38	0.38	0.39	0.38
r_∞	0.26	0.16	0.15	0.10	0.01
g	0.67	0.42	0.37	0.26	0.02
f_1	0.05	0.20	0.24	0.33	0.44
f_2	0.28	0.38	0.39	0.41	0.54
χ_R^2	1.01	0.99	0.99	0.99	1.02

a) τ, fluorescence lifetime; ϕ_1, ϕ_2, rotational correlation times; f_1, fractional contribution to anisotropy decay owing to ϕ_1; f_2, fractional contribution to anisotropy decay owing to ϕ_2; r_0, limiting anisotropy; r_∞, residual anisotropy; g, fraction of fluorescence arising from slow motion of probes corresponding to limiting anisotropy ($g = r_\infty/r_0$). Typical errors in r_∞, r_0, f_1 and f_2 are ± 0.02, error in g is ± 0.03.

Table 4.4 Time-resolved fluorescence anisotropy decay data of R6G in 10 mM, pH=7.4 Tris buffer solution and in 0.75 wt % SiO_2 in the presence of varying levels of Ac-KWK.[a]

	R6G in Ludox					
	0 mM Ac-KWK	0.6 mM Ac-KWK	1 mM Ac-KWK	2 mM Ac-KWK	5 mM Ac-KWK	6 mM Ac-KWK
τ, *ns*	3.93 ± 0.002	3.96 ± 0.005 (93.3%) 1.97 ± 0.01 (6.7%)	3.98 ± 0.004 (93.8%) 1.98 ± 0.008 (6.2%)	3.89 ± 0.004 (93.4%) 1.88 ± 0.01 (6.54%)	3.89 ± 0.005 (92.8%) 1.88 ± 0.02 (7.2%)	3.88 ± 0.005 (94.0%) 1.96 ± 0.01 (6.0%)
χ_R^2	1.14	1.10	1.08	1.11	1.09	1.09
ϕ_1, *ns*	0.18± 0.05	0.21± 0.04	0.20± 0.04	0.16± 0.03	0.20± 0.03	0.19± 0.03
ϕ_2, *ns*	3.9 ± 0.4	4.9 ± 0.8	4.5± 0.6	3.1± 0.7	3.0± 0.7	3.3± 0.9
r_0	0.38	0.39	0.37	0.39	0.40	0.40
r_∞	0.26	0.22	0.22	0.17	0.16	0.12
g	0.67	0.56	0.59	0.44	0.40	0.30
f_1	0.05	0.08	0.10	0.27	0.35	0.43
f_2	0.28	0.36	0.31	0.29	0.25	0.27
χ_R^2	1.01	1.03	1.00	0.99	1.01	1.07

a) τ, fluorescence lifetime; ϕ_1, ϕ_2, rotational correlation times; f_1, fractional contribution to anisotropy decay owing to ϕ_1; f_2, fractional contribution to anisotropy decay owing to ϕ_2; r_0, limiting anisotropy; r_∞, residual anisotropy; g, fraction of fluorescence arising from slow motion of probes corresponding to limiting anisotropy ($g = r_\infty/r_0$). Typical errors in r_∞, r_0, f_1 and f_2 are ± 0.02, error in g is ± 0.03.

Table 4.5 Time-resolved fluorescence anisotropy decay data of R6G in 10 mM, pH 7.4 Tris buffer solution and in 0.75 wt % SiO_2 in the presence of varying levels of EWE.[a]

	R6G in Ludox					
	0 mM EWE	0.6 mM EWE	1 mM EWE	2 mM EWE	5 mM EWE	10 mM EWE
τ, *ns*	3.93 ± 0.002	4.03 ± 0.005 (96.4%) 2.02 ± 0.01 (3.6%)	4.01 ± 0.004 (97.0%) 2.01 ± 0.007 (3%)	3.99 ± 0.004 (97.0%) 2.01 ± 0.02 (3%)	3.97 ± 0.005 (96.8%) 1.79 ± 0.008 (3.2%)	3.93 ± 0.004 (95.0%) 1.96 ± 0.007 (5.0%)
χ_R^2	1.14	1.08	1.05	1.07	1.09	1.06
ϕ_1, *ns*	0.18± 0.05	0.18± 0.09	0.16± 0.09	0.19±0.052	0.14± 0.05	0.23± 0.76
ϕ_2, *ns*	3.9 ± 0.4	4.6 ± 0.7	4.5 ± 0.4	4.3± 0.9	4.5 ± 0.9	14.0 ± 7.3
r_0	0.38	0.38	0.40	0.38	0.40	0.36
r_∞	0.26	0.27	0.28	0.25	0.27	0.30
g	0.67	0.71	0.70	0.66	0.68	0.72
f_1	0.05	0.07	0.07	0.08	0.06	0.05
f_2	0.28	0.22	0.23	0.26	0.26	0.23
χ_R^2	1.01	1.03	0.97	1.03	1.04	0.98

a) τ, fluorescence lifetime; ϕ_1, ϕ_2, rotational correlation times; f_1, fractional contribution to anisotropy decay owing to ϕ_1; f_2, fractional contribution to anisotropy decay owing to ϕ_2; r_0, limiting anisotropy; r_∞, residual anisotropy; g, fraction of fluorescence arising from slow motion of probes corresponding to limiting anisotropy ($g = r_\infty/r_0$). Typical errors in r_∞, r_0, f_1 and f_2 are ± 0.02, error in g is ± 0.03.

Table 4.6 Time-resolved fluorescence anisotropy decay data of R6G in 10 mM, pH 7.4 Tris buffer solution and in 0.75 wt % SiO_2 in the presence of varying levels of Ac-EWE.[a]

	R6G in Ludox					
	0 mM Ac-EWE	0.6 mM Ac-EWE	1 mM Ac-EWE	2 mM Ac-EWE	5 mM Ac-EWE	10 mM Ac-EWE
τ, *ns*	3.93 ± 0.002	4.00 ± 0.004 (96.7%) 2.00 ± 0.01 (3. 3%)	4.01 ± 0.003 (96.3%) 2.00 ± 0.01 (3.7%)	3.97 ± 0.004 (97.6%) 2.01 ± 0.02 (2.4%)	3.95± 0.001 (96.7%) 1.97 ± 0.01 (3.3%)	3.95 ± 0.006 (95.2%) 1.98 ± 0.01 (4.8%)
χ_R^2	1.14	1.08	1.02	1.05	1.09	1.09
ϕ_1, *ns*	0.18± 0.05	0.21± 0.06	0.18± 0.04	0.19± 0.02	0.19± 0.01	0.17± 0.06
ϕ_2, *ns*	3.9 ± 0.4	4.1 ± 0.5	4.0 ± 0.4	4.9 ± 0.9	5.1 ± 1.3	3.9± 0.3
r_0	0.38	0.37	0.37	0.37	0.38	0.39
r_∞	0.26	0.26	0.24	0.22	0.27	0.26
g	0.67	0.70	0.64	0.61	0.71	0.66
f_1	0.05	0.02	0.02	0.04	0.02	0.05
f_2	0.28	0.28	0.33	0.35	0.27	0.29
χ_R^2	1.01	1.00	0.99	0.97	1.02	1.03

a) τ, fluorescence lifetime; ϕ_1, ϕ_2, rotational correlation times; f_1, fractional contribution to anisotropy decay owing to ϕ_1; f_2, fractional contribution to anisotropy decay owing to ϕ_2; r_0, limiting anisotropy; r_∞, residual anisotropy; g, fraction of fluorescence arising from slow motion of probes corresponding to limiting anisotropy ($g = r_\infty/r_0$). Typical errors in r_∞, r_0, f_1 and f_2 are ± 0.02, error in g is ± 0.03.

In the presence of increasing levels of Lysine-containing peptides (KWK, Ac-KWK), there is a decrease in g value, consistent with the increased coverage of the silica surface by the peptide at higher concentrations, which causes more R6G to be present in solution. In addition, the fraction of fluorescence associated with ϕ_2 increases as KWK concentration increases, suggesting preferential adsorption of KWK on larger Ludox colloids, which would have a higher surface area available for binding to the peptide. A similar redistribution of fractional fluorescence values was previously observed upon adsorption of polymers[15] and organosilanes[16] to R6G-doped Ludox samples.

Using the anisotropy decay data it is possible to obtain an estimate of the degree of adsorption of the peptide onto the Ludox particles as a function of peptide concentration. For example, considering the 5 mM KWK samples, the g value gradually decreased from 0.67 (Ludox without KWK) to 0.02, with the fractional fluorescence of the nanosecond component increasing from 28% to 54% and that of the picosecond component increasing from 4% to 44%. Since the emission properties of R6G do not change upon adsorption,[15] we assume that the total fluorescence from the nanosecond and residual anisotropy components ($g + f_2$) corresponds to the fraction of bound dye. The degree of adsorption of peptide (D) can be found from the equation:

$$D = 1 - \frac{(g + f_2)_P}{(g + f_2)_0} \qquad (2)$$

where $(g + f_2)_0$ is obtained in the absence of peptide and $(g + f_2)_P$ is obtained in the presence of a given concentration of peptide. Using this approach for the other KWK concentrations, it is clear that the degree of adsorption of KWK onto the silica surface increases as the concentration of KWK increases, reaching a maximum value of 41% at 5 mM as shown in Figure 4.4. Higher peptide concentrations lead to the

flocculation of Ludox, suggesting that the presence of two Lys residues within the peptide, coupled with the positively charged N-terminus, may provide a means to form bridges between two separate colloidal particles at higher peptide concentrations, thus leading to flocculation prior to complete coverage of the silica surface.

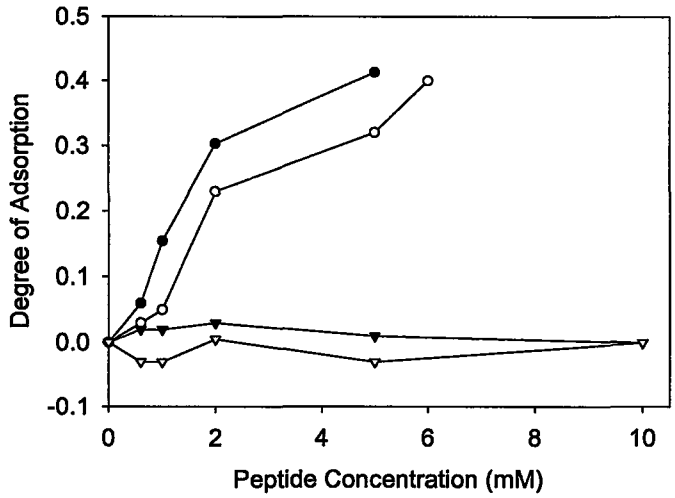

Figure 4.4. Degree of adsorption of KWK (●), Ac-KWK (○), EWE (▼) and Ac-EWE (▽) on the surface of Ludox particles as a function of peptide concentration as determined by indirect monitoring of R6G anisotropy decay parameters. Typical error on adsorption degree values is ± 0.04.

Figure 4.4 also shows the adsorption data obtained for the other three peptides. As was the case with the steady-state anisotropy data for R6G, the maximum degree of adsorption and the concentration of peptide required to saturate the surface depend on the number of amine groups in the peptide, and is most dependent on the presence of Lys residues. Based on the data in Figure 4.4, it can be concluded that the maximum degree of adsorption is 40% for Ac-KWK (6 mM), and essentially 0% (within error) for both EWE and Ac-EWE (at 10 mM).

It is important to note that the estimated surface coverage from steady-state anisotropy measurements of silica modified with cationic peptides (~ 60 - 70%) are higher than those obtained by time-resolved anisotropy (*ca.* 40%). Slightly higher degrees of adsorption were also obtained for anionic peptides using steady-state anisotropy (3-6%) relative to TRFA (~0% for both peptides). This trend has been previously observed for organosilanes coated Ludox surfaces.[16] The difference lies in the presence of the nanosecond component, which corresponds to bound dye that has relatively rapid rotational motion. Thus, the redistribution of dye between large and small structures contributes to the decrease in R6G steady-state anisotropy (Fig. 4.2), which can be mistakenly interpreted as a higher fraction of free dye, and thus a higher surface coverage of silica by the peptide, when only average anisotropy values are measured. This clearly demonstrates that steady-state anisotropy values overestimate the amount of "free" probe, and hence the extent of surface modification. Using TRFA, it is possible to distinguish between free dye and dye that is bound to rapidly rotating particles, providing a more accurate measurement of the true amount of adsorption. This highlights the importance of using time-resolved anisotropy decays to accurately assess the distribution of dye in Ludox systems.

4.3.4 Atomic force microscopy

Atomic force microscopy experiments were performed to further assess the binding properties of KWK and Ac-EWE on Ludox silica particles at different peptide:SiO_2 ratios. Two peptide levels were selected for further AFM study: 2 mM which corresponds to half maximum binding and 5 mM which corresponds to maximum binding of KWK to the silica surface, each of which was incubated with 0.75 wt% SiO_2.

Figure 4.5A and 4.5B show height and phase AFM images obtained for Ludox particles without any peptide present. As shown, Ludox is composed predominantly of particles with radii between 6 and 7 nm and there is also the presence of smaller particles (1~3 nm radius), which supports our interpretation of the ~3 ns rotational correlation being due to the binding of R6G on smaller Ludox particles.[24] Ludox particles showed a regular and close-packed array in the absence of peptide and did not show any contrast in the phase image, which means those Ludox particles are homogeneous and there are no other phases with different mechanical properties.

Upon addition of a low level of KWK (2 mM initial concentration), the Ludox particles appear to change in shape from spherical and uniform to irregular shapes, which is evident in both height and phase contrast AFM images. In the height image, there is evidence for significant aggregation of particles, and there is an almost complete absence of discrete particles, which is consistent with partial surface coverage of the Ludox particle and the beginning of particle aggregation/flocculation. Phase contrast AFM image gives the information of particle aggregation and particle shape changes, however, at the low KWK concentration the phase image is still predominated by the Ludox particles, and the KWK is not influencing the image to a large degree.

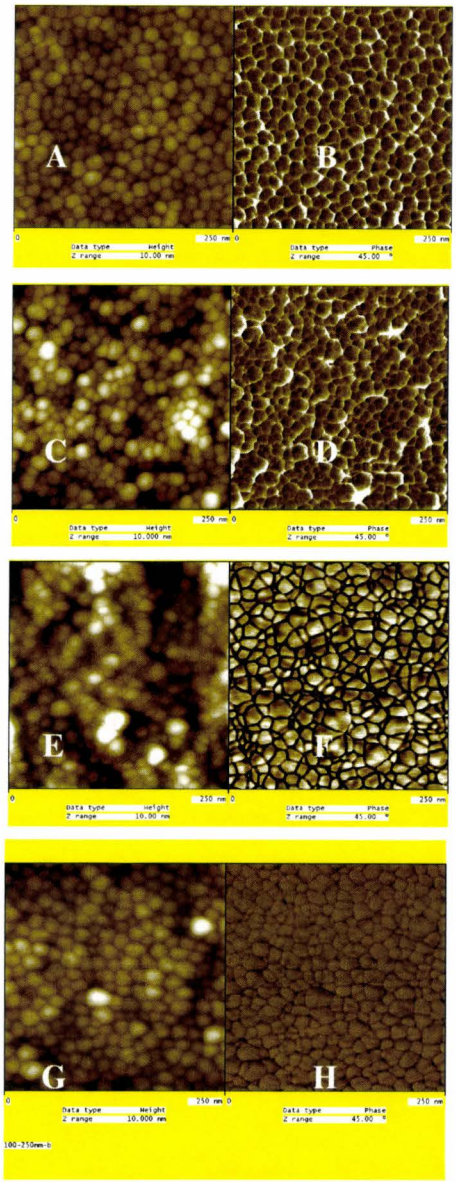

Figure 4.5 Height and phase contrast atomic force microscopy images of Ludox silica particles (0.75 wt % SiO_2). a) Height image of unmodified particles; b) phase image of unmodified particles; c) height image of Ludox particles exposed to 2 mM KWK; d) phase image of Ludox particles exposed to 2 mM KWK; e) height image of Ludox particles exposed to 5 mM KWK; f) phase image of Ludox particles exposed to 5 mM KWK, g) height image of Ludox particles exposed to 5 mM Ac-EWE; f) phase image of Ludox particles exposed to 5 mM Ac-EWE.

Addition of a higher level of KWK to Ludox (1 mol%) (Figures 4.5E and 4.5F) leads to a situation where there should be high coverage of the Ludox surface by KWK. At this KWK level there are significant changes in the particle distribution. Based on the height image, a halo appears to surround the Ludox particles and this causes aggregation of the silica particles, which is likely due to adsorbed KWK on the Ludox particle surface. The silica particles show irregular and random packing, with some aggregates clearly present. These aggregates would be expected to lead to particle flocculation in solution. The phase image clearly shows the presence of dark regions between larger light regions. The contrast mechanism in the phase image is due to variations in the mechanical properties of the sample. In this case, light areas are harder than dark areas. Thus, the phase contrast image is consistent with a KWK layer (dark regions) being present between the silica particles (light regions). The presence of a darker ring around each spherical particle in the height images suggests that KWK makes some specific contact angle with the beads such that a wetting layer is present in between the silica particles. This would result in the dark bands around the particles (as seen in the height images) and it is also consistent with the phase images. Taken together with the fluorescence data, it is clear that at the highest level of KWK, the peptide adsorbs on the surface of the silica particles.

In contrast, Figures 4.5G and 4.5H show AFM images of Ludox after exposure to 5 mM of EWE. These images appear to be very similar to those obtained for unmodified Ludox, with no evidence for particle aggregation in the height image or regions with different mechanical properties in the phase image. This provides further evidence that the EWE peptide does not adsorb to the Ludox surface, and supports the data obtained by TRFA.

4.4 Conclusions

Monitoring the R6G anisotropy during the incremental addition of peptide to aqueous Ludox sols resulted in the ability to measure the degree of peptide adsorption to silica particles. Our data show that R6G has different correlation times depending on whether it is dissolved in water or silica-bound. The fractions of respective correlation times are accurately determined from TRFA decays and reflect the distribution of R6G between the aqueous and silica phases. From the fraction of silica-bound R6G, it is possible to calculate the degree of adsorption of small peptides onto the Ludox particle surface. Indeed, the extent of adsorption follows the expected trend, wherein highly cationic peptides with the largest number of binding sites show greater adsorption as a function of concentration. Potential advantages of the indirect TRFA method for probing interactions of compounds with surfaces include: 1) no need for labeling the competing compound, which may be difficult, or may introduce unwanted changes; 2) the ability to use the method for many different species (polymers, peptides, proteins) and; 3) the ability to change the nature of the probe to assess different types of interactions (electrostatic, H-bonding, hydrophobic), providing a more versatile method for studying interactions of compounds with surfaces. On the other hand, the indirect method had difficulty detecting the adsorption of weakly binding peptides, such as EWE, which could be observed by direct measurement of Trp anisotropy. This suggests that weakly binding molecules cannot effectively compete with R6G for binding to the surface. In this case, a weaker binding fluorescent probe may be more suitable for adsorption studies. It should also be noted that neither method can provide absolute quantitation of surface coverage, but rather they provide only an assessment of *relative* changes in adsorption as a function of peptide charge and concentration. Even so, the indirect measurement

method still has significant utility, particularly for evaluating potential surface modification methods that may be used to reduce adsorption. Thus, TRFA measurements should be useful for characterization of the adsorption behavior of biomaterials, antifouling surfaces and new chromatographic stationary phases.

4.5 References

1. Jin, W; Brennan, J.D. *Anal. Chim. Acta* **2002**, *461*, 1.
2. Gill, I. *Chem. Mater.* **2001**, *13*, 3404.
3. Wang, R.; Narang,U.; Prasad, P.N.; Bright, F.V. *Anal. Chem.* **1993**, 65, 2671.
4. Flora,K.; Brennan, J.D. *Chem. Mater.* **2001**, 13, 4170.
5. Gottfried, D. S.; Kagan, A.; Hoffman, B. M.; Friedman, J.M. *J. Phys. Chem. B* **1999**, 103, 2803.
6. Jordan, J. D.; Dunbar, R.A.; Bright, F.V. *Anal. Chem.* **1995**, 67, 2436.
7. Baker, G.A.; Jordan, J.D.; Bright, F.V. *J. Sol-Gel Sci. Technol.* **1998**, 11, 43.
8. Doody, M. A.; Baker, G.A.; Pandey, S.; Bright, F. V. *Chem. Mater.* **2000**, 12, 1142.
9. Khan,I.; Shannon, C. F.; Dantsker, D.; Friedman, A.J.; Apodaca, J. P.-G.-de.; Friedman, J.M. *Biochem.* **2000**, 39, 16099.
10. Geddes, C. D.; Birch, D. J. S. *J. Non-Cryst. Solids* **2000**, *270*, 191.
11. Birch, D. J. S.; Geddes, C. D. *Phys. Rev. E.* **2000**, *62*, 2977.
12. Geddes, C. D.; Karolin, J.; Birch, D. J. S. *J. Fluoresc.* **2002**, *12*, 113.
13. Geddes, C. D.; Karolin, J.; Birch, D. J. S. *J. Fluoresc.* **2002**, *12*, 135.
14. Geddes, C. D. *J. Fluoresc.* **2002**, *12*, 343.
15. Tleugabulova, D.; Duft, A.M.; Brook, M.A.; Brennan, J. D. *Langmuir* **2004**, *20*, 101.

16. Tleugabulova, D.; Zhang, Z.; Chen, Y.; Brook, M.A.; Brennan, J.D. *Langmuir*, **2004**, *20*, 848.

17. Coradin T., Durupty O., Livage J. *Langmuir*, **2002**, *18*, 2331.

18. Zheng, L.; Reid, W.R.; Brennan, J.D. *Anal. Chem.* **1997**, *69*, 3940.

19 Tleugabulova, D., Duft, A. M.; Zhang, Z.; Chen, Y.; Brook, M. A.; Brennan, J. D.; *Langmuir* **2004**; *20*, 5924.

20. Geddes, C. D.; Karolin, J.; Birch, D. J. S. *J. Phys. Chem. B* **2002**, 106, 3835.

21. Tleugabulova, D.; Sui, J.; Ayers, P.; Brennan, J.D. *J. Phys. Chem. B*, in press.

22 Lakowicz, J. R., Maliwal, B., Cherek, H., Balter, A. *Biochemistry* **1983**, *22*, 1741.

23. Durupthy, O.; Coupe, A.; Tache, L.; Rager, M.-N.; Maquet, J.; Coradin, T.; Steunou, N.; Livage, J. *Inorg. Chem.* **2004**, *43*, 2021.

24 Tleugabulova, D.; Sui, J.; Ayers, P.; Brennan, J.D. J. Phys. Chem. B, 2005, 109, 7850.

Chapter 5

Using a Long-lived Fluorescent Quinolinium Dye to Probe Protein Adsorption on Native and Modified Colloidal Silica Nanoparticles by Time-Resolved Fluorescence Anisotropy

This chapter is based on work that was performed solely by me with input from both Dr. Brennan and Dr. Tleugabulova. Dr. Brennan and I were responsible for the design of the majority of the experiments, while Dr. Tleugabulova suggested model systems to investigate modified silica surfaces. I was responsible for writing the first draft of the chapter, while Dr. Brennan provided editorial input.

This chapter is targeted for submission to *Langmuir*.

Abstract

Recently, we reported on the use of time-resolved fluorescence anisotropy of rhodamine 6G (R6G) to monitor adsorption of polymers and small peptides onto colloidal silica surfaces based on partitioning of the dye between bound and free states. The present work extends the application of TRFA to monitor protein adsorption onto plain and modified silica particles. A recently reported cationic long-lifetime quinolinium dye, CG437, which strongly binds to anionic silica particles through electrostatic interactions, was used to directly probe alterations in the rotational correlation time of Ludox particles resulting from increases in the diameter of the rotating body upon binding of protein to the silica surface. The results were correlated to those obtained by monitoring the flocculation and intrinsic Trp steady-state anisotropy of anionic (Human Serum Albumin, HSA) and cationic (monellin) proteins present in Ludox sols. The results showed that the TRFA analysis of the long-lived probe provided data that correlated well with that obtained by direct monitoring of the protein anisotropy, and showed that monellin bound to plain silica surfaces, resulting in concentration-dependent increases in rotational correlation times, while HSA did not. Modification of the silica surface with the cationic silane aminopropyltriethoxysilane (APTES) blocked the binding of monellin and did not promote adsorption of HSA, indicating that such modified surfaces can significantly reduce protein adsorption. CG437 time-resolved fluorescence anisotropy in Ludox sols show that rotation correlation time increases as a function of monellin concentration, however the similar change is not found in control protein HSA. The study shows that TRFA analysis of long-lived cationic probes such as CG437 can provide an effective method to investigate interactions between proteins and modified silica surfaces, extending the utility of the TRFA method.

5.1 Introduction

The development of sol–gel derived materials used to encapsulate biological species such as enzymes, antibodies and other proteins in a functional state has been an area of intense interest in the past decade.[1,2] Typical applications of these sol-gel biomaterials include selective coatings for optical and electrochemical biosensors,[3-8] stationary phases for affinity chromatography,[9,10,11] immunoadsorbent and solid-phase extraction media,[12,13] controlled release agents[14-22] and development of solid-phase biosynthesis platforms.[23-26]

The interaction of entrapped proteins with the internal silica surfaces can cause significant decreases in protein dynamics and may lead to protein denaturation. Such interactions are typically evaluated using time-resolved fluorescence anisotropy (TRFA), which can assess the rotational dynamics of fluorescently labeled proteins after entrapment in sol-gel derived materials.[27 - 33] Unfortunately, the size and complexity of proteins and the range of different microenvironments within sol-gel derived silica results in a wide array of different protein motions that occur on different timescales. This situation can make the anisotropy decay complicated and very difficult to interpret. To overcome such issues, it is necessary to develop appropriate model systems that display reliable and easily interpretable dynamic motions, and yet provide sufficient complexity to allow insights into the parameters that affect protein-silica interactions.

Recently, our research group demonstrated that a simple system involving the cationic fluorophore rhodamine 6G (R6G) bound to anionic Ludox nanoparticles could be used in conjunction with TRFA measurements to assess the degree of silica surface modification and peptide:silica interactions.[34,35,36] In such a system, short (ps timescale) rotational correlation times correspond to probe that is free in solution,

long (ns scale) rotational correlation times correspond to dye molecules that are electrostatically bound to primary anionic silica nanoparticles, while residual anisotropy (r_∞) values correspond to dye molecules that are rigidly bound to larger (> 4.5 nm radius) particles, and thus rotate too slowly to cause fluorescence depolarization during the emission lifetime of R6G.[34] It was shown that the modification of silica particles with polymers, organosilanes or tripeptides caused a higher proportion of R6G to be in solution relative to that adsorbed to unmodified surfaces (i.e., higher fraction of the ps decay component), indicating that adsorption of the dye could be blocked using appropriately modified surfaces.

While the use of R6G:Ludox system has allowed monitoring of surface modification, attempts to extend this system to the monitoring of protein adsorption revealed several drawbacks. Firstly, the system is designed to have a very low probe loading (1 probe for every 14 particles), and thus adsorption of large species such as proteins, does not lead to significant repartitioning of probes. This is possibly due to preferential binding of proteins to larger Ludox particles, which could accommodate both the bound probe and the protein, preventing repartitioning of probe. Secondly, adsorption of protein to R6G:Ludox systems does not lead to any observable changes in rotational correlation times. Again, this suggested binding of protein to larger Ludox particles, which rotate too slowly to be observed using the short-lived R6G (~4 ns decay), and thus contribute only to the residual anisotropy. Finally, it is not possible to use the R6G:Ludox system to monitor protein adsorption to polymer or organosilane-modified surfaces, since the modification blocks binding of R6G, making it impossible to assess binding of secondary species to the modified surfaces.

To overcome the problems with short lived probes and to extend our studies to modified surfaces, we have examined the use of a long-lived cationic fluorescent

probe, CG437 (6-methoxy-1-(3-propanol) quinolinium bromide), which was recently reported by Geddes *et al.*,[37] to directly measure the rotational correlation time of large Ludox particles. By using a dye loading that is relatively high, most of the particles are expected have at least one dye bound. Upon addition of protein the radius of the rotating body should increase, and thus the value of the longest decay time should increase in proportion to the amount of protein that is bound to the silica surface. This method should also be able to assess protein interactions with modified silica surfaces, since even heavily modified surfaces are expected to be able to bind at least one dye molecule, which will remain bound and thus able to report on particle rotation even after a protein binds.

Herein, we examine the adsorption of cationic and anionic proteins to native and APTES modified silica surfaces using time-resolved fluorescence anisotropy of CG437, and compare the results to those obtained by flocculation studies and by directly monitoring Trp steady-state anisotropy from the proteins. The results demonstrate that TRFA of the CG437/Ludox system provides a useful new tool for probing the interactions of proteins with both native and modified silica surfaces.

5.2 Experimental Section

5.2.1 Chemicals

Monellin from *Dioscoreophyllum cumminsii* (serendipity berry), human serum albumin (HSA, essentially fatty acid free), melittin, ribonuclease T1, lyzozyme, polylysine (MW 2,500 and 41,000) and polyglutamic acid (MW 17,000) were obtained from Sigma (St. Louis, MO). Ludox AM-30, (30 wt% SiO_2 in water, d=1.210, average particle radius of 6 nm, specific surface area of 220 $m^2 \cdot g^{-1}$), (3-aminopropyl)triethoxysilane (APTES), 6-methoxyquinoline and 3-bromo-1-propanol

were purchased from Aldrich (Milwaukee, WI). All water was distilled and deionized using a Milli-Q Synthesis A10 water purification system. All other reagents were of analytical grade and were used as received.

5.2.2 Procedures

5.2.2.1 *Synthesis and Characterization of CG437*

Synthesis of the fluorescent probe was done according to the method described by Geddes and Birch.[37] 19 g (0.12 mol) of 6-methoxyquinoline and 16.8 g (0.12 mol) of 3-bromo-1-propanol were heated under reflux for 3 h at 70 °C. After cooling, 300 ml of acetone was added and the mixture was stirred continuously for 20 h. After continual washing with acetone, the resulting white precipitate was recovered to give 17.9 g (51% yield) of product. The structure was characterized by ^{1}H NMR, mass spectrometry, infrared, UV-Vis and fluorescence spectroscopy. All spectra conformed to the expected product (see supplementary data).

5.2.2.2 *Labeling of HSA*

Labeling of HSA at cysteine-34 using fluorescein-5-maleimide was done according to standard procedures.[38] Briefly, 100 μM HSA was combined with a 25-fold molar excess of fluorescein-5-maleimide in a buffer system consisting of 20 mM HEPES buffer containing 100 mM NaCl and 5 mM EDTA and reacted for 24 h in the dark. The labeled protein was then purified four times by size-exclusion chromatography using a Sephadex G-25 column. The concentration of labeled protein was found using $\varepsilon_{473} = 83000\ M^{-1}\ cm^{-1}$ for fluorescein (dianion)[39] and $\varepsilon_{277} = 36000\ M^{-1}\ cm^{-1}$ for HSA.[40] The labeling efficiency was determined to be 44%.

5.2.2.3 *Sample Preparation*

All samples were prepared daily and contained Ludox (0 - 14 wt% SiO_2) and 0 - 20 μM protein diluted with 10 mM HEPES buffer, pH 7.5. In cases where the protein or modifier induced flocculation of Ludox particles, a lower protein or modifier concentration was used to assure optical transparency and sample stability during the TRFA measurement. The samples for CG437 anisotropy studies contained 40 μM of the probe in addition to the protein, modifier and Ludox. Under these conditions, there are ~3 probe molecules bound per Ludox particle (in the absence of protein), based on the specific surface area, density and the radius of Ludox particles and assuming complete adsorption of CG437 molecules to the silica particles.

5.2.2.4 *Modified Colloidal Silica*

2 mL of Ludox (1.5 wt%) in 10 mM HEPES buffer, pH 7.5 was mixed with 1 – 10 μL of APTES and allowed to react for 10 min, after which CG437 was added to a final concentration of 40 μM followed by the addition of various concentrations of protein (0 – 20 μM of HSA or monellin). The upper limit of APTES concentration under these conditions was 0.5 wt%, after which the sample underwent flocculation. Below this limit, the surface-modified sols showed excellent colloidal stability for at least 1 week. Only optically transparent, nonflocculated sols were used for fluorescence measurements.

5.2.2.5 *Silica Flocculation Study*

Initial studies focused on flocculation of silica by proteins with varying pI values and sizes as a preliminary screen of protein-silica interactions. Flocculation measurements were performed on samples containing 50 μL of 1.5 wt% SiO_2 by

measuring absorbance at 410 nm from samples containing 0 – 500 μM of protein in 96 well plates using a TECAN Safire absorbance/fluorescence platereader. In this case all absorbance changes are due to scattering of light owing to protein-induced flocculation of silica as a result of protein-silica interactions. The values reported represent the average of 20 measurements each on three different samples.

5.2.2.6 *Fluorescence Measurements*

Steady-state fluorescence anisotropy measurements were performed using a SLM 8100 spectrofluorimeter (Spectronic Instruments, Rochester, NY) as described elsewhere.[41] Single point fluorescence anisotropy measurements were made for Ludox in the presence of 100 μM protein solutions at λ_{ex} = 370 nm, λ_{em} = 437 nm for CG437, at λ_{ex} = 295 nm, λ_{em} = 335 nm for Trp and at λ_{ex} = 495 nm, λ_{em} = 552 nm for fluorescein-5-maleimide labeled HSA. The values reported represent the average of 5 measurements each on three different samples.

Time-resolved fluorescence intensity and anisotropy decays were acquired in the time-domain using an IBH 5000U time-correlated single photon counting fluorimeter with a TBX-04 PMT detector, as described elsewhere using a pulsed NanoLED source for excitation at 370 nm and monitoring emission at 437 nm.[34-36] For anisotropy decay analysis, the experimentally obtained parallel and perpendicular fluorescence decays were used to generate the sum, *S(t)*, difference, *D(t)* and time-resolved anisotropy, *r(t)*, functions as follows:[42,43,44]

$$r(t) = \frac{I_{VV}(t) - I_{VH}(t)}{I_{VV}(t) + 2I_{VH}(t)} = \frac{D(t)}{S(t)} \quad (1)$$

The anisotropy decay was fit to a two-component hindered rotor model according to the following equation:[45]

$$r(t) = f_1 r_0 \exp(-t/\phi_1) + f_2 r_0(-t/\phi_2) + g r_0 \quad (2)$$

where r_0 is the limiting anisotropy at $t = 0$, ϕ_1 ($\phi_1 < \phi_2$) reflects average of isotropic rotational motions for CG437 bound to small silica particles, ϕ_2 reflects the slower average reorientation time of CG437 bound to larger silica particles, f_1 is the (small) fraction of fluorescence originating from ϕ_1, f_2 is the fraction of fluorescence originating from ϕ_2, and g is the fraction of fluorescence due to CG437 that is rigidly bound to very large particles that rotate more slowly than can be measured with the CG437 probe ($\phi > 450$ ns, radius > 8 nm) and thus is assessed as "non-motion". It should be noted that the value of gr_0 is equivalent to the residual anisotropy, r_∞, which is the anisotropy at $t \rightarrow \infty$. Fits were considered acceptable if the reduced chi-squared (χ_R^2) was close to 1.0 and the residuals showed a random pattern.

5.3 Results and Discussion

5.3.1 Characterization of Synthesized Probe

The structure of the fluorescent probe is shown in Figure 5.1.

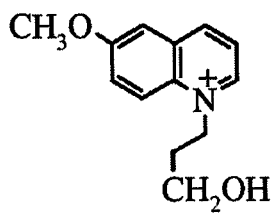

Figure 5.1 CG437 Structure

Figures 5.2 and 5.3 show ^{1}H NMR (D_2O) and IR spectra of both the reactant 6-methoxyquinoline and the product CG437. For 6-methoxyquinoline ^{1}H NMR (D_2O): δ 3.8 (s, 3H), 7.4-8.7 (m, 6H); IR: 1591, 1622 and 2937cm^{-1}. For CG437 ^{1}H NMR

(D_2O): δ 2.3 (m, 2H), 3.7 (t, 2H), 4.0 (s, 3H), 5.1 (t, 2H), 7.7-9.0 (m, 6H); IR: 1591, 1622, 2937 and 3261cm^{-1}.

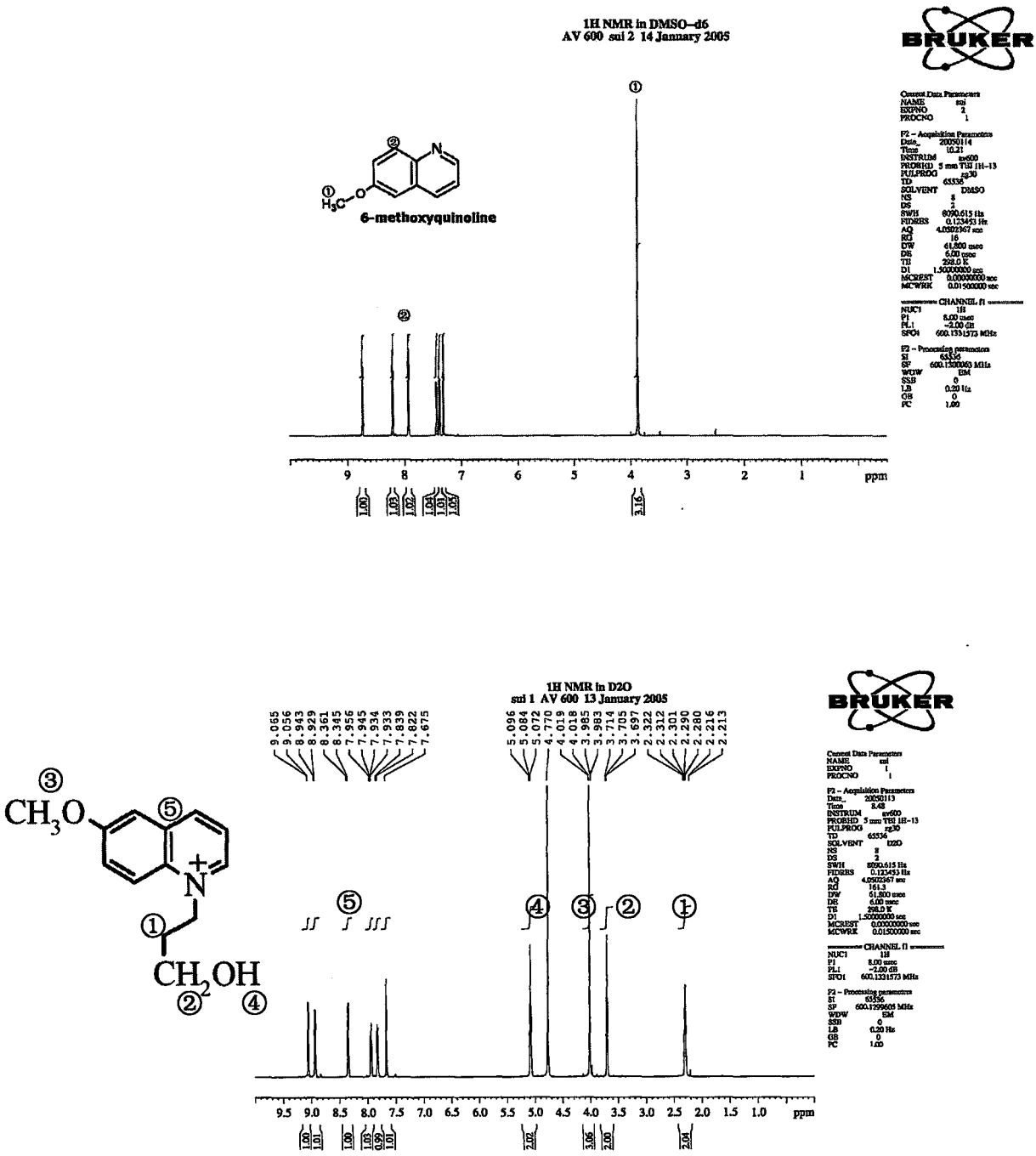

Figure 5.2 ^1H NMR (D_2O) of 6-methoxyquinoline and CG437

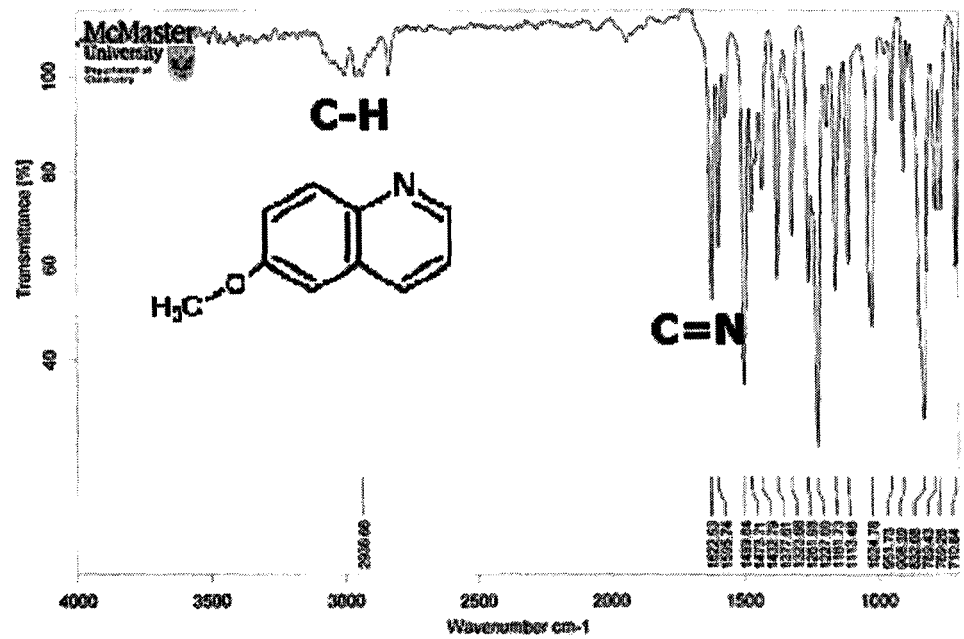

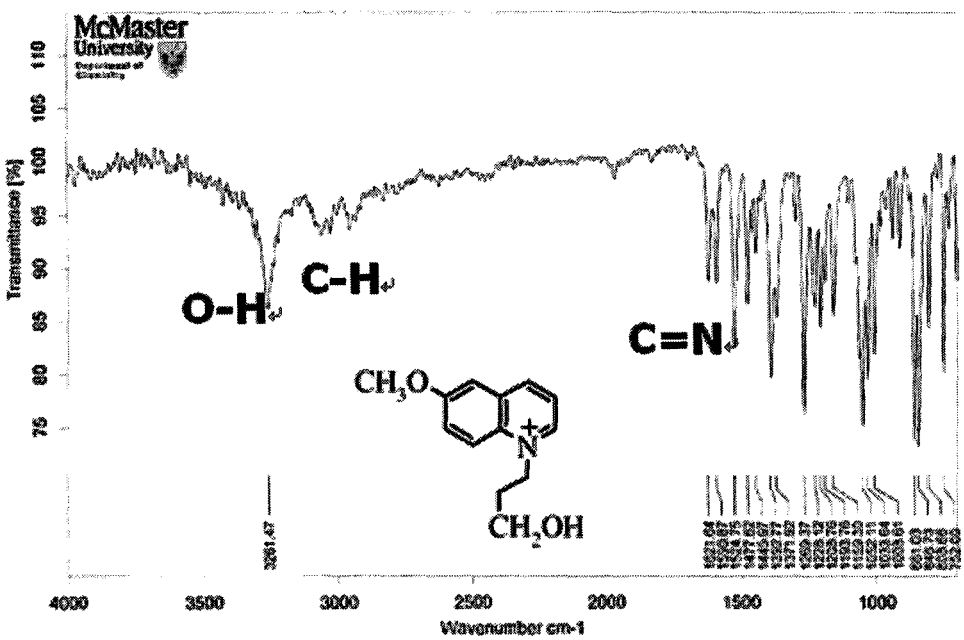

Figure 5.3 IR spectra of 6-methoxyquinoline and CG437

MS of CG437 (Figure 5.4): m/z 218.2 (M^+). Absorption spectra of 40 μ M CG437 show two peaks with λ_{max} at 320nm and 345nm (Figure 5.5), which are in accordance with the spectra provided by Geddes et al.[37] The emission spectrum (Figure 5.6) shows the expected peak at 437 nm in both buffer and diluted Ludox solutions.

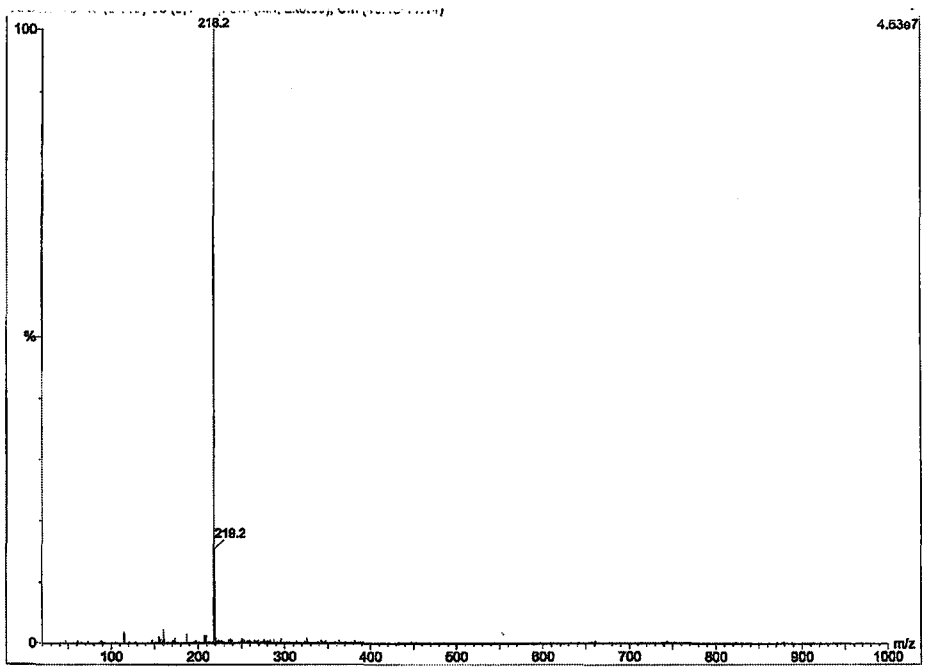

Figure 5.4 MASS Spectrum of CG437

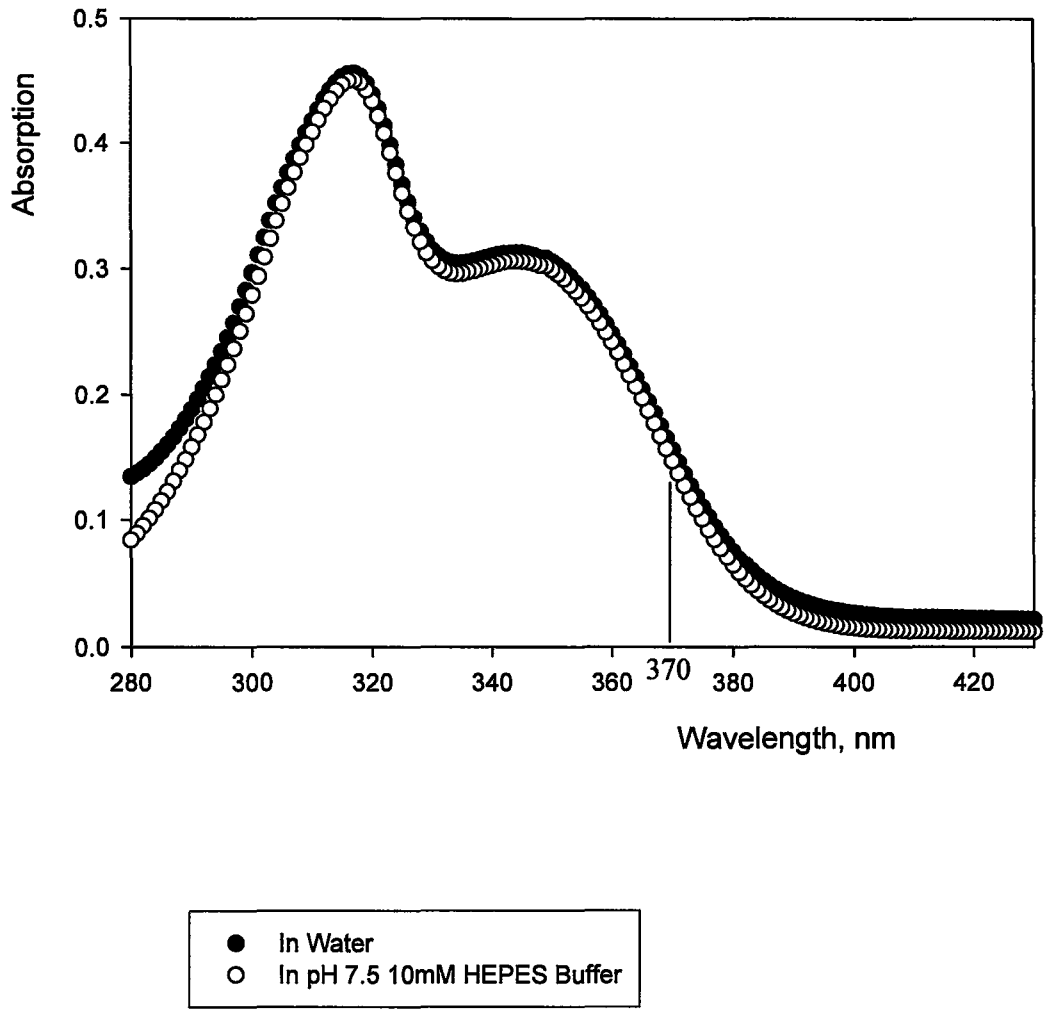

Figure 5.5 Absorption spectra of 40μM CG437

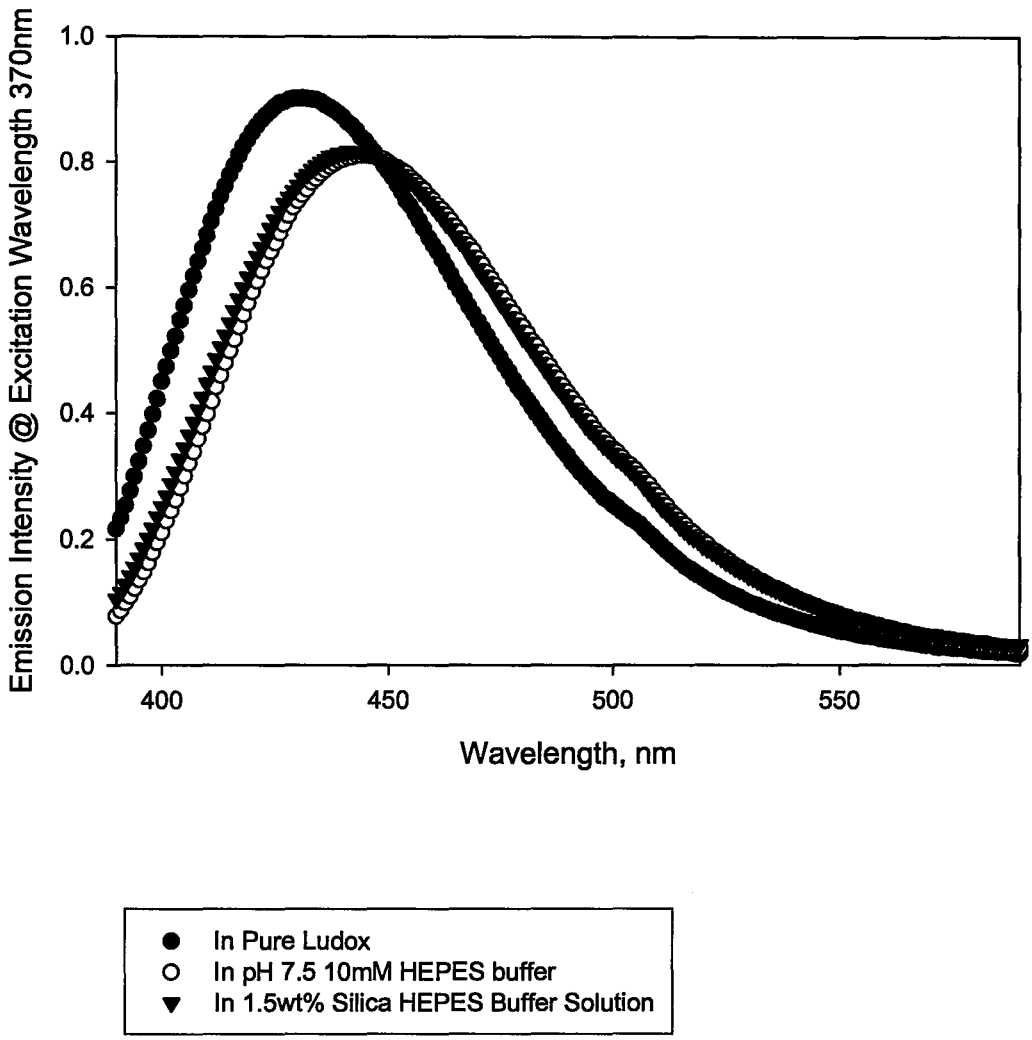

Figure 5.6 Emission spectra of 40μM CG437

5.3.2 Silica Flocculation

Preliminary screening of protein:silica interactions was done by monitoring the flocculation limits of Ludox in the presence of various proteins with different sizes and pI values, based on the assumption that such interactions would lead to bridging between individual particles and cause increased flocculation. The proteins studied included HSA (pI 5.6, MW 60,000), melittin (pI 12.8, MW 2,800), RNAse T1 (pI 2.9, MW 11,000) lysozyme (pI 11.0, MW 14,000) and monellin (pI 9.3, MW 10,700),

each of which have at least one Trp residue to allow for further examination of protein:silica interactions using intrinsic fluorescence measurements. Polylysine (PL, MW 2500 and 41,000, pI = 9.59) and polyglutamic acid (PGA, pI 3.2, MW 17,000) were used as model non-fluorescent cationic and anionic peptides to provide positive and negative controls. These proteins and peptides bracket the physiological pH range (pH 7.4) and thus will be cationic (Lysozyme, melittin, monellin, PL) or anionic (HSA, RNAse T1, PGA) under the conditions used in this study.

As shown in Figure 5.7, the absorbance of Ludox (which results from light scattering) containing the negative model peptide PGA shows a negligible change as the peptide concentration increases over the range of 0 – 500 μM, indicative of no interaction between the anionic peptide and anionic silica surface. However, all other proteins and peptides showed increases in absorbance as a function of their concentrations, owing to increased light scattering upon flocculation of Ludox. In the absence of Ludox the absorbance of the samples at 410 nm was negligible even at protein concentrations up to 500 μM, (data not shown) indicating that the observed changes in absorbance were not due to protein aggregation.

The extent of flocculation was dependent on both the nature and concentration of the protein. Cationic proteins such as lysozyme, monellin and melittin, and the cationic peptide PL (both MW 2500 and 41,000) led to significant flocculation, which increased with biomolecule concentration, consistent with interactions between the cationic proteins and the anionic silica surface. The extent of flocculation does not appear to depend on the molecular weight of the protein/peptide, with both the small peptide monellin and the large (41 kDa) PL peptide producing similar levels of flocculation. The anomalously high flocculation for lysozyme is not fully understood

at this time, but may relate to an ability to bridge several particles and produce larger overall aggregates.

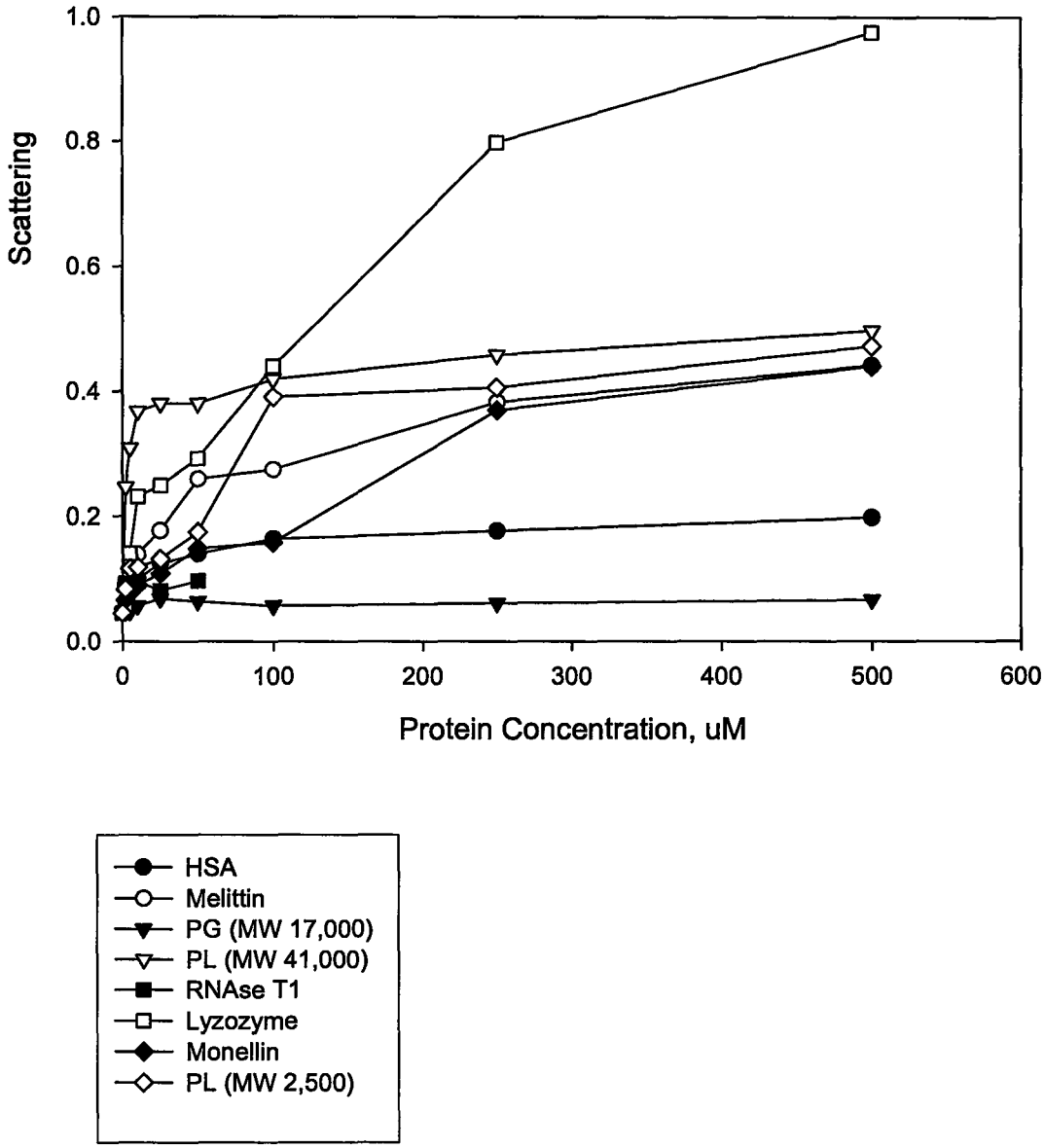

Figure 5.7. Absorption changes to monitor the flocculation of Ludox (1.5 wt%) by HSA, melittin, PG (MW 17,000), RNAse T1, lysozyme, monellin, PL (MW 41,000) and PL (MW 2,500)

Flocculation occurred to a much lesser extent for anionic proteins such as HSA and RNAse T1, and was particularly low for HSA even at concentrations up to 100 μM, indicating that there are only weak interactions between HSA and silica particles. RNAse T1 studies were done only up to 50 μM owing to the low concentration of the stock solution available for this enzyme. Overall, Figure 5.7 shows that the pI value of the protein is the key factor determining the flocculation properties with silica particles, consistent with electrostatic interactions being the predominant driving force for protein-silica interactions.

5.3.3 Monitoring of Protein Adsorption via Trp Steady-State Anisotropy

To further evaluate the extent of protein:silica interactions, the steady-state fluorescence anisotropy of the Trp residue within HSA and monellin was monitored as a function of Ludox concentration. These were chosen as model proteins because 1) at pH 7.5 they have opposite charges, which should make them have different binding properties with silica particles, 2) both proteins have only one tryptophan residue which provides a spectroscopic handle to allow direct observation of protein adsorption on native and modified silica via Trp fluorescence anisotropy; 3) the proteins are sufficiently large that they would be expected to cause a significant alteration in the rotational correlation time of the Ludox particle, allowing for extension to studies using CG437 (described below).

Figure 5.8 shows the changes in Trp steady-state anisotropy for both HSA and monellin as a function of increasing Ludox concentration. To ensure that the changes in anisotropy were due to alterations in rotational correlation times rather than artifacts due to increased scatter, two control experiments were done. Firstly, the

anisotropy of N-acetyltryptophanamide, which is not expected to bind to Ludox, was monitored as Ludox concentration was increased up to 7.5 wt%.

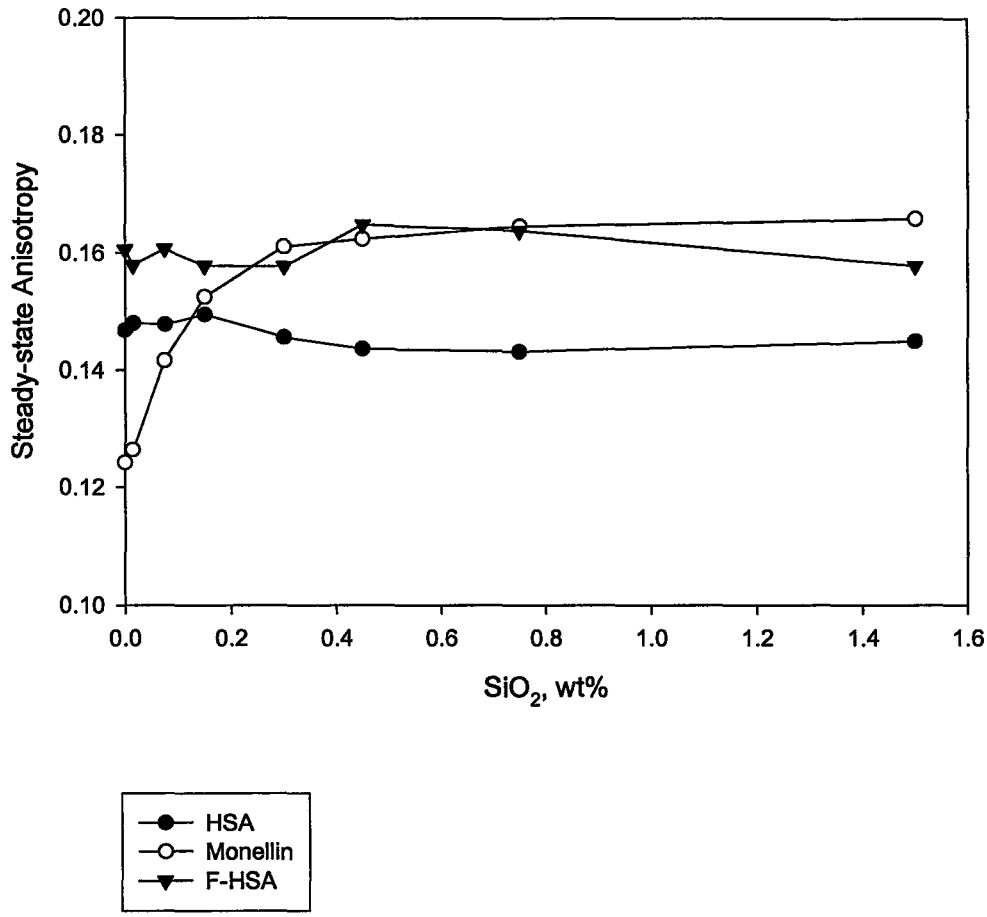

Figure 5.8. Steady-state fluorescence anisotropy of HSA (●), Monellin (○) and F-HSA (▼) at λ_{ex} = 295 nm, λ_{em} = 335 nm and for HSA-F at λ_{ex} = 495 nm, λ_{em} = 552 nm as a function of silica concentration. Samples contained 100 μM of the Monellin, HSA and 20 μM F-HSA. NOTE: 20μM is the maximum concentration of F-HSA that could be obtained after four times of purification by size-exclusion chromatography using a Sephadex G-25 column.

No changes in either intensity levels (I_{VV} or I_{VH}) or anisotropy were observed in this case, indicating that non-flocculated Ludox did not lead to increased anisotropy values. Secondly, the intensity observed in the emission channel of the fluorimeter was monitored under parallel and perpendicular polarization conditions with excitation at 295 nm and emission at 335 nm as Ludox as added to a sample of 41 kDa PL. In this case, signals resulting solely from increased scattering owing to particle flocculation can be measured to allow for correction of Trp anisotropy values. The intensity values in both the parallel and perpendicular channels were observed to be negligible relative to the intensity of the Trp signal form HSA and monellin (<1%), indicating that the Trp anisotropy values were reliable even when Ludox was partially flocculated. It should be noted that at a protein concentration of 100 μM, Ludox samples containing both monellin and HSA showed a similar (low) level of scattering, suggesting that flocculation was not significant for these samples.

As shown in Figure 5.8, monellin displayed increases in anisotropy as a function of the silica concentration, and reached a maximum anisotropy of 0.165 at 0.45 wt% silica, after which the anisotropy value plateaued. In the case of HSA, the anisotropy started from a higher anisotropy value ~0.145 than monellin (~0.125) due to the larger molecular size and more restricted rotational freedom of the Trp residue. However, addition of Ludox led to no increase in HSA anisotropy, and indeed appeared to produce a small decrease in anisotropy. Given the large size of HSA, it is possible that adsorption may occur through a site that is far removed from the Trp residue, and would thus allow freedom of movement for domain II (containing the Trp residue), minimizing changes in anisotropy. To ensure that the lack of an increase in anisotropy did correlate to a lack of adsorption, the protein was labelled in at Cys 34

in domain I with fluorescein. As shown in Figure 5.8, the anisotropy was still unaffected by the addition of Ludox, confirming that the protein did not adsorb to the surface.

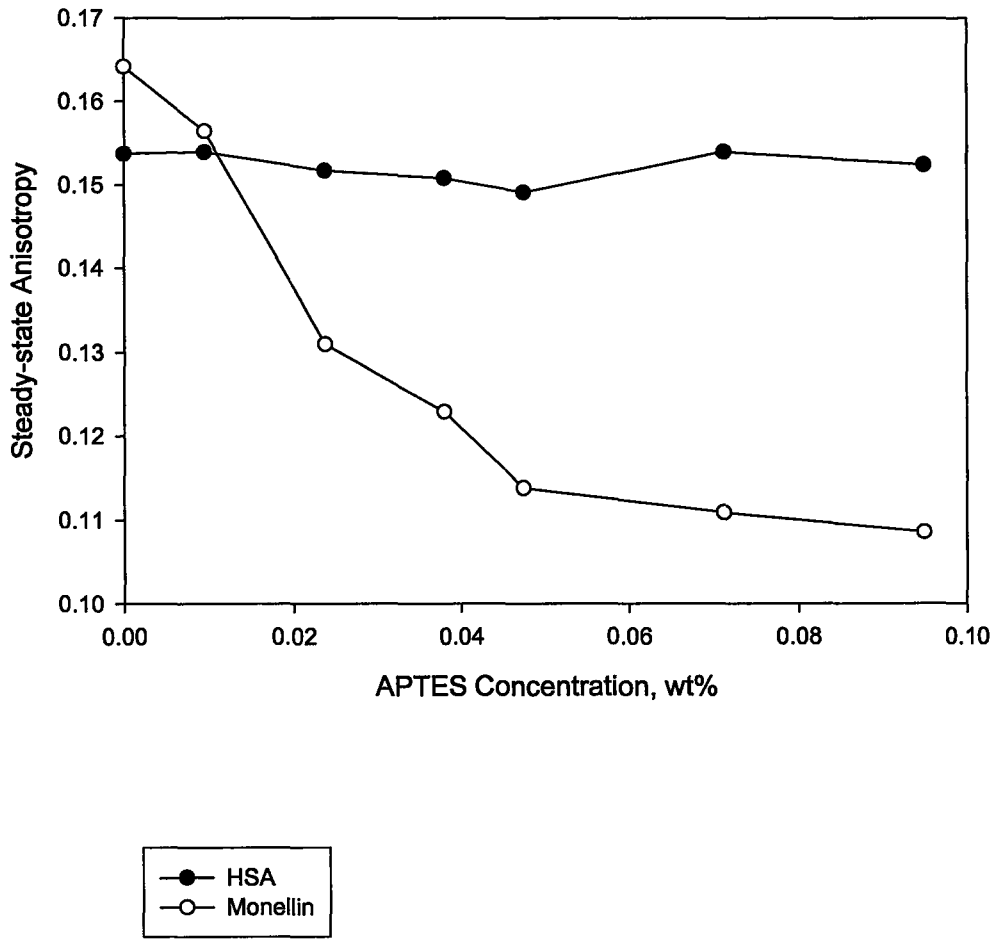

Figure 5.9 Steady-state fluorescence anisotropy of HSA (●) and Monellin (○) at λ_{ex} = 295 nm, λ_{em} = 335 nm as a function of APTES concentration. Samples contained 100 μ M of the proteins and 1.5 wt% silica.

Previous studies from our group have shown that low levels of APTES can be used to obtain significant surface modification of Ludox, with up to 80% of the

particle surface being covered by APTES.[35] As a preliminary step toward examining the interaction of proteins with modified silica surfaces, the anisotropy of both HSA and monellin was examined in HEPES solutions containing 1.5 wt% silica modified with different amount of APTES prior to the addition of protein. As shown in Figure 5.9, the anisotropy of monellin decreased dramatically as amount of APTES increased, returning to a values that was similar (indeed slightly lower) than that obtained form monellin in aqueous solution. This decrease in anisotropy is consistent with APTES binding to the silica surface and thus blocking the binding of the cationic protein monellin. This is in agreement with previous studies from our group, which have shown that modification of Ludox with APTES leads to a decrease in the binding of cationic fluorescent probes, such as R6G, to the silica surface.[35] On the other hand, the anisotropy of HSA remained essentially constant even at the highest level of APTES, suggesting that the anionic protein did not bind to cationic amino groups present on the silica surface. This is consistent with previous reports, which suggest that the ammonium group of APTES will undergo electrostatic interactions with siloxide groups on the Ludox surface, preventing the ammonium group from binding to anionic species present in solution.[35]

5.3.4 TRFA of CG437 Protein/Ludox Mixtures

To obtain more detailed information on the binding of the proteins to the Ludox particles, time-resolved fluorescence anisotropy was used to assess the individual rotational motions of CG437 in native and APTES-modified Ludox systems containing HSA or monellin. Table 5.1 shows all fitting parameters of the CG437 anisotropy decays as a function of protein concentration. The intensity decays of CG437 in Ludox and Ludox/protein mixtures were bi-exponential, with two lifetimes

of ~ 12ns (~ 45%) and ~ 27ns (~ 55%), which is slightly different from the results of Geddes [18.50 ± 0.66ns (38.6%) and 28.24 ± 0.13ns (61.4%) CG437/H_2O]. The origin of this result is not fully understood, but may be due to the presence of the Ludox, which could alter the electronic properties of the positively charged probe when it adsorbs to the silica surface.

The adsorption of CG437 to Ludox also causes a significant reduction in the rotational anisotropy of the probe, which is consistent with significant damping of the isotropic rotation of the CG437 dipole. As a result, as shown in Table 5.1, the anisotropy of CG437 does not decay to a value of zero (g ~ 0.18 for Ludox and Ludox/protein systems), indicative of a significant fraction of dye that is rigidly bound to silica structures that rotate too slowly to cause fluorescence depolarization during the emission lifetime of this probe. In the case of CG437, using a mean lifetime of 20 ns, this would correspond to rotational correlation times of >300 ns (15 τ), which would relate to dyes that are rigidly bound to particles larger than 6 nm in radius. Furthermore, a second rotational correlation time of ca. 24 ns appears in the nanosecond time range, which we attribute to binding of CG437 to smaller particles with an average radius diameter of 2.6 nm present in the Ludox sol.[46] Taken together, the percentage of bound dye, given by (f_2 + g), is on the order of 98%, and thus it is likely that the majority of CG437 molecules are bound to the silica surface in the Ludox sample. The small proportion of a faster correlation time (ca. 2% of a 2 – 3 ns rotational component) may reflect "wobble" motion of CG437 bound to the silica particles or could be an average of rotational motions for free CG437 and dye bound to very small silica nanoparticles. However, the small proportion of this value, and the fact that is does not change significantly upon introduction of proteins, along with the fact that the f_1, f_2 and g values remain constant within error as protein concentration

increases, indicates that CG437 adsorbs strongly to the silica surface and cannot be replaced by the adsorption of proteins onto the surface.

While the proportions of the various rotational components were not affected by the addition of protein, Figure 5.10 shows that increased levels of monellin led to corresponding increases in the longer rotational correlation time, from 24.3 ns (0 μM monellin) to 35.9 ns at 20 μM monellin, indicative of an increase in particle size as more protein bound. The final particle diameter was ca. 3 nm, representing an apparent increase in diameter of 0.4 nm. While this is much smaller than would be expected for binding of a monolayer of protein to the surface (protein diameter is ca. 2 nm), it must be noted that the correlation times were obtained at relatively low monellin levels (20 μM), and hence only a small fraction of silica particles would be expected to have a protein bound, leading to the relatively small increase in the average rotational correlation time. This is also in general agreement with the results from both the flocculation study and the measurement of Trp fluorescence, which indicated that saturation of monellin binding to the silica surface occurred at much higher protein levels (*ca.* 250 μM). In the case of HSA, the rotational correlation time remained essentially constant up to 20 mM of protein, indicating no detectable binding between HSA and silica particles, consistent with the flocculation and steady-state fluorescence anisotropy results.

5.3.5 TRFA of CG437 in APTES modified Ludox

Table 5.2 shows the fits to the CG437 intensity and anisotropy decays in APTES-Ludox solutions with and without proteins. Several features merit special attention. Firstly, the presence of APTES resulted in CG437 exhibiting a three component decay, with a small proportion (~4%) of a 4 ns lifetime being present. This additional

Table 5.1. Time-resolved fluorescence anisotropy decay parameters of CG437 in 10 mM, pH=7.5 HEPES buffer solution and in 1.5wt% SiO_2 in the presence of varying levels of proteins.[a]

a) ϕ_1, ϕ_2, rotational correlation times; f_1, fractional contribution to anisotropy decay owing to ϕ_1; f_2, fractional contribution to anisotropy decay owing to ϕ_2; g, fraction of fluorescence arising from slow motion of probes corresponding to limiting anisotropy ($g = r_\infty/r_0$). Typical errors in r_∞, r_0, f_1 and f_2 are ± 0.02, error in g is ± 0.03.

	Ludox+CG437	1μM Monellin	5μM Monellin	15μM Monellin	20μM Monellin	1μM HSA	5μM HSA	15μM HSA	20μM HSA
τ, ns^a	11.4 ± 0.06 (43.92%) 26.4±0.450 (56.08%)	11.4 ± 0.672 (45.52%) 26.7±0.533 (54.48%)	11.1 ± 0.615 (44.12%) 26.2±0.470 (55.88%)	10.7 ± 0.07 (42.83%) 25.7±0.510 (57.17%)	12.1 ± 0.37 (44.33%) 27.6±0.596 (55.6%)	11.2 ± 0.17 (43.60%) 26.6±0.120 (56.40%)	11.7 ± 0.28 (46.84%) 25.9±0.516 (53.16%)	11.9 ± 0.54 (44.60%) 26.6±0.12 (55.40%)	12.2 ± 0.85 (50.05%) 28.9±0.84 (49.95%)
χ_R^2	1.09	1.11	1.12	1.20	1.20	1.14	1.07	1.12	1.20
ϕ_1, ns	2.47 ± 0.278	1.98 ± 0.249	2.19 ± 0.273	2.55 ± 0.198	2.27 ± 0.248	1.91 ± 0.287	2.81 ± 0.72	2.77 ± 0.717	2.76 ± 0.24
ϕ_2, ns	24.3 ± 1.49	28.5 ± 1.51	30.43 ± 1.67	33.16 ± 1.31	35.90 ± 1.64	25.2 ± 1.44	24.6 ± 2.09	21.8 ± 0.83	23.4 ± 0.95
r_0	0.297	0.307	0.318	0.299	0.293	0.289	0.289	0.291	0.293
r_∞	0.178	0.180	0.196	0.185	0.180	0.172	0.177	0.168	0.176
g	0.599	0.586	0.616	0.619	0.614	0.590	0.612	0.577	0.601
f_1	0.021	0.017	0.017	0.021	0.029	0.014	0.019	0.025	0.021
f_2	0.380	0.397	0.367	0.360	0.357	0.394	0.369	0.397	0.379
χ_R^2	1.06	0.96	1.00	1.13	0.98	1.01	1.02	1.03	1.03

Table 5.2. Time-resolved fluorescence anisotropy decay parameters of CG437 in 10 mM, pH=7.5 HEPES buffer solution and in 1.5 wt % SiO_2, 0.0475% APTES, in the presence of varying levels of proteins.[a]

	APTES Ludox Blank	20μM HSA	20μM Monellin
τ, ns^a	4.74 ± 0.52 (4.16%) 13.7 ± 0.12 (61.51%) 29.3 ± 0.12 (34.33%)	3.73 ± 0.33 (3.05%) 13.5 ± 0.09 (62.37%) 29.1 ± 0.10 (34.58%)	4.46 ± 0.33 (4.35%) 13.8 ± 0.09 (61.18%) 30.1 ± 0.10 (34.46%)
χ_R^2	1.17	1.11	1.04
ϕ_1, ns ϕ_2, ns	0.525± 0.164 28.5 ± 1.45	0.655 ± 0.132 27.1 ± 1.17	0.629 ± 0.174 28.5 ± 1.49
r_0	0.292	0.301	0.287
r_∞	0.156	0.170	0.160
g	0.534	0.565	0.557
f_1	0.005	0.006	0.006
f_2	0.462	0.429	0.436
χ_R^2	0.97	1.05	0.98

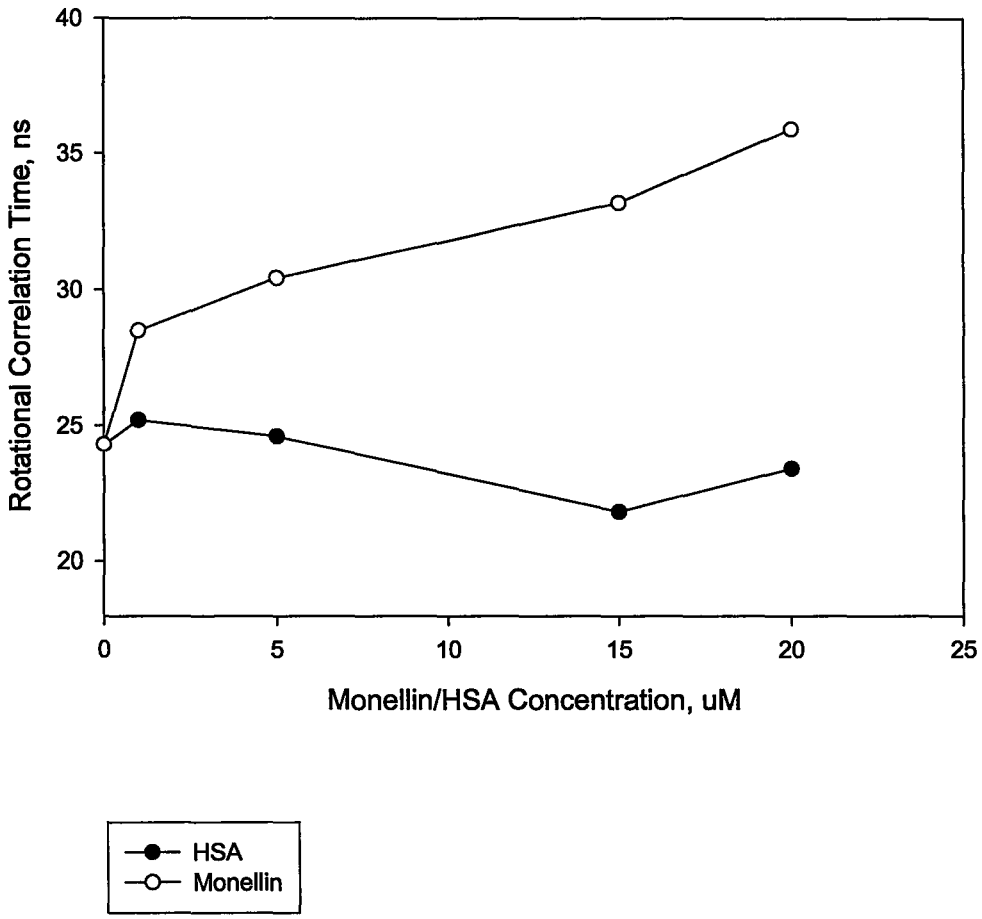

Figure 5.10 CG437 time-resolved fluorescence anisotropy rotational correlation time changes in Ludox silica sols (10 mM HEPES buffer, pH = 7.5, 1.5 wt % SiO_2) at different concentrations of HSA (●) and Monellin (○).

lifetime component may result from the environmental change around the dye due to addition of APTES. Secondly, the faster rotational correlation time decreased from ~2.5 ns without APTES to only 0.5 ns with APTES, but at the same time the proportion of the short lifetime dropped from 2% to ~0.5%, which suggests that this could be a simple fitting artifact. It should be noted that a 0.5 ns correlation time would be at the lower limit of correlation times accessible to the dye, given the average lifetime of 20 ns. Thirdly, the f_2 value increases at the expense of the g value for APTES coated materials, suggesting a slight repartitioning of the dye to smaller particles. This is in agreement with previous studies of Ludox using R6G, which showed an increase in the fractional contribution of the longer correlation time and a dramatic decrease in the g value upon addition of APTES.[35] This has been interpreted as being due to preferential modification of larger particles with APTES. Even though there are small changes in f_2 and g, the data show that ~99.5% of the CG437 dye remains bound in the presence of APTES and can thus report on adsorption of proteins to such particles.

The last point to consider is the effect of both the APTES and proteins on the rotational correlation times of the particles. The addition of APTES results in the value of ϕ_2 increasing from ~24 ns to 28.5 ns, consistent with an increase in the average particle diameter from 2.6 nm to 2.8 nm upon binding of APTES. While this increase is smaller than would be expected from a complete monolayer of APTES, it should be noted that TRFA measures the hydrodynamic radius, i.e. the radius of the particle and the bound water. The addition of APTES could significantly alter the amount of bound water, and thus lead to a lower than expected increase in particle size. Even so, the increase in particle size upon addition of APTES is consistent with binding of the organosilanes to the silica surface. The addition of either monellin or

HSA at levels of up to 20 μM did not lead to any further increase in the rotational correlation time, and hence the diameter, of the APTES modified Ludox particle. This suggests that the APTES effectively blocked adsorption of both the cationic and anionic proteins, consistent with the Trp anisotropy data.

5.4 Conclusions

Previous studies have revealed that TRFA analysis of short-lived probes can be used to assess the adsorption of polymers and peptides to silica nanoparticles. In such cases, the key data relates to the changes in the proportions of the various rotational correlation times. In this work, TRFA analysis of a long-lived fluorescent quinolinium dye, CG437, was shown to be useful for assessing the interaction of biomolecules with both native and modified silica surfaces based on changes in the longer correlation time value, which reveal increases in particle diameter upon adsorption of proteins. The specific changes in hydrodynamic radius are likely to be related to a combination of increases in particle size due to protein adsorption and alterations in the amount of bound water, hence the establishment of the amount of surface coverage from changes in particle diameter is not straightforward. However, the method could show promise in assessing the relative degree of surface modification in cases where a maximum correlation time value can be reached, since adsorption values could then be normalized to the maximum particle size. The data clearly show the power of time-resolved fluorescence anisotropy decay measurements for characterization of the adsorption behavior of proteins, antifouling surfaces and new chromatographic stationary phases.

5.5 References

1. Jin, W; Brennan, J.D. *Anal. Chim. Acta* **2002**, *461*, 1.

2. Gill, I. *Chem. Mater.* **2001**, *13*, 3404.

3. Dave, B.C.; Dunn, B.; Valentine, J.S.; Zink, J.I. *Anal. Chem.* **1994**, 66, 1120A.

4. Lev, O.; Tsionsky, M.; Rabinovich, L.; Glezer, V.; Sampath, S.; Pankratov, I.; Gun, J. *Anal. Chem.* **1995**, 67, 22A.

5. MacCraith, B.D.; McDonagh, C.; McEvoy, A.K.; Butler, T.; O'Keeffe, G.; Murphy, V. *J. Sol–Gel Sci. Technol.* **1997**, 8, 1053.

6. Brennan, J.D., *Encyclopedia of Analytical Chemistry*; John Wiley and Sons, Ltd., Chichester, **2000**, pp. 383-403.

7. Lin, J.; Brown, C.W. *Trends Anal. Chem.* **1997**, 16, 200.

8. Wu, X.J.; Choi, M.F. *Analytica Chimica Acta* **2004**, 514, 219.

9. Tanaka, N.; Kobayashi, H.; Nakanishi, K.; Minakuchi, H.; Ishizuka, N. *Anal. Chem.* **2001**,73, 420A.

10. Tanaka, N.; Nagayama, H.; Kobayashi, H.; Ikegami, T.; Hosoya, K.; Ishizuka, N.; Minakuchi, H.; Nakanishi, K.; Cabrera, K., D. ; Lubda, D. *J. High Resol. Chromatogr.* **2000**, 23, 111.

11. Hodgson, R.; Chen, Y.; Zhang, Z.; Tleugabulova, D.; Long, H.; Zhao, X.; Organ, M. G.; Brook, M. A.; Brennan, J. D. *Anal. Chem.,* **2004**, 76, 2780.

12. Arthur, C.L.; Pawliszyn J. *Anal. Chem.* **1990**, 62 , 2145.

13. Schedl, M.; Wilharm, G.; Achatz, S.; Kettrup, A.; Niessner R.; Knopp D. *Anal. Chem.* **2001**,73, 5669.

14. Sieminska, L.; Ferguson M.; Zerda, T.W.; Couch, E. *J. Sol–Gel Sci. Technol.* **1997**, 8, 1105.

15. Kortesuo, P., Ahola, M., Kangas, M., Yli-Urpo, A., Kiesvaara, J., Marvola, M. *Int. J. Pharm.* **2001**, 221,107.

16. Radin, S.; Ducheyne, P.; Kamplain, T.; Tan, B.H. *J. Biomed. Mater. Res.* **2001**, 57, 313.

17. Aughenbaugh, W.; Radin, S.; Ducheyne, P. *J. Biomed. Mater. Res.* **2001**, 57, 321.

18. Ahola, M.S.; Sailynoja, E.S.; Raitavuo, M.H.; Vaahtio, M.M.; Salonen, J.I.; Yli-Urpo, A.U.O.; *Biomater.* **2001**, 22, 2163.

19. Böttcher, H.; Slowik, P.; Suss, W. *J. Sol–Gel Sci. Technol.* **1998**, 13, 277.

20. Nicoll, S.B.; Radin, S.; Santos, E.M.; Tuan, R.S.; Ducheyne, P. *Biomater.* **1997**, 18, 853.

21. Santos, E.M.; Radin, S.; Ducheyne, P. *Biomater* **1999**, 20, 1695.

22. Böttcher H.; Jagota, C.; Trepte, J.; Kaiiles, K.H.; Haufe, H. *J. Control Release* **1999**, 60, 57.

23. Obert, R.; Dave, B.C. *J. Am. Chem. Soc.* **1999**, *121*, 12192.

24. Gill,I.; Ballesteros, A. *J. Am. Chem. Soc.* **1998**, 120, 8587.

25. Reetz, M.T.; Wenkel, R.; Avnir, D. *Synthesis* **2000**, 6, 781.

26. Badjic, J.D.; Kadnikova, E.N.; Kostic, N.M. *Org. Lett.* **2001**, 3, 2025

27. Wang, R.; Narang,U.; Prasad, P.N.; Bright, F.V. *Anal. Chem.* **1993**, 65, 2671.

28. Flora,K.; Brennan, J.D. *Chem. Mater.* **2001**, 13, 4170.

29. Gottfried, D. S.; Kagan, A.; Hoffman, B. M.; Friedman, J.M. *J. Phys. Chem. B* **1999**, 103, 2803.

30. Jordan, J. D.; Dunbar, R.A.; Bright, F.V. *Anal. Chem.* **1995**, 67, 2436.

31. Baker, G.A.; Jordan, J.D.; Bright, F.V. *J. Sol-Gel Sci. Technol.* **1998**, 11, 43.

32. Doody, M. A.; Baker, G.A.; Pandey, S.; Bright, F. V. *Chem. Mater.* **2000**, 12, 1142.

33. Khan,I.; Shannon, C. F.; Dantsker, D.; Friedman, A.J.; Apodaca, J. P.-G.-de.; Friedman, J.M. *Biochem.* **2000**, 39, 16099.

34. Tleugabulova, D.; Duft, A.M.; Brook, M.A.; Brennan, J. D. *Langmuir* **2004**, *20*, 101.

35. Tleugabulova, D.; Zhang, Z.; Chen, Y.; Brook, M.A.; Brennan, J.D. *Langmuir* **2004**, *20*, 848.

36. Sui J.; Tleugabulova, D.; Brennan J. D. *Langmuir* **2005**, *21*, 4996.

37. Geddes, C.D.; Apperson, K.; Birch, D.J.S. *Dyes Pigments* **2000**, *44*, 69.

38. Flora, K. K.; Brennan, J. D.; Baker, G. A.; Doody, M. A.; Bright, F. V. *Biophys. J.* **1998**, 75, 1084.

39. SjÖback, R.; Nygren, J.; Kubista, M. *Spectrochim. Acta, A* **1995**, 51A, L7-L21.

40. Pico, G. A. Int. J. Biol. Macromol. **1997**, 20, 63-73.

41. Zheng, L.; Reid, W.R.; Brennan, J.D. *Anal. Chem.* **1997**, *69*, 3940.

42. Demas, J. N. *Excited-State Lifetime Measurements*; Academic Press: New York, 1983.

43. Lakowicz, J. R.; Gryczynski, I. In *Topics in Fluorescence Spectroscopy*; Lakowicz, J. R., Ed.; Plenum: New York, 1991; Vol. 1, Chapter 5.

44. a) Bright, F. V.; Betts, T. A.; Litwiler, K. S. *CRC Crit. Rev. Anal. Chem.* **1990**, *21*, 389, b) Bright, F. V. *Appl. Spectrosc.* **1995**, *49*, 14A.

45. Geddes, C. D.; Karolin, J.; Birch, D. J. S. *J. Phys. Chem. B* **2002**, 106, 3835.

48. Iler, R. K. The Chemistry of Silica: Solubility, Polymerization, Colloid and Surface Properties, and Biochemistry, Wiley-Interscience Publication, New York, 1979, p. 348.

49. Tleugabulova, D.; Zhang, Z.; Chen, Y.; Brook, M.A. and Brennan, J.D. *Langmuir* **2004**, 20, 848.

46. Tleugabulova, D.; Sui, J.; Ayers, P. and Brennan, J.D.. *Journal of Physical Chemistry B*, **2005**, 109, 7850.

Chapter 6

Conclusions and Future Outlook

6.1 Summary and Conclusions

The research contained in this thesis strived to achieve three main goals. These were: (i) to assess the nature of the R6G:silica interaction to determine the dynamics of adsorbed R6G and ultimately validate the model used to fit the TRFA data and gain further insight into the physical meaning of the anisotropy decay parameters, (ii) to assess the electrostatic binding of four model peptides to the silica surface using TRFA methods and compare information obtained from direct monitoring of peptide fluorescence to that obtained from R6G, and (iii) to investigate a new method for analysis of surface modification based on changes of ϕ_2, rather than f_1, f_2 and g, to extend our studies from the realm of small peptides toward larger biomolecules such as proteins, and to extend the Ludox system to allow examination of interactions between proteins and surface-modified silica.

The first project explored the TRFA parameters of R6G in a number of silica systems and provided new insight into the physical meaning of the nanosecond decay component ϕ_2. We found that the fraction of ϕ_2 was generally higher in Ludox than in aqueous sodium silicate and decreased with increasing silica concentration; ϕ_2 vanished upon gelation of sodium silicate at pH 7 leading to a total loss of R6G depolarization ($r(t) = const$). These results rule out the presence of local R6G wobbling when bound ionically to the colloidal silica and indicate that ϕ_2 is associated with the rotation of small nanoparticles, the presence of which is supported by TEM measurements. The data also support the rigid sphere model to describe the TRFA decays for R6G-Ludox, and show that TRFA data are entirely supported by steady-

state anisotropy data and structural considerations for the R6G molecule and the silica surface.

Knowing the correct model to interpret the TRFA decays from the R6G/Ludox system, the second objective was to assess the electrostatic binding of four model peptides to the silica surface using TRFA methods. Chapter 4 described the measurements of steady-state anisotropy and TRFA of R6G in Ludox sols to characterize the extent of the ionic binding of the probe to silica particles in the presence of varying levels of tripeptides of varying charge, including Lys-Trp-Lys (KWK), N-acetylated Lys-Trp-Lys (Ac-KWK), Glu-Trp-Glu (EWE) and N-acetylated Glu-Trp-Glu (Ac-EWE). The results were compared to those obtained by direct observation of peptide adsorption using the steady-state anisotropy of the intrinsic tryptophan residue. Ionic binding of the peptides to Ludox particles produced an increase in the steady-state Trp anisotropy that was dependent on the number of cationic groups present, but the limiting anisotropy values were relatively low, indicating significant rotational freedom of the indole residue in the adsorbed peptides. On the other hand, R6G showed significant decreases in anisotropy in the presence of cationic peptides, consistent with the addition of cationic peptides blocking the adsorption of the dye to the silica surface. The results showed that R6G was able to indirectly report on the binding of peptides to Ludox particles and that the competitive binding method could be used to assess the binding of various biologically relevant compounds onto silica surfaces, which demonstrates the potential of TRFA for probing peptide:silica and protein:silica interactions.

The third major objective of this work was to extend our studies from the realm of small peptides toward larger biomolecules such as proteins, and to extend the Ludox system to allow examination of interactions between proteins and surface-modified

silica. As described in chapter 5, the long-lived cationic quinolinium probe CG437 could be used to directly measure the rotational correlation times of both native and modified Ludox particles. The binding of a protein leads to an increase in the average correlation time of the particles, owing to the increase in average particle size when protein adsorbs, thus allowing direct observation of protein:Ludox interactions. The study shows that TRFA analysis of variations in ϕ_2 values of long-lived cationic probes such as CG437 can provide an effective method to investigate interactions between proteins and modified silica surfaces, extending the utility of the TRFA method.

Overall, the research findings outlined in this thesis expand the application of time-resolved fluorescence anisotropy in a new field: evaluating peptide:silica, protein:silica and protein:modified silica interactions. The studies show that TRFA analysis with short lifetime probes such as R6G provides a sensitive method to investigate interactions between small biomolecules such as peptides with native silica surfaces, without having to label peptides first. It provides a convenient method to calculate degree of silica surface modification by various kinds of peptides from the TRFA fitting parameters f_1, f_2 and g. TRFA of long-lived cationic probes such as CG437 provides an effective method to investigate interactions between larger biomolecules such as proteins and native or modified silica surfaces by monitoring the changes of ϕ_2 extending the utility of the TRFA method.

6.2 Future Outlook

Time-resolved fluorescence anisotropy has proven to be a powerful tool to investigate the interactions between entrapped biomolecules and sol-gel materials in-situ. Potential advantages of the approach outlined in this thesis include the ability to

work with very low quantities of protein, (micromolar concentration), the ability to use fluorescence to monitor the adsorption of non-fluorescence species such as polylysine and polyglutamic acid, and the ability to provide information on the binding of species to both native and modified surfaces. However, there are also several potential drawbacks to the TRFA approach. Firstly, while the TRFA fitting parameters f_1, f_2 and g provide a simple method to calculate the relative degree of silica surface modification by various kinds of peptides, methods must be developed to allow assessment of absolute surface coverage, in molecules per nm^2 surface area, to allow comparison of TRFA modification data to that obtained by other methods. Secondly, this method is currently limited to cationic probes such as R6G and CG437 bound to anionic surfaces. Changing the nature of the probe may allow us to assess different types of interactions (electrostatic, H-bonding, hydrophobic), providing a more versatile method for studying interactions of compounds with surfaces. Thirdly, the use of silica nanoparticles as a model system suffers from issues such as flocculation, which limits the concentration range analytes and modifiers that can be evaluated by TRFA measurements.

Another area where TRFA needs to be further explored in terms of both surface modification and protein adsorption is in monolithic sol-gel derived matrices. Such as system would avoid issues with flocculation and would provide a means to study a higher range of modifier concentrations. On the downside, such a system could potentially suffer from issues such as a distribution of microenvironments or variations in biomolecule conformation throughout the matrix, which would complicate TRFA analysis. However, by monitoring the rotational properties of a competitive probe, such as R6G, rather than the dynamics of the protein, it may be possible to more carefully evaluate protein:silica interactions within such materials.

Finally, efforts must be made to relate the data from the TRFA studies to that obtained from other methods, such as surface analysis or frontal affinity chromatography (FAC). Methods such as TIRF and FAC overcome the flocculation problem and allows insight into the interactions between analytes and silica based columns, namely non-specific binding, with or without surface modifiers such as APTES, GLTES, etc. Such studies may provide very useful information on how to better interpret the TRFA data, and may ultimately lead to the development of improved sol-gel processing conditions and surface modification schemes that can decrease non-specific interactions to improve the performance of protein-doped devices.